ABSTRACT

Title of dissertation: UNDERSTANDING PHASE TRANSITIONS, SYMMETRY BREAKING, AND INTERACTION-ENHANCED SENSING IN OPTOMECHANICAL AND COLD ATOMIC SYSTEMS

Stephen James Ragole
Doctor of Philosophy, 2018

Dissertation directed by: Professor Jacob M. Taylor
Department of Physics

We focus on the interaction of light and matter in atomic and optomechanical systems. These highly controllable and engineerable systems present access to new regimes and research opportunities that often do not exist outside the laboratory. As such, they frequently depart from more commonplace systems which are well understood. We extend our understanding of thermodynamic phase transitions, spontaneous symmetry breaking, and quantum-enhanced sensing to new regimes.

Traditionally, phase transitions are defined in thermodynamic equilibrium. However, inspired by the success of the phase transition paradigm in non-equilibrium fields, we derive an effective thermodynamics for the mechanical excitations of an optomechanical system. Noting the common frequency separation between optical and mechanical components, we study the dynamics of the mechanical modes under the influence of the steady state of the optical modes. We identify a sufficient set of constraints which allow us to define an effective equilibrium for the mechanical

system. We demonstrate these constraints by studying the buckling transition in an optomechanical membrane-in-the-middle system, which spontaneously breaks a parity symmetry. Having established a thermodynamic limit, we characterize the nature of the phase transition, which can change order based on system parameters. We extend our framework, proposing an photonic systems which realizes an SO(N) symmetry breaking transition of the same nature as the membrane-in-the-middle system. While we have treated these systems in the classical limit, their open nature has pronounced effects when other noise sources are suppressed. We study the canonical optomechanical system to unravel the origin of the semiclassical force and potential on the mechanics. We find that this force, while conservative with respect to the mechanics, deeply depends on the quantum back-action due to photon loss from the cavity.

Additionally, we study the ability of cold atoms to sense rotation. We consider bosonic atoms confined to a one-dimensional ring. Employing Luttinger liquid theory to study the excitations, we find that in the strongly-repulsive regime, atomic currents can be manipulated and superposed by controlling a laser barrier. These superpositions provide a Heisenberg-limited rotation sensing method. When we include noise, the precision is reduced, but the performance still surpasses the standard quantum limit. We comment on the applicability of such a sensor for inertial sensing.

UNDERSTANDING PHASE TRANSITIONS, SYMMETRY BREAKING, AND INTERACTION-ENHANCED SENSING IN OPTOMECHANICAL AND COLD ATOMIC SYSTEMS

by

Stephen James Ragole

Dissertation submitted to the Faculty of the Graduate School of the
University of Maryland, College Park in partial fulfillment
of the requirements for the degree of
Doctor of Philosophy
2018

Advisory Committee:
Professor Victor M. Galitski, Chair
Professor Jacob M. Taylor, Advisor
Professor Gretchen K. Campbell
Professor Jay D. Sau
Professor Mohammad Hafezi

Acknowledgments

This thesis would not have been possible without the contributions of countless people who have helped me throughout my life. Indeed, the whole enterprise of science depends not just on the hard work of individual scientists, but also the collaboration of teams and the network of colleagues, friends, and family who support us in this work.

I owe a great deal to my parents, who have always made education a priority, even when it meant shuttling their children to afternoon activities or far away schools. Their encouragement and support has been invaluable throughout the years. My brothers and sister-in-law continue to serve as role models in exploring the world and having fun doing it.

One does not sign up for this much school without having fantastic teachers. Throughout my education I have had the good fortunate of having caring, devoted teachers who were always willing to engage my curiosity and push my thinking. Additionally, I am grateful for the teachers who saw something more than I did and challenged me to accomplish things I had not imagined.

In research, I am deeply thankful for the Special Undergraduate Enrichment Programs at CU Boulder, without whose funding it would have been challenging to consider a career in science. The opportunities granted by the program led me to this exciting field of atomic, molecular and optical physics. To that end, Professor Chris Greene and Dr. Jose D'Incao were wonderful mentors who cemented my love of atomic physics research.

In graduate school, I benefitted greatly from guidance and support of my advisor, Professor Jake Taylor. I learned a tremendous amount about how to tackle scientific problems and which ones to go after. I am also grateful for the helpful discussions from my committee: Professors Campbell, Hafezi, Galitski, and Sau. Thanks to the members of the Taylor group, postdocs: Michael Gullans, Vanita Srinavasa, Tom Purdy, Shelby Kimmel, Jianxin Chen, Justyna Zwolak, Xingyao Wu, and Dan Carney, and graduate students: Prabin Adhikari, Dvir Kafri, Haitan Xu, Xunnong Xu, Chiao-Hsuan Wang, Andrew Glaudell, Sandesh Kalantre, Shangjie Guo, Minh Tran, and Brittany Richman, for numerous helpful discussions and support. I am particularly appreciative of my office mates from different groups, Aftaab Dewan, Ranchu Mathew, Abhinav Deshpande, and Ali Hamed Moosavian, who were always willing to engage in my frequent questions.

I am also thankful that Jake supported my wild idea to move across the country and finish writing at JILA. JILA, yet again, proved to be a wonderful place to work and I thank Professor Ana Maria Rey and her group for their generous hospitality and support.

Thank you my friends and student leaders on Graduate Student Committee and the Mental Health Task Force for providing me with meaning and productive outlets throughout graduate school. Graduate school adds a lot of unnecessary stress and difficulty to an already difficult task. Thanks to the department leadership, who helped us with their devotion to improving the department: Donna Hammer, Jessica Crosby, Peter Shawhan, and Steve Rolston. I will always be proud that we were part of the long, hard work to address these issues.

While the simple work of physics research is hard enough, the whole ordeal of graduate school, beginning with moving across the country to live with strangers can be overwhelmingly challenging. I am thankful for the Seven Seas, which was a fantastic place for me to call home at the start of graduate school.

I also want to thank my friends: Courtney Cowper, Zach Eldredge, Ryan Galginaitis, Rachel Gartner, Alex Hansen, Matt Harrington, Anna Lieb, Joe Murray, Mitesh Shridhar, David Somers, Antony Speranza, Chris Wall, and Ken Wright. Your support has been invaluable.

Finally, Gina, I could not have gotten here without your support, kindness, humor, and intellect. You make every day better.

Table of Contents

List of Tables

List of Figures

Chapter 1: Introduction

1.1 Motivation

Frequently in physics there are discoveries of new areas, or advances in technology, that allow access to never before considered regimes. These new areas may be described by entirely new theories or extensions of well known standards. In either case, the notion of analogies is a particularly relevant and useful concept. When we discover something new about the behavior of physical objects, it adds to our previous understanding, but also implicitly asks, what can be done with this understanding? Can one take concepts from other areas which resemble, however slightly, this new system and implement them? Testing these analogies gives more insight into the new system and potentially allows for the creation of new technologies built off of previous results. As an example one can consider the incredibly successful exploration of matter waves: Louis de Broglie realized that matter could have wave-like properties in 1924. These properties were soon confirmed (accidentally) by Davisson and Germer [1]. It was only a brief time before these wave-like properties were utilized to create an entirely new method of observation, the electron microscope [2]. Electron microscopy quickly blossomed into an important field which to this day drives understanding of crystal structures and features that are

smaller than reasonable wavelengths for photon-based imaging. While most analogies are not as successful, the technique of extending our understanding from old systems to new ones is particularly fruitful. I begin with a description of the history of optomechanics and atomic physics to set the stage for the analogies we discuss.

1.2 Optomechanics

The fact that photons can exert a force on objects is important over a range of scales and therefore to many different fields of physics. The force was originally proposed by Kepler to explain why the tail of a comet always points away from the Sun. While the magnitude of radiation pressure force is not particularly large, (at Earth's orbit, solar radiation pressure is $\sim 10\ \mu N/m^2$), it is important factor in astrophysics and has been used to propel satellites as far as Venus [3]. On the surface of the Earth, other forces overwhelm radiation pressure and its effect is difficult to quantify. While Maxwell's equations predicted that electromagnetic radiation should exert this pressure, it was not until 1900 that it was successfully measured [4, 5]. Over the last century, however, this force has become increasingly important and experimentally accessible. Since the invention of the laser [6, 7], we have enjoyed incredible control and engineerability in creating coherent, stable sources of light. This ability to generate light has been augmented by our ability to create structures that modify the properties of light for storage, amplification and transmission. In particular, we focus on the ability to "trap" light in an optical resonator. The traditional resonator is a cavity composed of two mirrors, at least one of which is

imperfect, to allow light from the outside to transmit into the cavity. There are numerous other methods of creating resonator structures, such as those employing dielectric material (for a review of these, see Ref [8]). Within the resonator, the boundary conditions determine a resonant set of modes. If the externally coupled light overlaps with these resonant modes, they will be excited within the resonator. The modes are generally long lived, with a lifetime set by the cavity decay rate, κ, which means that driving with even small external power can result in a large number of excitations within the cavity. This large population, of course, means many photons can interact with matter, either through the electric field or, in our case, by imparting momentum to a mechanical object. These combined optical and mechanical (optomechanical) systems have found a wide range of applicability. Such systems can form sensors which push the boundaries of measurement, typically at the nanoscale [9], but including the massive Laser Interferometry Gravitational-Wave Observatory (LIGO), which recently detected gravitational waves from two merging black holes [10]. Additionally, the success of optical fiber for information transmission has increased the need for devices which can interact with guided light, including the development of optomechanical memory elements [11].

For the first part of the thesis, I focus on processes where the light exerts a force on mechanical resonators. These interactions can become incredibly important within optical resonators and when the mechanical objects are low mass. This optical force is non-linear, depending on the number of photons, and competes with mechanical restoring forces. It is sometimes useful to view the interaction not as a force, but as a modification of the frequency of the resonant modes. Within this

framework, it is more obvious how density waves in dielectric material can couple mechanical oscillations to photonic ones. Typically one considers mechanical systems with linear restoring forces and while generic systems may have more complicated dynamics, a decomposition to normal modes renders our consideration of harmonic oscillators fairly general.

Optomechanical interactions can be engineered in numerous optically dense materials, including gases of cold atoms (e.g., [12–14]), where the optical length of a cavity now depends on the density of the atomic gas within. The oscillations of density are nearly harmonic, creating an equivalent system. These systems also typically feature an enhanced optomechanical coupling due to the fact that all of the atoms interact with the same light field. Additionally, they can be prepared at very low temperatures, allowing explorations of quantum effects. Optomechanical systems in the quantum regime have proved remarkably sensitive, providing measurements of some of the smallest forces to date, [9, 15].

However, optomechanical systems are fundamentally driven and dissipative, meaning that coupling to the external environment is crucial to their operation. Due to this external drive and loss, these systems are not in thermodynamic equilibrium, coupling to at least two reservoirs. Many traditional systems in physics, and especially within quantum mechanics, are treated as closed, or at equilibrium with a single reservoir at a well-defined temperature. The absence of a single bath complicates the picture and invites us to consider whether equilibrium concepts such as phase transitions extend to these non-equilbrium cases. One interesting feature of optomechanical interactions is the ability to connect excitations which have

resonant frequencies which are very well separated. This ability to transduce excitations from one regime to the other underlies most of the optomechanical sensing (i.e., reading information about the mechanics from the optical field) and may find use in transmitting quantum information [16]. The separation in time scales means we may be able to consider the dynamics of the mechanics assuming that the optical modes instantaneously reach their steady state. From this point of view, we look for a new effective equilibrium description of the mechanical system. While phase transitions exist classically, the ability to cool optomechanical systems invites the study of such behavior in the quantum realm. However, the introduction of loss means that, quantum mechanically, information is leaking out of the system, which potentially has strong effects on the dynamics of the mechanics [13, 17, 18]. We will pursue this line of reasoning in Appendix A.

1.3 Quantum gases

As alluded to in the previous section, atomic gases have generated a tremendous interest in the past decades. Arising concurrently and symbiotically with our ability to create and manipulate light, our understanding of atomic physics has driven a revolution in the ability to control and manipulate quantum systems. Indeed, the key ideas of the laser were pursued to allow more precise study of atomic and molecular states [19]. Nowadays, atomic and molecular systems are used as state of the art clocks and sensors which continue to push the envelope of precision (for a review of quantum sensing, see Ref. [20]). Some experiments have even con-

strained possible additions to the Standard Model [21, 22] and there are proposals to use cold atomic gases detect gravitational waves [23, 24].

In addition to static electric and magnetic fields, with the advent of the laser, it was possible to imagine controlling atomic states and motion with coherent light [25, 26]. An important goal at the time was controlling the motion of atoms or ions to decrease the thermal noise on spectroscopic properties. The absolute limit to this "laser cooling" for bosonic atoms is the realization of a Bose-Einstein condensate (BEC). At low temperatures, bosonic atoms lack enough states to occupy thermally and a macroscopic number of these atoms "condense" into the ground state of the potential [27]. The creation of BECs (as well as their fermionic counterpart, the degenerate Fermi gas) has driven an immense amount of research in atomic physics, opening up an entirely new toolbox of investigation.

1.3.1 Sensing with BECs

In particular, the condensation of many atoms into the same quantum state provides an avenue for precise sensing. Atoms have many excited states whose energies depend strongly on external factors, such as magnetic field or rotation. If one creates a superposition of two states which have different energies in such an external field, this superposition will gain a phase that depends on the strength of the field. Reversing the superposition can map this phase into a population difference between the states, which can be measured if the atom is imaged in a state selective manner. With a BEC, one can effectively conduct this single atom

experiment millions of times with a single run. Indeed, such experiments have provided incredible results in gravitational gradiometry, rotation sensing, and have promise in detecting gravitational waves [23, 28–30].

However, using a single atom technique in this ensemble manner leads to a natural noise which grows like $\sqrt{N}$ where N is the number of atoms. This noise forms what is sometimes called the Standard Quantum Limit for sensing, as it prevents higher precision measurements from being made. The limit is a result of averaging and can be overcome using quantum correlations, e.g., entanglement [31–33]. In some cases, quantum systems can correlate in such a way that they respond as a collective system to an external field. In that case, the state of the system is not a tensor product of a series of single atom superpositions, but instead a single superposition of the whole system in two different configurations. The phase accumulated between the states grows as N while the noise of a single measurement is constant. This "Heisenberg limit" is the fundamental limit on quantum sensing.

Perhaps unsurprisingly, performing measurements beyond the standard quantum limit has proven difficult, in part due to the strong response entangled states have to external factors, which can lead to decoherence [33]. Additionally, one must engineer or exploit interactions between atoms to create the relevant entangled states. While there have been some experimental successes [18, 34–36], even theoretically studying interacting many-body systems is generically difficult and common perturbative techniques such as mean field theory are often unable to describe maximally entangled states. Indeed, an exciting avenue for cold atom physics is the simulation of systems which are difficult to understand theoretically. However,

there are some restricted domains which can be studied due to useful approximations.

In particular, in one-dimension, the restricted motion allows one to consider an effective theory of phonons and topological excitations (such as currents) known as Luttinger liquid theory. This theory was originally applied to fermions in confined nano-wire structures [37] but it was later discovered that, since particles cannot exchange places without scattering, both bosonic and fermionic systems can be considered in the same framework [38–40]. This theory opens up a wide range of interacting systems for analysis and includes many-body superpositions (such as between two distinct currents) which are necessary for attempting Heisenberg limited sensing. We explore the possibility of using such systems for rotation sensing.

1.4 Thesis outline

Chapter 2 introduces a generic framework for understanding when optomechanical systems can be described as having an effective equilibrium phase transition. While these systems are typically far from equilibrium, following Ref. [41], we consider optomechanical systems when the relevant optical frequencies are much faster than the mechanical ones. This separation allows us to eliminate the optical modes and focus on the induced dynamics for the mechanical modes. We identify a sufficient set of constraints that the optical modes must follow defining our thermodynamic limit. Additionally, we note that optically induced forces are generically non-conservative.

Building on this framework, we describe a explicit realization of a phase transition in Chapter 3. We study an optomechanical membrane-in-the-middle system inspired by the experimental observation of a buckling transition, which we include as Appendix B [42]. We walk through the previously identified constraints to show that this system has a well defined thermodynamic limit. Further, we identify an order parameter and characterize the nature of the phase transition. Additionally, this introduces the notion of spontaneous symmetry breaking in optomechanical systems.

In Chapter 4, we broaden our consideration to include systems which break a continuous symmetry (such as $U(1)$) instead of the discrete $\mathbb{Z}_2$ symmetry described in Chapter 3. We propose a Hamiltonian based on a reparametrization of our model of the $\mathbb{Z}_2$ system which has an $SO(N)$ symmetry. This Hamiltonian can be realized with optomechanically coupled photonic nanobeams. We show that this system has a transition which spontaneously breaks the $SO(N)$ symmetry as the driving strength increases. We conclude with comments on the constraints necessary for a thermodynamic limit, as described in Chapters 2 and 3, including commenting on a related cold atom experiment [43] which spontaneously breaks a $U(1)$ symmetry.

Moving to consider atomic systems more fundamentally, Chapter 5 describes a proposal for an interaction-enhanced quantum rotation sensor. Here, we assume the optical fields only dictate the potential landscape for the atoms, which we imagine trapped in a one-dimensional ring. To consider effects beyond mean-field and into the strongly interacting regime, we use Luttinger liquid theory. We identify a method to generate and interfere many-body superpositions of atomic current. We

study the ability of these states to measure rotation, which affects neutral atoms analogously to the effect of magnetic fields on charged particles. We demonstrate an improvement beyond the standard quantum limit and comment on potential applications in sensing and elsewhere.

In Appendix A, we consider how quantum effects, essential to Chapter 5, will manifest in the systems considered in Chapters 2-4. In particular, non-linear features like bistability are prohibited by the linearity of quantum mechanics. However, these optomechanical systems are open, which means the photons leave the system while carrying information about the mechanical resonator. We seek to understand the effect of photon loss on the wavefunction of the mechanics by using a quantum jumps framework [44, 45]. We demonstrate that the standard semiclassical potential used in optomechanics appears on average from the combination of these photon jumps and the conservative dynamics of the system.

Chapter 2: Phase Transitions in Optomechanical Systems [1]

2.1 Introduction

Phase transitions provide a remarkably powerful framework to study phenomena in many different regimes. While traditionally phase transitions have been studied in classical, equilibrium systems, the most fundamental aspect is the non-analytic behavior of an observable at large system sizes. Looking more generally to non-analytic behavior, others have considered situations that do not meet the strict requirements of thermodynamic equilibrium. In particular, phase transitions have been proposed or observed in systems that are non-equilibrium [46], dissipative [47], dynamical [48, 49], and even quantum mechanical [50–54]. In non-equilibrium systems, numerous analogies with traditional equilibrium phase transitions have been explored, e.g., in lasers [55, 56], the Gunn effect [57], and in tunnel diodes [58, 59]. These analogies are fairly broad in consideration, and are readily generalized to other non-equilibrium, non-linear systems, such as those studied in optomechanics.

In recent years, scientific advances have enabled the creation of numerous op-

[1] This chapter appears as part of "Thermodynamic limits for optomechanical systems with conservative potentials," by S. Ragole, H. Xu, J. Lawall, and J. M. Taylor in Physical Review B 96 (18), 184106

tomechanical systems over a range of scales (see Ref. [8] for a review). These systems combine the engineerability and control of optical systems with the simplicity of a mechanical harmonic oscillator. Impressive results, including a self-structuring of atoms [51–54] and a buckling of an optomechanical membrane [42] suggest that stable structural rearrangements of the mechanical modes can be described by an order parameter.

Here we show that the dynamics of the slow modes (the mechanics) can be described by an effective thermodynamic theory despite being an open, non-equilibrium system. Our approach works provided that the fast modes (the optics) obey certain properties, analogous to approaching an optical steady state, defining our thermodynamic limit. This is conceptually similar to integrating out high frequency or short wavelength behavior, but here the process takes a non-equilibrium problem to an equilibrium one, in contrast to the usual formulation of phase transitions. Specifically, we construct a sufficient set of constraints that allow the definition of a thermodynamic limit, and phase transitions, in optomechanical systems. While the limit we define is possible in some cases, we also show a generic optomechanical system may not have such a limit or even be described by a thermodynamic potential. We illustrate our general approach with an example, a phase transition following [42], showing along the way that these constraints are satisfied. While our approach takes into account quantum fluctuations, we do not consider quantum phase transitions in this work.

2.2 Identification of Thermodynamic Limit

We will consider a driven, dissipative system comprising many optical modes coupled to many mechanical modes. Such optomechanical systems have been realized over a wide range of scales, from LIGO to nanoscale resonators or cold atoms [8]. Examples of non-analytic behavior in these systems is depicted in Figure 2.1. These systems are, however, far from equilibrium. In the limit that the optics respond instantaneously with respect to the mechanical modes, (i.e., the dynamics for each optical mode are much faster than any of the mechanical frequencies), we may consider the behavior of the optical steady state. Typically, this is accomplished by adiabatically eliminating the optical modes and replacing them with steady state values that depend parametrically on the mechanical modes [41]. Here we show that we can construct a limit in which the mechanical steady state values are effectively thermodynamic, and identify order parameters in systems with phase transitions.

To ensure that a thermodynamic description holds, we need the system to have conservative dynamics, be stable, have optical forces that are at least as large as mechanical forces and to only couple to bath(s) at a single temperature in the large size limit. Theses constraints (C1-C6) are enumerated in Table 2.1.

We adopt a Hamiltonian formulation for the system, then follow the usual conventions to derive Heisenberg-Langevin equations of motion. As such, we will not specify many of the details of the Hamiltonian, instead focusing on the resulting

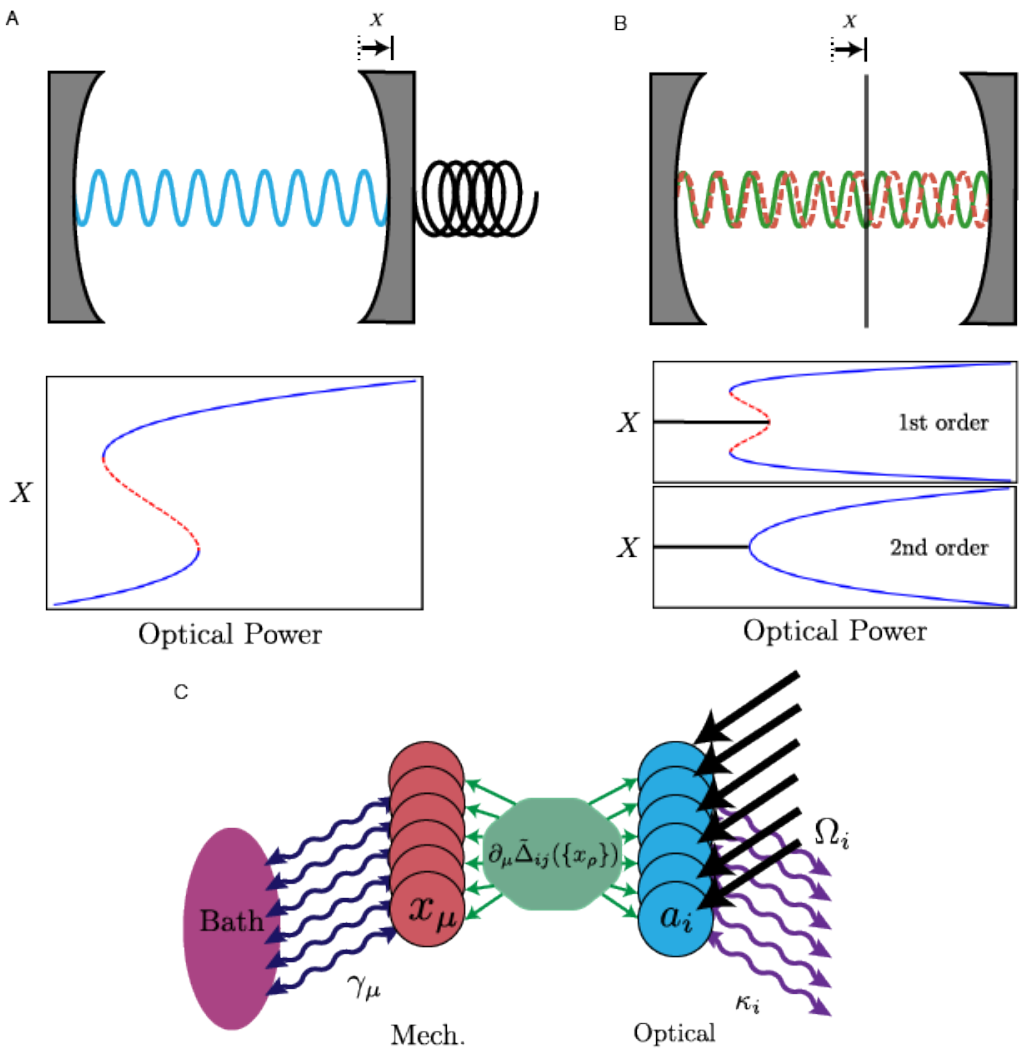

Figure 2.1: Examples of non-analytic behavior in the steady state mechanics of optomechanical systems. A. Competition between mechanical and optical springs creates bistability as a function of laser power. The stable (unstable) solution is shown as a solid (dashed) line. B. A membrane-in-the-middle system shows a Z_2 phase transition which has either a first- (with unstable solutions as dashed lines) or second-order characteristics. C. A cartoon of the generic system with many mechanical (x_μ, on the left) and optical modes (a_i, on the right) coupled optomechanically and with laser drive (Ω_i) on the optics.

Table 2.1: The constraints for realizing a thermodynamic limit of an optomechanical system.

C1	The optical force must have a vanishing curl.
C2	The total cavity detuning must remain negative (red-detuned).
C3	The optical force must be comparable to the mechanical restoring force.
C4	The linearized optical restoring force must remain comparable to the mechanical restoring force.
C5	The optically induced damping in the linearized equations must vanish.
C6	The optically induced noise in the linearized equations must vanish.

equations of motion. Still, in principle our system plus bath is described by

$$H = H_{\rm opt} + H_{\rm mirror} + H_{\rm mech} + H_{\rm optbath} + H_{\rm mechbath} \ , \tag{2.1}$$

where all terms with optical mode operators are assumed to be bilinear or linear in such operators, but may also depend upon the mechanical degrees of freedom. This means that we can write down equations of motion for the optical modes that have no troubles with commutator order, but the addition of optical loss through the mirror into the optical bath will lead to an effective, non-Hermitian picture in the equations of motion approach.

The system obeys the following equations (in the frame rotating with the laser

drive frequency for each mode):

$$\dot{a}_i = i\tilde{\Delta}_{ij}(\{x_\rho\})a_j - i\Omega_i + \sqrt{\varkappa_{ij}^{ex}}a_j^{in} \ , \tag{2.2}$$

$$\dot{x}_\mu = M_{\mu\nu}^{-1}p_\nu \ , \tag{2.3}$$

$$\dot{p}_\mu = -K_{\mu\nu}x_\nu - \Gamma_{\mu\nu}p_\nu + a_i^\dagger\partial_\mu\tilde{\Delta}_{ij}(\{x_\rho\})a_j + \sqrt{\Gamma_{\mu\nu}}p_\nu^{in} \ , \tag{2.4}$$

where we use Einstein summation notation, with optical modes, a_i, indexed by Roman indices, coupled to the set of mechanical modes, represented by x_μ, p_μ, indexed by Greek indices. $\tilde{\Delta}_{ij}(\{x_\rho\}) = \Delta_{ij}(\{x_\rho\}) + \frac{i}{2}\kappa_{ij}(\{x_\rho\})$ is the non-Hermitian matrix, due to $H_{\rm opt} + H_{\rm mirror} + H_{\rm optbath}$, which describes the dynamics of the optical modes in addition to all of the couplings to the mechanical modes. We note that this generic coupling includes standard dispersive couplings ($i = j$), beam-splitter-like terms ($i \neq j$), and dissipative couplings. $M_{\mu\nu}$, $K_{\mu\nu}$, and $\Gamma_{\mu\nu}$ are the matrices, due to $H_{\rm mech} + H_{\rm mechbath}$, giving the effective masses, couplings, and decay rates for the mechanical modes. Ω_i is the laser drive, $\varkappa_{ij}^{ex}$ is the decay rate matrix for the optical baths, and a_j^{in}, p_ν^{in} are the fluctuations of corresponding optical and mechanical bath fluctuations, respectively. We note that the derivatives of $\tilde{\Delta}_{ij}$ with respect to mechanical coordinates correspond to the vacuum radiation pressure force. Thus, when the optical modes have finite occupation, we will have a finite force.

2.3 Explicit calculation of constraints around steady state

To separate the steady state effects from the fluctuations, we make the following expansion:

$$a_i = A_i + \delta a_i \ , \tag{2.5}$$

$$x_\mu = X_\mu + \delta x_\mu \ , \tag{2.6}$$

$$p_\mu = P_\mu + \delta p_\mu \ , \tag{2.7}$$

where the capital letters (A_i, X_μ, P_μ) represent the noiseless, classical variables and the δ variables are proportional to the fluctuations. We can consider the noiseless variables in the optical steady state ($\dot{A}_i = 0$) and study the induced force on the mechanical modes:

$$F_\mu^{opt} = A_i^\dagger(\{X_\rho\})\partial_\mu \tilde{\Delta}_{ij}(\{X_\rho\})A_j(\{X_\rho\}) \ . \tag{2.8}$$

2.3.1 Constraints on steady state values

Our first requirement (C1) is that the curl of this force vanishes, $\epsilon_{\rho\nu\mu}\partial_\nu F_\mu = 0$. If this requirement holds, then the mechanics can be described by a conservative potential. This curl has the form:

$$\begin{aligned}\epsilon_{\rho\nu\mu}\partial_\nu F_\mu = -\epsilon_{\rho\nu\mu}\Bigg(&\partial_\nu \tilde{\Delta}_{il}^\dagger(\{X_\rho\})\frac{1}{\tilde{\Delta}_{lm}^\dagger(\{X_\rho\})}\partial_\mu \tilde{\Delta}_{mj}(\{X_\rho\}) \\ &+ \partial_\mu \tilde{\Delta}_{il}(\{X_\rho\})\frac{1}{\tilde{\Delta}_{lm}(\{X_\rho\})}\partial_\nu \tilde{\Delta}_{mj}(\{X_\rho\})\Bigg)A_i^\dagger A_j \ ,\end{aligned} \tag{2.9}$$

where we have used the fact that partial derivatives commute. There are many possible instances where the curl vanishes. Some example cases are if there is only a

single mechanical mode, a single optical mode, or if $\tilde{\Delta}_{ij}(\{x_\rho\})$ is Hermitian – though the lack of damping in the optical modes may violate our adiabatic assumption. We will show a simple case where a non-Hermitian $\tilde{\Delta}_{ij}(\{x_\rho\})$ possesses a potential and describes a system with a phase transition. Intriguingly, cases with two or more damped optical modes and multiple mechanical modes generically have a curl, owing to the matrix nature of $\tilde{\Delta}_{ij}(\{x_\rho\})$ and the inclusion of optical loss. Though these cases may have interesting dynamics, including potentially topological properties and limit cycle behaviors, we will not focus on them here.

In the case where the curl vanishes, we need to ensure additional constraints hold to use equilibrium statistical mechanics to describe our system. We need the optical modes to remain red-detuned overall (C2) otherwise instability (via gain) will result. We also require that the optically induced forces remains comparable to the mechanical restoring force in $\{X_\rho\}$ (C3) and in $\{\delta x_\rho\}$ (C4) otherwise the system simply becomes mechanical. While C3-C4 are identical in linear systems, they are distinct in more complicated systems. In stable, open systems considered here, there are (at least) two baths, one optical and one mechanical. For a well-defined (single-temperature) thermodynamic limit, we need the mechanical system to experience a single temperature bath. These restrictions (C5-C6), linked by the fluctuation-dissipation theorem, mean that both the optically-induced mechanical damping and optically-induced mechanical noise must vanish in our limit.

2.3.2 Constraints on linearized fluctuations

To find the optically-induced forces and the corresponding damping and noise, we study the linearized dynamics of the fluctuations $(\delta a_i, \delta x_\mu, \delta p_\mu)$ which contain the influence from optical and mechanical noise. To first order, the linearized variables have the following equations of motion:

$$\delta\dot{a}_i = i\tilde{\Delta}_{ij}(\{X_\rho\})\delta a_j + i\partial_\mu\tilde{\Delta}_{ij}(\{X_\rho\})\delta x_\mu A_j + \sqrt{\varkappa_{ij}^{ex}}a_j^{in} \ , \tag{2.10}$$

$$\delta\dot{x}_\mu = M_{\mu\nu}^{-1}\delta p_\nu \ , \tag{2.11}$$

$$\begin{aligned}\delta\dot{p}_\mu = &-K_{\mu\nu}\delta x_\nu + A_i^\dagger\partial_\mu\tilde{\Delta}_{ij}(\{X_\rho\})\delta a_j + \delta a_i^\dagger\partial_\mu\tilde{\Delta}_{ij}(\{X_\rho\})A_j \\ &+ A_i^\dagger\partial_\nu\partial_\mu\tilde{\Delta}_{ij}(\{X_\rho\})\delta x_\nu A_j - \Gamma_{\mu\nu}\delta p_\nu + \sqrt{\Gamma_{\mu\nu}}p_\nu^{in} \ ,\end{aligned} \tag{2.12}$$

where a_i^{in}, p_μ^{in} are the bath-induced fluctuations in the optical and mechanical modes respectively.

This is a set of linear equations and can be solved. The solution determines the local stability of the system, and can include both damping and gain, depending upon eigenvalues of $\tilde{\Delta}_{ij}(\{X_\rho\})$. We note that this linearized theory is entirely compatible with the full quantum system, but may not capture the full phase diagram of the system outside of our area of focus – particularly in the regime of limit cycle or oscillator behavior.

We now examine the linear regime in detail. In both the noiseless and linearized equations, we need the optical forces to be comparable to the mechanical forces (C3-C4). Following our steady state assumption for the optical modes,

$A_i = \tilde{\Delta}_{ij}(\{X_\rho\})^{-1}\Omega_j$, we can Fourier transform the equations for the fluctuations, $\delta a_i(t) = \int \mathrm{d}\omega \tilde{a}_i(\omega) e^{-i\omega t}$, expanding in ω:

$$\begin{aligned}\tilde{a}_i &= \frac{-1}{\omega\delta_{ij} + \tilde{\Delta}_{ij}(\{X_\rho\})}\left(A_k\partial_\mu\tilde{\Delta}_{jk}(\{X_\rho\})\tilde{x}_\mu - i\sqrt{\varkappa_{jk}^{ex}}\tilde{a}_k^{in}\right) \ , \\ &\approx \frac{-1}{\tilde{\Delta}_{ij}(\{X_\rho\})}\left(A_k\partial_\mu\tilde{\Delta}_{jk}(\{X_\rho\})\tilde{x}_\mu - i\sqrt{\varkappa_{jk}^{ex}}\tilde{a}_k^{in}\right) \\ &\qquad + \omega\frac{1}{\tilde{\Delta}_{ij}(\{X_\rho\})}\frac{1}{\tilde{\Delta}_{jk}(\{X_\rho\})}\partial_\mu\tilde{\Delta}_{kl}(\{X_\rho\})\tilde{x}_\mu A_l \ , \end{aligned} \tag{2.13}$$

where we assume the noise fluctuations are small compared to the optomechanical term $\left(|\sqrt{\varkappa_{jk}^{ex}}\tilde{a}_k^{in}| < |A_k\partial_\mu\tilde{\Delta}_{jk}(\{X_\rho\})\tilde{x}_\mu|\right)$.

Now, inputing the expanded "steady state" optical modes into the Fourier transform of equation 2.12, we see a coupling to the optical bath which could disrupt the emergence of a thermodynamic limit. These damping and noise effects from $\tilde{a}_i$ must vanish for the mechanics to have a single bath (C5-C6). These six requirements, listed in Table 2.1, form a set of conditions which must be satisfied as the mechanical modes go to their thermodynamic limit (we envision $X_\mu \propto V^\alpha$, $\alpha > 0$, where V is the volume of the mechanical resonator and $V \to \infty$). In Figure 2.2, we show a simplified view of our approximation and thermodynamic limit process.

2.4 Conclusion

If all of these conditions (C1-C6) are met, then the mechanical modes will experience a potential modified by the optics but will not have any additional damping or noise contributions. In this case, the modes will thermalize only to the mechanical reservoir, with no contribution from the optical reservoir. In such a situation, we

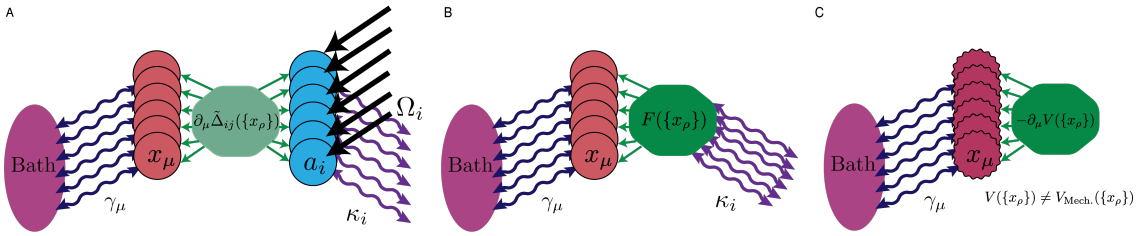

Figure 2.2: A schematic view of the thermodynamic limit we construct. A. The original system is a generic, driven optomechanical system with an arbitrary number of optical and mechanical modes. B. Using our adiabatic assumption, we use the steady state values for the optical modes, which results in an effective force on the mechanics, including a dissipative component from the optical bath. C. Following the constraints, we ensure that the force in B is conservative (C1), stable (C2), comparable to the mechanical force (C3-C4), and that the optical bath fluctuations are negligible (C5-C6), resulting in a mechanical system with a modified potential.

can compute the partition function and upon integration of the mechanical modes, determine a free energy for an order parameter if one exists in the system.

There are interesting systems which do not meet these conditions, however, we restrict ourselves to the case where our effective thermodynamic theory applies. In particular, in the next chapter, we demonstrate the existence of a $\mathbb{Z}_2$ phase transition in the defined thermodynamic limit of an optomechanical membrane-in-the-middle system.

Chapter 3: The Thermodynamic Limit for the $\mathbb{Z}_2$ System [1]

3.1 Introduction

We consider an optomechanical system with two optical modes, $a_{1,2}$, coupled oppositely to a single mechanical mode, x, with resonant frequency Ω_m, where each optical mode has equal drive and decay, ($\Omega_{1,2} = \Omega,\ \kappa_{1,2} = \kappa$),. Explicitly, we define $\Delta_{11} = \Delta_1 + gx$ and $\Delta_{22} = \Delta_2 - gx$, where $\Delta_1 = \Delta_2 = \Delta$ is the detuning of the modes when $x = 0$. As an example, one can consider a cavity with a dielectric membrane-in-the-middle [42, 60–62] where we drive two modes with opposite responses to the membrane motion, depicted in Fig. 2.1B. This system has been realized experimentally and shows the characteristics of a phase transition [42], which we expand upon.

To demonstrate that such a system has a thermodynamic limit, we need to determine how the constraints from Chapter 2 (C1-C6) are held. We choose the "bad cavity limit," $\kappa_i \gg \Omega_m, \gamma$, such that the optical decay is much faster than any mechanical frequency. C1 is satisfied immediately because the curl of a one-

[1] This chapter appears as part of "Thermodynamic limits for optomechanical systems with conservative potentials," by S. Ragole, H. Xu, J. Lawall, and J. M. Taylor in Physical Review B 96 (18), 184106

dimensional force vanishes identically. We expand the variables (a_1, a_2, x, p) and imagine that $X \propto V^\alpha \to \infty$, as above. We also consider the scaling of the membrane mass, $m = \rho V$, the coupling, $g = \omega_c d^{-1}$, and the cavity decay, $\kappa = cd^{-1}\mathcal{F}^{-1}$ where ρ is the mass density and $\omega_c, d, \mathcal{F}$ are the cavity frequency, length, and finesse, respectively. We can consider a variety of options for the cavity length, d, and adjust the other parameters, such as finesse and cavity frequency, to ensure the following scaling arguments hold. Two options for the cavity scaling are depicted in Figure 3.1. With C1 automatically satisfied, the rest of the constraints become a set of scaling relations that determine a region of parameter space in which the defined thermodynamic limit exists.

To ensure the cavity stays red-detuned (C2) we must impose that $\Delta \propto -|gX|$. Taking the steady state solutions for $A_i, \tilde{a}_i$ as described above, we can derive the optically induced force, damping, and noise in order to quantify the remaining constraints. The optical and linearized optical forces (C3-C4) are:

$$F^{opt} = -\frac{4\hbar g^2 \Delta |\Omega|^2}{(\Delta^2 + \frac{\kappa^2}{4})^2 + 2g^2X^2(\frac{\kappa^2}{4} - \Delta^2) + g^4X^4} X \ , \tag{3.1}$$

$$f^{opt} = -\frac{4\hbar g^2 \Delta |\Omega|^2 \left((\Delta^2 + \frac{\kappa^2}{4})^2 + 2g^2X^2(\Delta^2 + \frac{\kappa^2}{4}) - 3g^4X^4\right)}{\left((\Delta^2 + \frac{\kappa^2}{4})^2 + 2g^2X^2(\frac{\kappa^2}{4} - \Delta^2) + g^4X^4\right)^2} \delta x \ , \tag{3.2}$$

The optical force must be comparable to $m\Omega_m^2 X$, while the linearized optical force must be comparable to $m\Omega_m^2 \delta x$. Since $m\Omega_m^2$ remains finite in $2D$, the coefficient of these optical springs must not vanish. Given the linear nature of the coupling, C3 and C4 are identical constraints which are satisfied when $|\Omega|^2 \geq c_3|gX|^3$ and $\kappa \leq c_4|gX|$, where c_3, c_4 are fixed constants, and we used C2 to achieve this result.

Having established that the force is relevant for the steady state position and

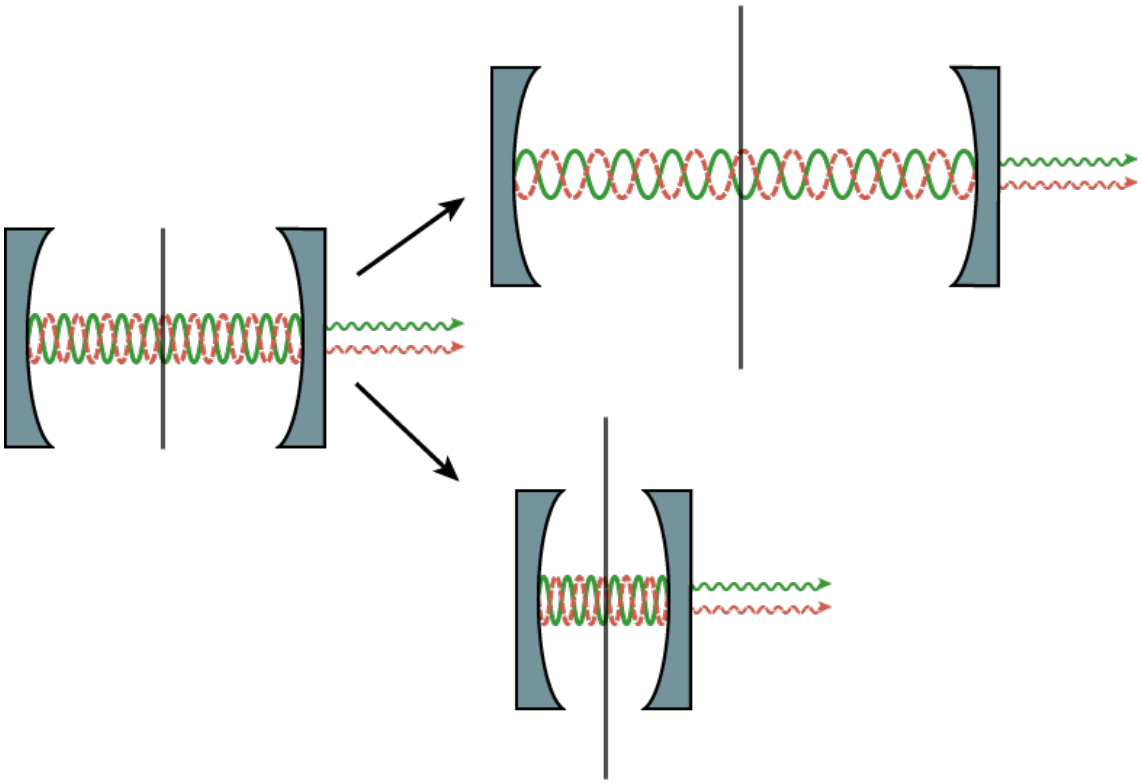

Figure 3.1: Two possible realization of the thermodynamic limit for the membrane-in-the-middle system. In the upper figure, we imagine the cavity growing with the membrane, while the finesse decreases to ensure κ stays large. In the lower figure, we consider shrinking the cavity, which meets our constraints so long as the finesse does not increase more quickly than the cavity shrinks. In each case, the power required to satisfy the other constraints grows.

its fluctuations, we can consider dissipative effects. The damping and noise will be carried into the mechanical equations from $\tilde{a}$. These terms must vanish if we are to achieve the desired single temperature bath (C5-C6). The damping is:

$$\gamma^{opt} = -\frac{4\hbar g^2|\Omega|^2\Delta\kappa}{m\left((\Delta^2+\frac{\kappa^2}{4})^2+2g^2X^2(\frac{\kappa^2}{4}-\Delta^2)+g^4X^4\right)^3}\times \left(5g^6X^6+g^4X^4(5\Delta^2+\frac{9\kappa^2}{4})+3g^2X^2(\frac{\kappa^4}{16}-\frac{1}{2}\Delta^2\kappa^2-3\Delta^4)-(\Delta^2+\frac{\kappa^2}{4})^3\right) , \tag{3.3}$$

which, following C1-C4, scales at most as $\frac{\Omega_m^2}{|gX|}$ and thus vanishes as $X\to\infty$, satisfying C5.

Finally, we consider the optically induced noise (C6). These noise terms have the form:

$$b_i^{in} = \frac{\hbar g|\Omega|\sqrt{\kappa}a_i^{in}}{\left((\Delta\pm gX)+\frac{i\kappa}{2}\right)^2} , \tag{3.4}$$

where b_i^{in} is the noise term in $\dot{p}$ and $i=1,2$ determines the sign of the gx.

These terms should be considered in relation to the mechanical noise, i.e., we should compute $\frac{\langle b^{in\dagger}b^{in}\rangle}{\langle p^{in\dagger}p^{in}\rangle}$ where p^{in} is the noise from the mechanical bath. Assuming the mechanics have an ohmic bath, this ratio is:

$$\frac{\langle b^{in\dagger}b^{in}\rangle}{\langle p^{in\dagger}p^{in}\rangle} = \frac{\hbar^2g^2|\Omega|^2\kappa}{\left((\Delta\pm gX)^2+\frac{\kappa^2}{4}\right)^2}\frac{1}{2m\gamma k_bT} , \tag{3.5}$$

where the plus (minus) corresponds to $b_{1(2)}$.

Following the scaling from above, this term is proportional to $\frac{\hbar\Omega_m^2\kappa}{2gX\gamma k_bT}=\frac{Q_{\rm mq}\kappa}{gX}$, where $Q_{\rm mq}=\frac{\hbar\Omega_m^2}{\gamma k_bT}$ is the quantum Q for the oscillator. From above, we need

$\kappa \leq c_4|gX|$ but we also need to consider how Q_{mq} behaves in the thermodynamic limit. From the scaling of X, we have $Q_{\mathrm{mq}} \propto \frac{1}{V^{2\alpha}\gamma}$ which vanishes so long as $\gamma > c_5 V^{-2\alpha}$, i.e., if the mechanical noise stays finite, it will overwhelm the optically induced noise and form the dominant noise contribution.

With this final constraint in place, we have demonstrated that our optomechanical system has a well defined potential with only relevant coupling to a single bath in the thermodynamic limit, which can be described by equilibrium statistical mechanics.

3.2 Mulitmode generalization of $\mathbb{Z}_2$ membrane buckling

We generalize this analysis to include many mechanical modes, such as those present in a membrane, each coupled to the optics in the same fashion (though, potentially with different values of g). We compute the partition function for these membrane modes and the optically induced potential. We will consider a membrane with the displacement field $u(r,t)$, a mass density ρ, and a Young's modulus, Y. As an order parameter, we identify $O(t) = \int \mathrm{d}^2x g(r)u(r,t)$, which appears in the optical potential, $V(O)$. We can write the classical membrane Hamiltonian and the full partition function including the optical potential:

$$H = \int \mathrm{d}^2 r \left[\frac{\pi(\vec{r},t)^2}{2\rho} + Y\left(\partial_\mu u(\vec{r},t)\right)^2 + f(r,t)u(r,t) \right] , \tag{3.6}$$

$$Z = \int \mathcal{D}u\mathcal{D}\pi \mathrm{d}O\mathrm{d}\lambda e^{-\beta(H[u,\pi]+V(O))} e^{i\lambda(O-\int \mathrm{d}^d r g(r)u(r,t))} , \tag{3.7}$$

where $f(r,t)$ is an external force that might break the symmetry, and we have added the order parameter, O, in as an auxiliary field.

After transforming to Fourier space and integrating out the membrane momentum, π, displacement, u, and λ, we can rewrite the partition function (up to normalization factors) purely in terms of the order parameter O:

$$Z' = \int \mathrm{d}O \exp\left(-\beta\left(\frac{1}{2}\left(\sum_{\vec{k}} \frac{g_{-k}^2}{\Omega_{m_k}^2}\right)^{-1}\left(O - \sum_k \frac{g_k f_k}{\Omega_{m_k}^2}\right)^2 + V(O)\right)\right) , \quad (3.8)$$

where g_k, f_k are the Fourier components of the optomechanical coupling and external forces respectively. From Eqn. 3.8, we can compute the integral and compute the free energy, F:

$$F = -\frac{1}{\beta}\log Z' . \quad (3.9)$$

Since O grows with system size (and the potential along with it), only the minima of the effective potential will have finite energy in the thermodynamic limit. These correspond to the usual saddle points in steepest descent approximations.

3.3 Characterization of the buckling phase transition

The locations of the minima of F change non-analytically as a function of laser power, resulting in a phase transition in the steady state of the coupled mode. Intriguingly, the order and onset of the phase transition are strongly dependent on the detuning of the optical modes from the cavity. To see this behavior, we study the values of the order parameter O which give zero "force". Renaming the effective "spring constant," $k = \left(\sum_{\vec{k}} \frac{g_{-k}^2}{\Omega_{m_k}^2}\right)^{-1}$, we compute the zero force condition:

$$0 = kO\left(1 - \frac{A}{O^4 + 2O^2(\frac{\kappa^2}{4} - \Delta^2) + (\Delta^2 + \frac{\kappa^2}{4})}\right) , \quad (3.10)$$

where we define $A = \frac{-4\hbar|\Omega|^2\Delta}{k}$, where Ω is the coupling to the laser drive. This quantity is positive since we are considering red-detuning ($\Delta < 0$) and is proportional to the input laser power. We also note that the second term has even parity, so solutions with $O \neq 0$ will appear in pairs, providing the $\mathbb{Z}_2$ symmetry of the steady state solutions anticipated.

The general solution for the non-trivial phase ($O \neq 0$) is

$$O^2 = \Delta^2 - \frac{\kappa^2}{4} \pm \sqrt{A - \Delta^2\kappa^2} \ . \tag{3.11}$$

For the solution to be valid, the right hand side needs to be real and positive. Enforcing realness, $A > \Delta^2\kappa^2$. Recalling that A is proportional to laser power, this constraint gives the minimum laser power for a transition to occur. To ensure positivity, we have to consider two cases, $|\Delta| < \frac{\kappa}{2}$ and $|\Delta| > \frac{\kappa}{2}$. In the first case, the square root term must be larger than the first two terms, so only the positive root can be a solution. For that to be the case, we need

$$\begin{aligned} A - \Delta^2\kappa^2 &> \left(\frac{\kappa^2}{4} - \Delta^2\right)^2 \ , \\ A &> \left(\frac{\kappa^2}{4} - \Delta^2\right)^2 + \Delta^2\kappa^2 \ , \\ A &> \left(\frac{\kappa^2}{4} + \Delta^2\right)^2 \ . \end{aligned} \tag{3.12}$$

When this equation is satisfied, there is only one solution for O^2. This case corresponds to a double well potential where the wells split from $O = 0$ as power is increased. The $O = 0$ solution becomes unstable and represents the peak of the barrier between the two wells at $O = \pm O_s$. However, in the case where $|\Delta| > \frac{\kappa}{2}$, once $A > \Delta^2\kappa^2$, a triple well develops with minima at $O = 0, \pm O_{s+}$, where O_{s+} is

the larger solution. We will show below that the smaller solution, O_{s-}, is unstable and forms the peaks of the barriers.

To study the stability of the solutions, necessary for the steepest descent approximation, we determine the local curvature of the potential at each of these critical points by computing the second derivative of the potential, $\partial_O^2 V(O)$. Defining $u = O^2$ and $D(u) = u^2 + 2u(\frac{\kappa^2}{4} - \Delta^2) + (\Delta^2 + \frac{\kappa^2}{4})$ for convenience,

$$\partial_O^2 V(O) = k\left[1 - \frac{A}{D(u)}\right] + \frac{kOA}{D(u)^2} D'(u) 2O \ . \tag{3.13}$$

The $O_s = 0$ solution is stable but decreasingly so until $\frac{A}{D(0)} = 1$ (which is the power at which as the $|\Delta| < \frac{\kappa}{2}$ case buckles) and the solution becomes unstable.

In the buckled state, we see the mechanical spring constant drops out immediately and the curvature is controlled by the optical response. The sign of the curvature is determined by $D'(O_{s\pm}^2) = \pm 2\sqrt{A - \Delta^2\kappa^2}$. Therefore, when $|\Delta| > \frac{\kappa}{2}$, the smaller solutions are unstable, leading to a first order phase transition, while the outer solutions and the solutions for $|\Delta| < \frac{\kappa}{2}$ are stable with a new, optically determined, spring constant. Thus, as a function of laser power, the steady state of the membrane will either experience a 1st or 2nd order phase transitions which spontaneously breaks the $\mathbb{Z}_2$ symmetry of the potential.

3.4 Conclusion

Exploring the thermodynamic limit defined in Chapter 2, we define an optomechanical membrane-in-the-middle system which possesses a phase transition of either 1st or 2nd order, controlled by the system parameters. Specifically, our theory

supports the experimental observation of spontaneous $\mathbb{Z}_2$ symmetry breaking corresponding to the buckling of the mechanical spring [42]. This experimental result is included as Appendix B.

We also find, more generally, that optomechanical systems which do not have conservative dynamics are generic, and are not well understood in our thermodynamic limit. Analysis of these systems may point to topological physics and connect with other related optomechanical systems, such as those with exceptional points [63]. While experimental efforts have included the ability to cool the mechanical system to its ground state [64], determining whether our framework for phase transitions persists at the quantum level will require further analysis to handle the effects of quantum fluctuations. However, the possibility of observing quantum phase transitions which spontaneously break symmetry remain quite compelling and will drive future theoretical work.

Chapter 4: $U(1)$ and $SO(N)$ spontaneous symmetry breaking in optomechanical systems

4.1 Introduction

Spontaneous symmetry breaking is a fascinating phenomenon where the state of a system takes on a specific value or range of values that are not determined entirely by the equations of motion. Some of the simplest examples occur in realizations of the Dicke phase transition [65–67], where the presence of a small number of bosonic modes can dramatically change the steady state behavior of atoms or mechanical resonators, spontaneously breaking an intrinsic parity symmetry [68, 69]. More complex examples include systems with additional gauge symmetries, and appear to describe superconductivity [70] and the Higgs mechanism [71–73]. The above cases are sometimes close to those provided by nature, but we can also study spontaneous symmetry breaking in optomechanical systems, where recent advances have allowed precise engineering of the mechanical modes [74–76], optical modes [77, 78] and their interaction [79, 80]. Furthermore, the concept is extensible even to open systems, where non-equilibrium mechanics can give rise to thermodynamic steady states described by a Gibbs ensemble, as in Ref. [81]. In that work, we demonstrated

that symmetry-breaking phase transitions can occur in such systems, and provided as an example the $\mathbb{Z}_2$ phase transition, realized in a membrane-in-the-middle cavity optomechanics experiment [42].

Here, inspired by recent experiments with atomic Bose-Einstein condensates [43], we generalize our framework to include systems that will show spontaneous symmetry breaking in more complex ways, involving groups with higher global symmetries, such as $U(1)$ and $SO(N)$. We note that to generate systems with spontaneously broken symmetries, one must begin with equations of motion that respect the symmetry to be broken. This restriction suggests natural systems in which one might imagine realizing such a symmetry. For instance, systems composed of the clockwise and counterclockwise whispering gallery modes of a mechanical resonator, excitations in equivalent optical cavities coupled to a central mode, or left and right circularly polarized light. These cases can typically have a "natural" symmetry which may be spontaneously broken.

We will largely follow the same strategy from Ref. [81]: define an optomechanical system where the optics evolve much more quickly than the mechanics, eliminate the optical modes, and study the steady state properties of the mechanics under the combined optomechanical potential. We defer a consideration of the damping and fluctuations in the thermodynamic limit to Appendix B of this chapter. We will identify cases where for low power, the steady state mechanics are at their mechanical equilibrium, but at high power, the steady state will achieve a new equilibrium where the squared sum of displacement for the modes is fixed, but the relative displacement of any given mode is free. Therefore, while the Hamiltonian, driving,

and loss are invariant under a global transformation (generalized rotation) of these modes, the steady state will have to assume a single value, spontaneously breaking the symmetry. Our suggested experimental approach takes the basic concept of $\mathbb{Z}_2$ breaking and by stacking together several such systems, achieves the higher symmetry $SO(N)$. Another key point of our approach: the "spontaneous" part of the breaking arises from the contact of the system to its bath.

4.2 Symmetries in beam-splitter optomechanics

As our starting point, we consider the Hamiltonian that describes a beamsplitter whose transmittivity depends upon a (mechanical) position variable, as used in Ref. [81]. Consider two optical modes of a cavity, with annihilation operators a_L and a_R, driven by laser detuned equally from the respective cavity resonances. This system can be recast by transforming to a symmetric/anti-symmetric basis for the optical modes, which makes the symmetry breaking manifest. Under such a transformation, we have an optomechanical interaction:

$$H_{\text{int}} = \hbar g a_0^\dagger \left(x a_i\right) + H.c. \ , \tag{4.1}$$

where g is the optomechanical coupling, $a_{0(i)}$ is the symmetric (anti-symmetric) combination of the driven modes, x is the position of the mechanical membrane, and $H.c.$ is the Hermitian conjugate of the first term. This interaction has the property that changes in sign of the x degree of freedom can be compensated by a simultaneous sign change in a_i, showing the (in this case $\mathbb{Z}_2$) symmetry which can be spontaneously broken.

In this form, we assume we only drive the symmetric mode, a_0, and the phase transition corresponds to a population of the a_i mode along with a displacement of the mechanical membrane, where the direction of the displacement and sign of the a_i mode are chosen spontaneously. Inspired by this interaction, we can consider the generalization to multiple optical and mechanical modes:

$$H_{\text{int}} = \hbar g a_0^\dagger \left(\sum_{i=1}^{N} x_i a_i \right) + H.c. \ , \tag{4.2}$$

where i indexes the multiple mechanical and optical modes coupled to the driven a_0 mode. Such a system can no longer be composed of symmetric and anti-symmetric combinations of cavity modes, however, we can construct the above interaction using directionally coupled, optomechanical waveguides [82].

If two waveguides approach each other, the dispersion in each waveguide changes due to evanescent field interactions, potentially strongly, e.g., in "zipper-cavities" [83, 84]. Excitations in such regions are naturally described by symmetric and anti-symmetric combinations of waves in each waveguide. We can view an traveling wave in a single waveguide as a superposition in this basis. The phase which accumulates between the symmetric and anti-symmetric modes over the interaction region depends on the dispersion modification, which depends on the distance between the waveguides [85]. Transforming back to the waveguide basis, the total phase sets the amount of light which transmits from one waveguide into the other. If we allow the waveguides to move, they act as a mechanically dependent beamsplitter. We imagine a system engineered such that the beamsplitters are dark if the mechanical modes are at their equilibrium position. We also imagine that these

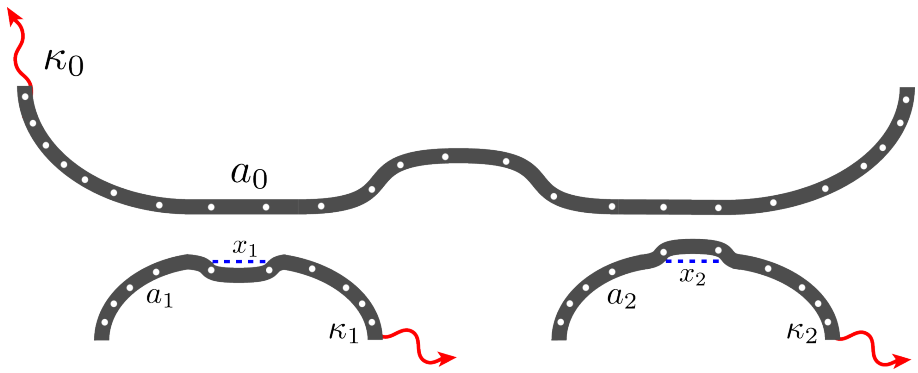

Figure 4.1: A cartoon of a proposed realization with $U(1)$ symmetry. Here the driven mode, a_0 occupies a long photonic nanobeam and is coupled evanescently to two smaller nanobeams with optical modes, a_i. These beams are free to deform and their displacements, x_i, modify the strength of the beamsplitter coupling.

waveguides have reflective boundaries, creating photonic cavities. Thus, we can construct our system by imagining a large, driven, cavity coupled to several other cavities in the manner detailed above and depicted in Fig. 4.1. For a more detailed derivation, see Appendix A of this chapter.

Following our intuition from the $\mathbb{Z}_2$ case, we see that such an interaction is invariant under a simultaneous rotation of the mechanical and optical modes. This global symmetry is described by the group of rotations in N dimensions, $SO(N)$. As we show below, it can be spontaneously broken above a threshold laser power. In the following chapter, we explore the phase transitions of this system. In Appendix B, we define a thermodynamic limit for this system and in Appendix C we provide some analysis of the similar spontaneous symmetry breaking in a cavity BEC system [43].

4.3 Characterizing phases transitions in beam-splitter optomechanics

We show that the above model can realize first- and second-order phase transitions and readily generalizes to higher dimensions. Following our analysis from Ref [81], we calculate the steady state values of the optics and determine the dynamics of the mechanical modes under the influence of the optical steady state. We can write down the full system Hamiltonian (in units of the mechanical harmonic oscillator length, $\ell_{\text{H.O.}} = 1$, and $\hbar = 1$):

$$H = -\Delta_0 a_0^\dagger a_0 + \Omega(a_0 + a_0^\dagger) + \sum_{i=1,2} \frac{\omega}{2}(p_i^2 + x_i^2) - \sum_{i=1,2} \Delta_i a_i^\dagger a_i - \sum_{i=1,2} g x_i (a_0^\dagger a_i + a_i^\dagger a_0), \tag{4.3}$$

where ω is the mechanical frequency, Ω is the external drive, Δ_0, Δ_i are the detunings for the respective optical modes, and we have transformed to a frame rotating with the drive laser.

We add fluctuations and dissipative terms in the equations of motion to account for the open nature of the cavities and dissipation on the mechanical modes. We also restrict ourselves to the symmetric case, where the detuning, decay, and damping rates are equal for the non-driven cavities. This leads to the following

Heisenberg-Langevin equations:

$$\dot{a}_0 = i(\Delta_0 + \frac{i\kappa_0}{2})a_0 + i\sum_{i=1,2} g x_i a_i + i\Omega + \sqrt{\kappa_0}a_0^{in} \ , \tag{4.4}$$

$$\dot{a}_i = i(\Delta_1 + \frac{i\kappa_1}{2})a_i + igx_i a_0 + \sqrt{\kappa_1}a_i^{in} \ , \tag{4.5}$$

$$\dot{x}_i = \omega p_i \ , \tag{4.6}$$

$$\dot{p}_i = -\omega x_i + g(a_0^\dagger a_i + a_i^\dagger a_0) - \gamma p_i + \sqrt{\gamma}p_i^{in} \ , \tag{4.7}$$

where $\kappa_{0,1}, \gamma$ are the damping terms for their respective modes and $a_{0,i}^{in}$, p_i^{in} are fluctuations.

In the limit that the optics are much faster than the mechanical modes, we expand the variables ($a \to A + \delta a, x \to X + \delta x$), around their steady state, assuming that the fluctuations will be proportional to the noise. We can find the steady state for the noiseless variables via solving the resulting matrix equation. With the steady state values for the optical modes, we can determine the force on the mechanical modes:

$$F_i^{opt} = -\frac{2g^2 X_i \Delta_1 |\Omega|^2}{(\Delta_0^2 + \frac{\kappa_0^2}{4})(\Delta_1^2 + \frac{\kappa_1^2}{4}) - 2g^2(X_1^2 + X_2^2)(\Delta_0\Delta_1 - \frac{\kappa_0\kappa_1}{4}) + g^4(X_1^2 + X_2^2)^2}. \tag{4.8}$$

This force has a vanishing curl and thus supports static, steady-state solutions for the mechanics. We also note the force respects the symmetry of the Hamiltonian, namely, it depends on the effective radial coordinate, $R^2 = X_1^2 + X_2^2$ and points in the radial direction. We can integrate the force in the radial direction to see what

addition it makes to the total mechanical potential:

$$V^{\text{opt}}(R) = \frac{2\Delta_1|\Omega|^2 \arctan\left(\frac{\frac{\kappa_0\kappa_1}{2} - 2\Delta_0\Delta_1 + 2g^2R^2}{\Delta_1\kappa_0 + \Delta_0\kappa_1}\right)}{(\Delta_1\kappa_0 + \Delta_0\kappa_1)}. \tag{4.9}$$

For red (negative) detunings, the argument of the arctan is negative but the prefactor is positive, giving the correct form to allow for a symmetry breaking transition. That is, when $|\Omega|^2$ is large enough, the minima of the combined optical and mechanical potential will not be at $R = 0$. Example cases of the radial potential at different driving strengths are displayed in Fig. 4.2. Above the threshold power, the radius will go to a fixed value, but the angle of the vector, i.e. the relative excitation of the modes, will be unconstrained, as shown in Fig. 4.3. This free angle results from the broken $SO(2)$ or $U(1)$ symmetry.

Since the angle is unconstrained, there is a zero energy mode which takes one steady state to another one with an infinitesimally different angle. We also note here that the nature of the potential is very similar to the potential in Refs. [42, 81] which means that the order of the phase transition will depend on the relative size of the detunings and the decay rates. For $\Delta_0\Delta_1 - \frac{\kappa_0\kappa_1}{4} > 0$, the system will have a first-order transition, with the metastable potential shown in Fig. 4.2 B., otherwise the transition will be second-order.

4.4 Extending to $SO(N)$ symmetries

This system easily generalizes to higher dimensions. By adding pairs of optical and mechanical modes, while maintaining the same type of interaction and constraints on the frequencies involved (i.e. the mechanics must be much slower

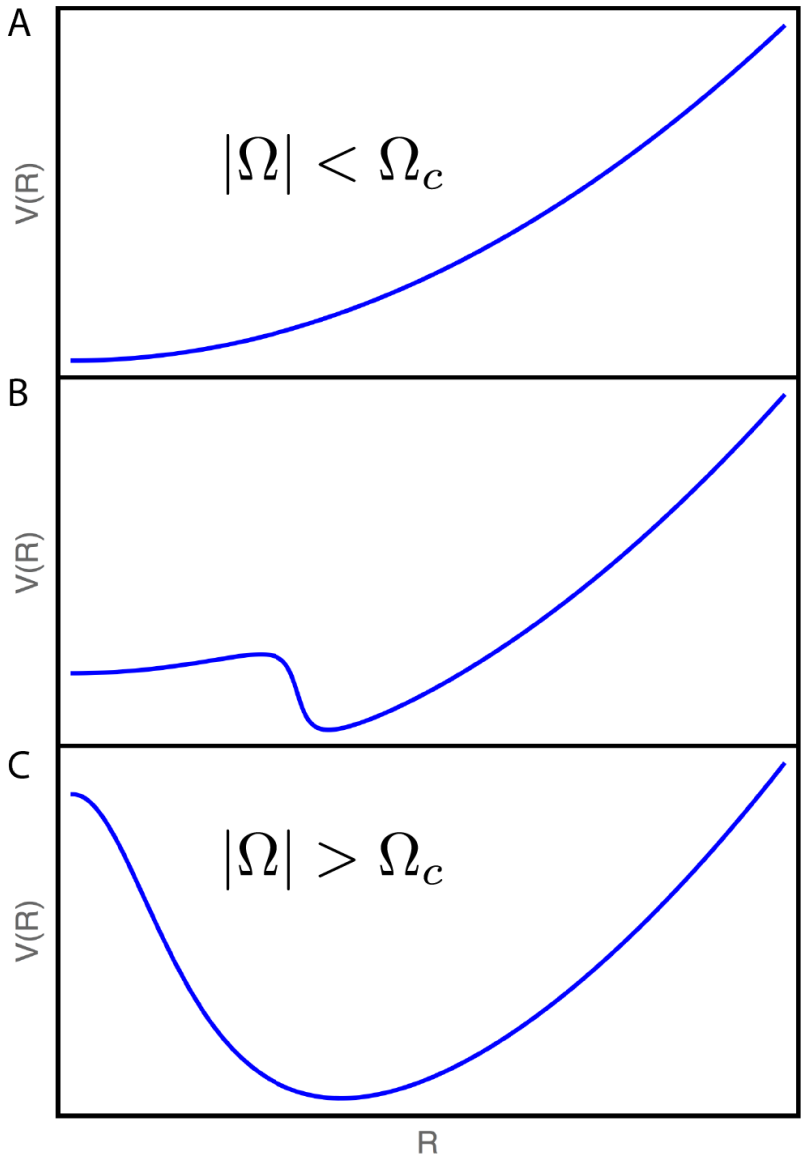

Figure 4.2: Examples of the combined mechanical and optical potential in the radial direction. A. At low power, the mechanical potential dominates and leads to $R = 0$. B. At higher powers, a minimum at $R \neq 0$ develops. If the detunings are large (see order analysis in main text), $R = 0$ becomes metastable at intermediate powers. C. At high powers, the optical effects overwhelm the mechanical effects and there is only one minimum, located at $R \neq 0$. In the case without metastability, this minimum develops at $R = 0$ and smoothly moves outward as power increases.

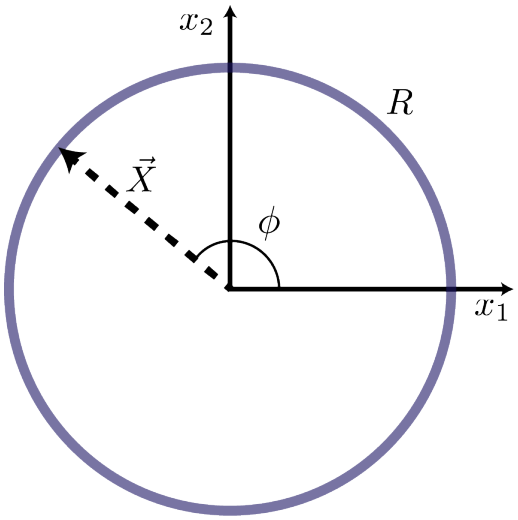

Figure 4.3: A representation for a specific steady state of the $U(1)$ system. Above a critical laser power, the steady state squared sum of oscillator positions ($R^2 = X_1^2 + X_2^2$) will be a fixed, non-zero value (represented by the circle), but the relative oscillator positions are unconstrained, represented by the angle ϕ.

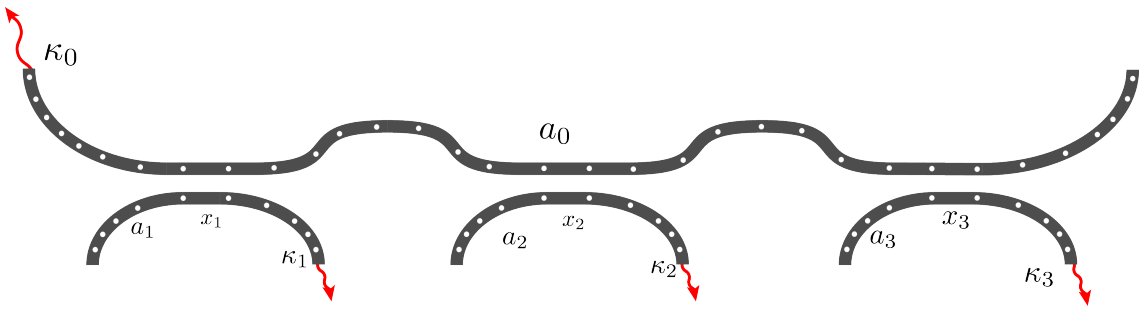

Figure 4.4: We can construct higher dimensional systems by adding more optomechanical, photonic cavities. While we denote each cavity decay rate, we take $\kappa_1 = \kappa_2 = \kappa_3$.

than relevant optical time scales), we enlarge the space and, in turn, allow for higher symmetries to be broken. We imagine experimentally realizing this by extending the driven photonic cavity and adding additional coupled cavities, as seen in Fig. 4.4. As we noted before, the interaction is invariant under rotations. Strictly speaking, we have two vectors, one optical and one mechanical. The nature of the interaction and our adiabatic elimination means that the optical "vector" is always parallel to the mechanical one, leaving the symmetry for rotations of a single vector, as opposed to two. To see this, consider the optical equations of motion in Cartesian coordinates:

$$\dot{a}_0 = i(\Delta_0 + \frac{i\kappa_0}{2})a_0 + i\sum_{i=1,2,3} g x_i a_i + i\Omega + \sqrt{\kappa_0}a_0^{in} \ , \tag{4.10}$$

$$\dot{a}_i = i(\Delta_i + \frac{i\kappa_1}{2})a_i + igx_i a_0 + \sqrt{\kappa_1}a_i^{in}, \tag{4.11}$$

We can solve the steady state for the a_0 mode and substitute it into the a_i equation:

$$\dot{a}_i = i(\Delta_i + \frac{i\kappa_1}{2})a_i + \frac{igx_i}{\Delta_0 + \frac{i\kappa_0}{2}} \left(gx_j a_j + \Omega - i\sqrt{\kappa_0} a_0^{in} \right) \ . \tag{4.12}$$

The steady state equation for a_i can now be recast as a matrix equation, $M_{ij}a_j + v_i = 0$ where $M_{ij} = (\Delta_i + \frac{i\kappa_1}{2})\delta_{ij} + \frac{1}{(\Delta_0 + \frac{i\kappa_0}{2})} g^2 x_i x_j$, $v_i = Cx_i$, and $C = \frac{\Omega - i\sqrt{\kappa_0}a_0^{in}}{(\Delta_0 + \frac{i\kappa_0}{2})}$ is a constant. Evidently, x_i is an eigenvector of M_{ij}, thus also an eigenvector of M_{ij}^{-1}. Therefore, when we solve for $a_i = -C(M_{ij})^{-1}x_j$, we find that a_i is always parallel to x_i. This fact results in a force that is always purely radial, preserving the curl-free condition and rotational symmetry of the mechanical system for arbitrary dimensions.

For 2 dimensions, when the system has a finite value for the "radial" coordinate, the spontaneous choice of an angle breaks the $U(1)$ symmetry. If we consider an additional optical and mechanical mode, then the relevant broken symmetry is $SO(3)$. Continuing to add pairs of optical and mechanical modes, generic $SO(N)$ symmetry breaking is possible.

To be explicit, we can write down the Hamiltonian for an $SO(3)$ system:

$$\begin{aligned} H = &-\Delta_0 a_0^\dagger a_0 + \Omega_0(a_0 + a_0^\dagger) + \sum_{i=1,2,3} \frac{\omega}{2}(p_i^2 + x_i^2) \\ &- \sum_{i=1,2,3} \Delta_1 a_i^\dagger a_i - \sum_{i=1,2,3} g x_i (a_0^\dagger a_i + a_i^\dagger a_0) \ , \end{aligned} \tag{4.13}$$

where again Δ_0, Δ_1 are the detunings for the respective optical modes (assuming the undriven modes are degenerate) in the frame co-rotating with the drive laser. We can derive the equations of motion for this system and study the steady state

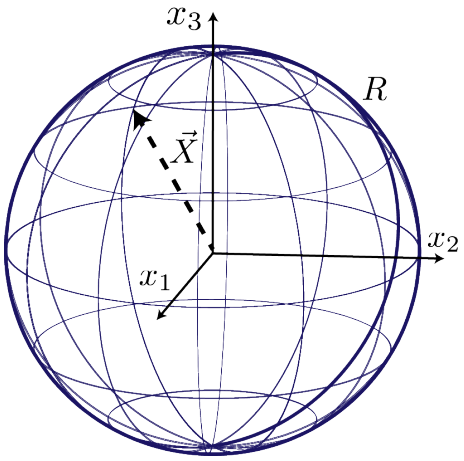

Figure 4.5: A representation for a specific steady state of the $SO(3)$ system. Above a critical laser power, the sum of squared amplitudes of the oscillators ($R^2 = X_1^2 + X_2^2 + X_3^2$) will be a fixed, non-zero value, represented by the wireframe sphere. The ratios of their excitations relative to each other, i.e., the angles of the vector, however, are unconstrained.

solutions. Again, the curl-free condition means that steady state solutions will have no angular momentum. This leaves only the radial degree of freedom, which will have an identical optical potential:

$$V^{\text{opt}}(r) = \frac{2\Delta_1|\Omega|^2 \arctan\left(\frac{\frac{\kappa_0\kappa_1}{2} - 2\Delta_0\Delta_1 + 2g^2r^2}{\Delta_1\kappa_0 + \Delta_0\kappa_1}\right)}{(\Delta_1\kappa_0 + \Delta_0\kappa_1)} \,. \tag{4.14}$$

It similarly has first- or second-order transitions as the optical potential contends with the mechanical spring. Above these transitions, the steady state value of the radius will be fixed, but now two angular variables will be unconstrained, as shown in Fig. 4.5.

4.5 Conclusion

We have generalized the notion of spontaneous symmetry breaking phase transitions to open systems which allow for an adiabatic elimination of "fast" modes. We consider optomechanical systems with interactions possessing a natural symmetry. Following Ref. [81], we adiabatically eliminate the optical modes and focus only on the dynamics of the mechanics. In particular, we propose a photonic nano-beam system which enables first- and second-order transitions that spontaneously break $SO(N)$ symmetry. These systems reduce to the system considered in Ref. [81], and must follow similar constraints to have a thermodynamic limit. We comment on the thermodynamic limit of the nanobeam system and a similar cavity BEC experiment, [43] in the appendices.

While we have primarily focused on realizing systems which spontaneously breaks a global $SO(N)$ symmetry, we can imagine other systems in which the interaction includes polarization and strain degrees of freedom for the optics and mechanics respectively. Additionally, if one were to realize the interaction locally, between the local strain field of a membrane and the electric field at the membrane surface, the interaction would possess a local symmetry. The spontaneous breaking of this local symmetry could allow simulation of phenomena more closely related to high energy or condensed matter physics [70–73]. However, in the optomechanical case, there is a great deal of control over the structure and dispersion of the fields involved.

4.6 Appendix A: Derivation of optomechanical coupling for directional couplers

Here we give a more detailed derivation of the interaction term for our proposed $SO(N)$ system. We consider two waveguides which are in close proximity for a small region. Assuming that the interaction between waveguides is weak, we will use coupled mode theory [85]. That is, we assume that the mode in each waveguide is largely unaltered by the presence of the other waveguide, except for the amplitude, which becomes a function of the propagation direction (defined as z). Explicitly, following the conventions from Ref. [85], we assume the electric field in each waveguide has the form $E_i = a_i(z)u_i(y)e^{-i\beta_i z}$ where $a_i(z)$ is the amplitude, $u_i(y)$ is the transverse mode shape, n_i is the index of refraction for waveguide i, and β_i is the phase accumulated per unit length. We assume the waveguides are width d, separated by a gap of width $2a$, which we allow to vary. This gap has an index of refraction, n.

Following the coupled mode equations from Ref. [85], we arrive at a transmission matrix, T_{ij}, relating the amplitudes at the beginning of the interaction region, $a_i(0)$, to those at the end, $a_i(z_0)$: $a_i(z_0) = T_{ij}a_j(0)$. This transmission matrix is determined by several factors:

$$C_{ij} = \frac{1}{2}\left(n_i^2 - n^2\right)\frac{k_0^2}{\beta_j}\int \mathrm{d}y u_i(y)u_j(y) \ , \tag{4.15}$$

$$\gamma^2 = \frac{(\Delta\beta)^2}{4} + C_{12}C_{21} \ , \tag{4.16}$$

where $\Delta\beta = \beta_1 - \beta_2$ is the difference in phase accumulation per unit length between

the waveguides and k_0 is the free space wavenumber.

As we are concerned with the coupling between modes, e.g., from $a_1(0)$ to $a_2(z_0)$, we focus on the off-diagonal terms. These off-diagonal terms are determined (up to a phase, which we can absorb) by $\frac{C_{ij}}{\gamma}\sin(\gamma z_0)$. Here we consider a phase-matched system. Phase-mismatched systems might also be able to realize this interaction, but we do not focus on them here.

For phase matched systems, the two waveguides are assumed to be identical. In this case, $\Delta\beta = 0$ and $C_{12} = C_{21} = C$, so $\gamma = C$. Additionally, we imagine constructing a coupler such that $Cz_0 = 2\pi m$ where m is an integer. Here we can engineer the coupling by assuming that the waveguides are allowed to move by some displacement x, changing the distance between them. This displacement will modify C:

$$\begin{aligned} C &= \frac{1}{2}\left(n_1^2 - n^2\right)\frac{k_0^2}{\beta_1}\int_a^{a+d} \mathrm{d}y u_1(y)u_2(y+x) \ , \\ &\approx \frac{1}{2}\left(n_1^2 - n^2\right)\frac{k_0^2}{\beta_1}\int_a^{a+d} \mathrm{d}y u_1(y)u_2(y) + x\frac{1}{2}\left(n_1^2 - n^2\right)\frac{k_0^2}{\beta_1}\int_a^{a+d} \mathrm{d}y u_1(y)u_2'(y) \ , \\ &\approx C_0 + C'x \ , \end{aligned} \tag{4.17}$$

where $u_2'(y)$ is the derivative of u with respect to y and we have renamed the integral C'. Since the unperturbed modes are identical but reflected, $u_1(y) = u_2(-y)$, we have a symmetric coupling.

In this case, we can expand the off-diagonal couping, $\sin\left(C_0 z_0 + C'xz_0\right) \approx C'xz_0$. This expansion results in the x-dependent beam-splitter interaction we require.

4.7 Appendix B: Thermodynamics of the beamsplitter model

While we have focused on the transition and spontaneous symmetry breaking in the finite size systems, we can also establish the existence of a thermodynamic phase transition as defined in Ref. [81] for the beamsplitter case. We demand that the curl must vanish (C1), the system must remain stable (C2), the optical and mechanical forces should be comparable in the steady state and linearized regime (C3-C4), and that the optically induced noise and damping must vanish (C5-C6). These restrictions define constraints that system parameters need to follow as the system grows macroscopic. We imagine the size of the optomechanical beams, $V \to \infty$ is growing large in our thermodynamic limit.

As we have seen in the main text, the optical force has a vanishing curl from the nature of the interaction, which automatically satisfies our constraint C1. To study the other constraints, we redefine our coordinates in a polar system and rotate our optical modes ($a_i \to a_{r,\phi}$). This is a decomposition of the optical modes into radial and angular excitations coincident with the steady state coordinates of the mechanics, which can be realized with rotation matrix R:

$$R = \begin{pmatrix} 1 & 0 & 0 \\ 0 & \cos\phi & \sin\phi \\ 0 & -\sin\phi & \cos\phi \end{pmatrix} . \tag{4.18}$$

We will include the $-i\dot{R}R^{\dagger}$ term to account for the potential of this frame being non-inertial. However, we know from the Cartesian version that the force has no curl, thus steady state solutions will have zero angular momentum, meaning the

frame is inertial. The system can spontaneously break the symmetry by choosing an angle (or the relative size of excitations in the mechanical modes) but this angle is fixed once chosen. With this transformation the Hamiltonian becomes:

$$H = -\Delta_0 a_0^\dagger a_0 + \Omega_0(a_0 + a_0^\dagger) + \frac{\omega}{2}(p_r^2 + \frac{l^2}{r^2} + r^2) \\ - \Delta a_r^\dagger a_r - gr(a_0^\dagger a_r + a_r^\dagger a_0) - \Delta a_\phi^\dagger a_\phi - i\frac{\omega l}{r^2}(a_r^\dagger a_\phi - a_\phi^\dagger a_r) \ , \tag{4.19}$$

Adding fluctuations and dissipation, we can write the equations of motion:

$$\dot{a}_0 = i(\Delta_0 + \frac{i\kappa_0}{2})a_0 + igra_r + i\Omega + \sqrt{\kappa_0}a_0^{in} \ , \tag{4.20}$$

$$\dot{a}_r = i(\Delta_1 + \frac{i\kappa_r}{2})a_r + igra_0 + \sqrt{\kappa_r}a_r^{in} - \frac{\omega l}{r^2}a_\phi \ , \tag{4.21}$$

$$\dot{a}_\phi = i(\Delta_1 + \frac{i\kappa_\phi}{2})a_\phi + \sqrt{\kappa_\phi}a_\phi^{in} - \frac{\omega l}{r^2}a_r \ , \tag{4.22}$$

$$\dot{r} = \omega_r p_r \ , \tag{4.23}$$

$$\dot{p}_r = -\omega r + \frac{\omega l^2}{r^3} + g(a_0^\dagger a_r + a_r^\dagger a_0) - \gamma p_r + \sqrt{\gamma_i}p_i^{in} - \frac{2i\omega l}{r^3}(a_r^\dagger a_\phi - a_\phi^\dagger a_r) \ , \tag{4.24}$$

$$\dot{\phi} = \frac{\omega l}{r^2} - \frac{i\omega}{r^2}(a_r^\dagger a_\phi - a_\phi^\dagger a_r) \ , \tag{4.25}$$

$$\dot{l} = -\frac{\gamma l}{r} + \sqrt{\gamma'}l^{in} \ , \tag{4.26}$$

we note that the equations for a_0, a_r are identical to the transformed equations from [81]. Of course, there is an extra mode a_ϕ which is coupled by l. We can solve for the steady state of these modes and find that, due to the curl-free condition, $L = 0$. Therefore, we now have exactly the transformed equations from Ref. [81] and thus can employ identical constraints to define our thermodynamic limit.

The constraints are unmodified, we simply demand that each mode satisfy them, e.g., $\Delta_0, \Delta_1 \propto -gR$, C2. The other constraints are straightforward, $|\Omega|^2 \geq c_3|gR|^3, \kappa_{0,1} \leq c_4 gR, \gamma > c_5 V^{-2\alpha}$. Therefore, we have identified a thermodynamic

limit in which the mechanical modes experience a modified potential, but thermalize to a single mechanical bath. As the angular optical mode does not contribute to dynamics, it needs no additional constraints. However, the addition of noise does affect the mechanical "angle," which is free to move through all values. Including the effects of noise, there will be a random force in the angular direction; ϕ will experience a Brownian motion-like trajectory, exploring the full space as a function of time.

The generalization to $SO(3)$ or generically $SO(N)$ will also follow the same procedure. A rotation into the proper (hyper-)spherical coordinates will show the system is simply two optical modes coupled by a radial excitation and other modes coupled by the angular momentum of the mechanical system. As these generalization also have no curl, the angular modes decouple completely and produce the same constraints as above on the coupled modes.

4.8 Appendix C: $U(1)$ symmetry breaking in an atomic optomechanical system

Transitions which spontaneously break the group $U(1)$ have been recently observed experimentally with a Bose-Einstein condenstate (BEC) in a cavity system [43]. This system served as an inspiration for our generalization. In this appendix, we analyze this experimental system and comment on the possibility of a thermodynamic limit. Here, we define our thermodynamic limit with the number of atoms N going to infinity.

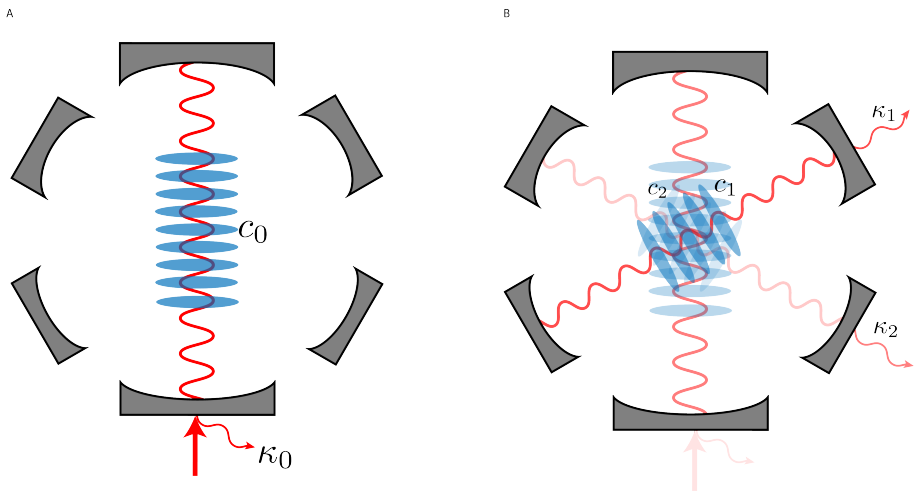

Figure 4.6: A cartoon of the cavity BEC system from Refs. [43, 86]. A. In the symmetric phase, there are no photons in either of the crossed cavities and the atoms occupy a 1D optical lattice generated by the driven central cavity. B. Past the critical point, photons scatter from the central cavity to the crossed cavities, simultaneously kicking atoms into the crossed lattices. Here we show a realization where cavity 1 has a higher occupation than cavity 2.

In the experiment, a BEC is trapped in the space where 3 optical cavities cross, as shown in Fig. 4.6A. The central cavity is driven externally with a laser, creating an optical lattice which the atoms occupy in the symmetric phase. However, through Raman processes, central cavity photons can scatter off of the atoms, populating one of the crossed cavities and simultaneously exciting the atoms into the generated lattice of the crossed cavity. When the external drive, λ, is large enough, these excitations become favorable, and atoms and light will populate the modes of the crossed cavities, depicted in Fig. 4.6B. However, the relative occupation of one crossed cavity to the other is undetermined, creating an "angular" degree of freedom

characteristic of a spontaneously broken $U(1)$ symmetry, which has been probed in Ref. [86]. We recast this experiment within our framework, adding in mechanical dissipation [81].

We will begin with the reduced Hamiltonian in Ref. [86], where we consider the coupling between photonic excitations (a_1, a_2) in two crossed optical cavities and the mechanical excitations (c_1, c_2) of a BEC into the lattices generated by these photons. We will assume that the driven cavity immediately takes its steady state value and ignore the effects of pump depletion as these are small compared to typical driving strengths and to the depletion of the central BEC mode, c_0. Finally, we transform to a frame that is rotating with the driving laser frequency. Therefore, we are left with a Hamiltonian describing two optical modes and two mechanical modes where the coupling between them is controlled by the laser power, λ, and the central BEC mode, c_0.

$$\begin{aligned} H &= \sum_{i=1,2} -\hbar\Delta_i a_i^\dagger a_i + \hbar\omega c_i^\dagger c_i + \frac{\hbar\lambda}{\sqrt{N}}\left(a_i^\dagger + a_i\right)\left(c_i^\dagger c_0 + c_0^\dagger c_i\right) \ , \\ &= \sum_{i=1,2} -\hbar\Delta_i a_i^\dagger a_i + \hbar\omega c_i^\dagger c_i + \frac{\hbar\lambda c_0}{\sqrt{N}}\left(a_i^\dagger + a_i\right)\left(c_i^\dagger + c_i\right) \ , \end{aligned} \tag{4.27}$$

where N is the total number of atoms, $c_0 = \sqrt{N - \sum_{i=1,2} c_i^\dagger c_i}$ represents the BEC occupation in the lattice of the central mode, which is constrained by the fixed number of atoms in the system, ω is the energy of the crossed lattices, which is set by the optical frequency, and $\Delta_i = \omega_p - \omega_{c_i}$ is the detuning of the cavity from the pump laser. $\lambda = -\frac{g\Omega_p\sqrt{N}}{2\sqrt{2}\Delta_a}$ is the coupling where g is the vacuum Rabi frequency, Δ_a is the detuning of the pump mode from the atomic resonance, and Ω_p is proportional

to pump power. We will consider the case were the cavities 1, 2 are identical and therefore drop the subscript on cavity parameters, such as Δ. Here we note that experimental frequencies for the optical modes are much larger than the mechanical modes, $\Delta,\ \kappa \sim 2\pi \times (100 - 1000)$ kHz while $\omega \sim 2\pi \times 4$ kHz [43]. This separation of time scales motivates our assumption that the optics will immediately equilibrate to their steady state values, with respect to the motion of the mechanical modes.

While the membrane-in-the-middle system relied on depletion of the driven optical modes to create the necessary nonlinearities [42, 81], here the finite number of atoms imposes a constraint on c_0 which plays this crucial role. However, we still control the transition with the strength of the external laser drive, λ. Having written the Hamiltonian, we can now derive Heisenberg-Langevin equations of motion:

$$\dot{a}_i = i\left(\Delta + \frac{i\kappa}{2}\right) a_i - \frac{i\lambda c_0}{\sqrt{N}}\left(c_i^\dagger + c_i\right) + \sqrt{\kappa} a_i^{in} \ , \tag{4.28}$$

$$\dot{c}_i = -i\omega c_i - \frac{i\lambda c_0}{\sqrt{N}}\left(a_i^\dagger + a_i\right) - \frac{\gamma}{2} c_i + \sqrt{\gamma} c_i^{in} \ , \tag{4.29}$$

where $\kappa, (\gamma),\ a_i^{in}, (c_i^{in})$ are the optical (mechanical) cavity loss and noise, respectively. From Eqn. 4.29, we find that force is curl-free, satisfying C1. Following Ref. [81], we will make an expansion of these variables, e.g., $a_i = A_i + \delta a_i$, where δ variables are proportional to the noise in the system. Then, we can find the steady state solution for the optics and find the imposed dynamics of the mechanical modes:

$$\dot{A}_i = i\left(\Delta + \frac{i\kappa}{2}\right) A_i - \frac{i\lambda\sqrt{(N - C_1^2 - C_2^2)}}{\sqrt{N}}\left(C_i^\dagger + C_i\right) \ , \tag{4.30}$$

$$A_i = \frac{\lambda\sqrt{(N - C_1^2 - C_2^2)}(C_i^\dagger + C_i)}{\sqrt{N}\left(\Delta + \frac{i\kappa}{2}\right)} \ , \tag{4.31}$$

$$\dot{C}_i = -i\left(\omega - \frac{i\gamma}{2}\right) C_i - \frac{i\lambda\sqrt{(N - C_1^2 - C_2^2)}}{\sqrt{N}}\left(A_i^\dagger + A_i\right) \ , \tag{4.32}$$

where we have substituted $C_0 = \sqrt{(N - C_1^2 - C_2^2)}$ to make the nonlinearity explicit. These equations are more manageable in their real and imaginary parts, substituting $C_i = \frac{1}{\sqrt{2}}(X_i + iP_i)$, one can solve for P_i in terms of X_i and find an effective force in terms of X_i. Further, to move to coordinates which makes the symmetry breaking apparent, we define R, ϕ, such that $X_1 = R\cos(\phi)$ and $X_2 = R\sin(\phi)$. In this transformed frame, ϕ vanishes from the equations of motion. This angle will be spontaneously selected when the system moves to the symmetry broken phase. We can integrate the effective force to find a "radial" potential, $V(R) = \frac{\hbar\omega}{2}\left(1 + \frac{\gamma^2}{\omega^2} + \frac{8\lambda^2\Delta}{\omega\left(\Delta^2 + \frac{\kappa^2}{4}\right)}\right) R^2 - \frac{2\hbar\lambda^2\Delta\left(\omega^2+\gamma^2\right)}{N\left(\Delta^2+\frac{\kappa^2}{4}\right)\omega^2} R^4$. Our demand that the cavity detuning is red ($\Delta < 0$), which satisfies C2, guarantees the stability of the system by ensuring a confining quartic potential.

The controlling parameter, $\lambda = \frac{g\Omega_p\sqrt{N}}{2\sqrt{2}\Delta_a}$, naturally grows as $\sqrt{N}$ and any attempt to decrease this scaling will result in a vanishing optical coupling. Therefore, we demand $\omega = \omega_0 N$, to ensure that the mechanical restoring force remains relevant, satisfying the constraints C3-C4.

Following our expansion, we can calculate the impact of the noise and dissipation induced on the mechanical modes by the optics. The damping has the

form:

$$\gamma^{\text{opt}} = -\frac{4\Delta\omega\lambda^2\left(N-R^2\right)\kappa}{N\left(\Delta^2+\frac{\kappa^2}{4}\right)^2}\ , \tag{4.33}$$

where we see that our previous stability constraint, $\Delta < 0$, (C2) now ensures that this term is damping, $\gamma_i > 0$, and not gain. Meanwhile, the noise has the form:

$$p_{in}^{\text{opt}} = \frac{\sqrt{2\kappa}\lambda\sqrt{(N-R^2)}a_i^{in}}{\sqrt{N}\left(\Delta+\frac{i\kappa}{2}\right)}\ . \tag{4.34}$$

The damping and the correlation of the noise, $\langle p_{in}^{\text{opt}\dagger} p_{in}^{\text{opt}}\rangle$, both grow linearly with N. We demand that these quantities be overwhelmed by their mechanical counterparts to satisfy C5-C6. These constraints mean that the mechanical damping, γ, must also grow as N. This scaling may be difficult to realize, which could prevent such systems having a thermodynamic limit within our framework. Thus, while possessing a transition, such behavior may mesoscopic in nature.

Chapter 5: Interacting atomic interferometry for rotation sensing approaching the Heisenberg Limit [1]

5.1 Introduction

Cold atomic systems have provided an exciting arena for studying aspects of quantum mechanics. The ability to coherently manipulate atoms has been employed to measure the properties of non-inertial frames, e.g. [28,29]. The recent realizations of toroidal traps [87–93] for atoms have presented the possibility for an atomic analogue of the SQUID and its application as a sensor and qubit, e.g. [94–99]. These systems are well understood when interactions between particles are comparatively weak. However, to achieve the maximum advantages in sensing and other applications, many-body superpositions must be understood and utilized. In this chapter, we propose a method for the reliable creation and manipulation of superpositions of many-body states of cold atoms, in particular, the persistent current states of atoms confined to a 1D ring. As a concrete example, we show how the system's sensitivity to rotation can be improved by strong interactions.

Previous approaches to atom interferometric sensing use the ability to trans-

[1] This chapter appears as "Interacting atomic interferometry for rotation sensing approaching the Heisenberg Limit" by S. Ragole and J. M. Taylor in Physical Review Letters 117 (20), 203002.

form phase evolution along different paths into population differences, but treat atomic interactions as deleterious to sensitivity [100, 101]. In these approaches, e.g., Ramsey interferometry, single atoms are put into superposition and the relative phase gained over some time contains information about the quantity to be measured. The far end of the interferometer converts these phases into measurable population differences. However, atoms can interact during this process, altering the phase and leading to a loss of single atom coherence, decreasing the final sensitivity of the measurement [100,101]. These experiments can be engineered to minimize the possibility of interaction and they have produced remarkably precise measurements of gravitation and rotation [28, 29]. This precision comes in part from conducting a large number of independent single atom measurements simultaneously. These ensemble measurements have a noise/signal ratio limited by the shot noise of N independent two-level systems. This noise/signal ratio goes as $\frac{1}{\sqrt{N}}$, known as the shot noise limit [102]. Sensitivities may be improved even to the limit from Heisenberg uncertainty, but only through atomic entanglement, such as squeezing [31].

This chapter describes a system designed to explore the effect of atomic interactions on the sensitivity of an atomic interferometer to rotational flux. We investigate whether there are situations in which atomic interactions can lead to the correlations necessary to beat the shot noise limit while not being too strongly dephased to prevent sensitivity improvements. We find that a strongly repulsive gas of atoms with a weak barrier can be manipulated to create persistent current state superpositions, which can be used to sense rotation with sensitivity that scales as $N^{-3/4}$, below the shot noise limit, but not approaching the Heisenberg limit. Sur-

prisingly, we do not find that SQUID-like systems with strong barriers are effective for this sensing technique. Instead, we utilize the atomic analogue of the phase-slip qubit [103].

5.2 Effective theory for a strongly interacting atomic gas

Strongly interacting systems are famously challenging to analyze. To reduce the difficulty of this problem, we study only the long wavelength behavior of a gas of atoms trapped in a ring geometry in the 1D limit. This dimensional reduction simplifies the physics involved and allows us to consider a variety of interactions and even statistics, though we focus on the bosonic case. While current experiments are weakly interacting and, at best, quasi-2D [89–93], 1D linear traps have been achieved with a range of interaction strengths, e.g., [104,105]. There remains substantial work to create strongly interacting ring systems described above and by others [106–110], but there are efforts in progress [111] and this chapter demonstrates an additional payoff of achieving such systems.

5.2.1 Luttinger liquid theory for cold atoms

Since we consider a wide range of atomic interactions, perturbative methods are not suitable. Mean-field approximations, such as those underlying the Gross–Pitaevskii equation, miss a crucial quantum effect: the ability to create superpositions of many-body excitations, which we find to be necessary for interaction-assisted metrological benefit. Instead, we employ Luttinger liquid theory, an effective field

theory which universally describes quantum systems in 1D with short-range interactions [38–40].

We require temperatures and time variations that are slow compared to the Luttinger energy scale, $E_{LL} \approx \frac{\hbar^2\pi^2\rho_0^2}{K}$, where $\rho_0 = \langle\rho\rangle$ is the average number of atoms per length. K, the Luttinger parameter, encodes the combined effects of statistics and interactions. For example, $K = 1$ corresponds to the Tonks–Girardeau gas (or free fermions) and $K \to \infty$ is the superfluid limit. The interaction strength of delta function-interacting bosons can be mapped to the Luttinger parameter, which allows us to consider the range of interactions for a repulsive Bose gas [40]. We find that $K \approx 1$ is ideal for the gyroscope. In this limit, we can express the Luttinger parameter in terms of the 3D scattering length, a_s, the transverse confinement, $l_\perp$, and ρ_0: $K = 1 + \frac{2\rho_0 l_\perp^2\left(1-\frac{Ca_s}{l_\perp}\right)}{a_s}$, where $C \approx 1.0325...$ is a constant [40]. This theory has the following free Hamiltonian (following conventions from [40]):

$$H_0 = \frac{\hbar v_s}{2\pi}\int_0^L \mathrm{d}x\left[K\left(\partial_x\phi(x)\right)^2 + \frac{1}{K}\left(\partial_x\Theta(x) - \pi\rho_0\right)^2\right] \tag{5.1}$$

where v_s is the speed of sound, L is the circumference of the ring, $\phi(x)$ is a local phase of the underlying field which we are abstracting away. $\partial_x\Theta(x)$ relates to the number density, ρ, by $\rho(x) = \frac{\partial_x\Theta(x)}{\pi}\sum_{l=-\infty}^{+\infty} e^{2il\Theta(x)}$. The Luttinger fields $\phi(x)$ and $\Theta(x)$ have the following commutation relation, $[\phi(x), \frac{\partial_{x'}\Theta(x')}{\pi}] = i\delta(x - x')$.

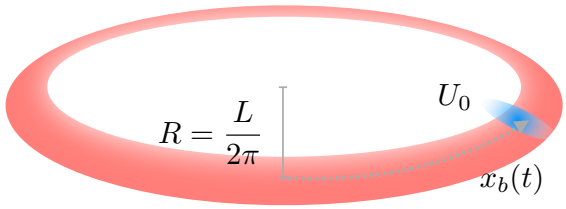

Figure 5.1: A cartoon of the system. Atoms are trapped in a 1D ring of length L with a blue-detuned laser crossing at a single point, $x_b(t)$. In the atom frame, the barrier rotates through the ring at a rate combining the laboratory frame rotation ($\omega_{frame} = \frac{2\pi v_{frame}}{L}$) and the externally controlled stirring rate ($\omega_{stir} = \frac{2\pi v_{stir}}{L}$).

5.2.2 Adding a laser barrier

To make the system sensitive to rotation, we break rotational symmetry by adding a blue-detuned laser beam as a localized potential barrier, shown in Fig. 5.1. We approximate the laser in the long wavelength theory as a (moving) barrier at a single point ($x = x_b(t)$) on the ring. When the barrier is smaller than E_{LL}, i.e., weak, it induces a new term in the Hamiltonian [39, 40, 112, 113]:

$$\begin{aligned} V &= \int_0^L \mathrm{d}x U_0 \delta(x - x_b(t))\rho(x) \\ &\approx 2NU_0 \cos(2\Theta(x_b(t))) \end{aligned} \tag{5.2}$$

where N is the particle number, and U_0 is the dipole potential from the laser. In this expansion, we have kept the lowest harmonics of the density (consistent with [39, 112, 113]). Though strong laser barriers have been used to create "weak-links," in 1D such barriers will destroy persistent current states. The weak barrier

considered here preserves the character of persistent current states and couples them perturbatively.

We perform a standard field expansion for periodic boundary conditions [40, 114]. This expansion defines the fields in terms of zero-modes (θ_0, ϕ_0), topological excitations (N, J) and phonons (b_q). Explicitly,

$$\Theta(x) = \theta_0 + \frac{\pi x}{L} N + \frac{1}{2} \sum_{q \neq 0} \left| \frac{2\pi K}{qL} \right|^{\frac{1}{2}} (e^{iqx} b_q + e^{-iqx} b_q^\dagger) \tag{5.3}$$

$$\phi(x) = \phi_0 + \frac{2\pi x}{L} J + \frac{1}{2} \sum_{q \neq 0} \left| \frac{2\pi}{qLK} \right|^{\frac{1}{2}} \mathrm{sgn}(q) (e^{iqx} b_q + e^{-iqx} b_q^\dagger) \tag{5.4}$$

In this expansion,

$$H_0 = \sum_{q \neq 0} \hbar \omega(q) b_q^\dagger b_q + \frac{\rho_0 L \hbar \omega_0}{8K^2} (N - \rho_0 L)^2 + \frac{\rho_0 L \hbar \omega_0}{2} J^2 \tag{5.5}$$

where $\omega_0 = \frac{4\pi^2 \hbar}{ML^2}$ is the rotation quantum for particles of mass M in a ring of circumference L and we use the relation $v_s K = \frac{\hbar \pi N}{ML}$ from Galilean invariance to achieve this form. We restrict our consideration to a fixed atom number ($N = \rho_0 L$). The current operator, J, has integer eigenvalues and represents the topological charge associated with persistent current in the ring. The phonon modes, b_q, are bosons with quasimomentum $q_n = \frac{2\pi n}{L}$ for $n \in \mathbb{Z}$ and $\omega(q) = \hbar v_s |q|$ for $q \ll \rho_0$.

5.2.3 Deriving the effective Hamiltonian

Now, we transform to a frame which is co-rotating with the barrier. The barrier rotates along with the lab frame and can be actively controlled relative to the lab frame to "stir" the gas. Noting $[J, 2\theta_0] = i$ and $[b_q, b_{q'}^\dagger] = \delta_{qq'}$, we transform

the Hamiltonian with $U_{\mathrm{RF}} = \exp\left(-i\left[\frac{2\pi x_b(t)N}{L}J + \sum_{q\neq 0} q x_b(t) b_q^\dagger b_q\right]\right)$.

The free Hamiltonian is invariant under the transformation, while $V \to 2NU_0\cos(2\Theta(0))$. We also gain the terms

$$\delta H = -i\hbar U_{\mathrm{rf}}^\dagger \dot{U}_{\mathrm{rf}} = -\hbar\omega_b(t)NJ - \hbar\sum_{q\neq 0} q\dot{x}_b(t) b_q^\dagger b_q \tag{5.6}$$

where $\omega_b(t) = \frac{2\pi\dot{x}_b(t)}{L}$ is the angular frequency of the barrier relative to the atoms.

We complete the square for the linear J term and ignore the constant term produced under our fixed atom number assumption. Thus, the transformation leads to a shift in the persistent current operator $J^2 \to \left(J - \frac{\omega_b(t)}{\omega_0}\right)^2$. The phonon term is easily absorbed by defining a new phonon dispersion relation, $\tilde{\omega}(q) = v_s|q| - \dot{x}_b(t)q$. This shifted frequency confirms the intuition that if the stirring speed, $\dot{x}_b$, grows larger than the sound velocity, v_s, our theory will become unstable.

Adding in a barrier breaks the Galilean invariance, and can couple phonons and topological excitations to themselves and each other, potentially decohering topological charge superpositions. We can expand the barrier term using eqn. 5.3

$$V = NU_0\left(e^{2i(\theta_0+\delta\theta(0))} + e^{-2i(\theta_0+\delta\theta(0))}\right) \tag{5.7}$$

where $\delta\theta(0) = \frac{1}{2}\sum_{q\neq 0}|\frac{2\pi K}{qL}|(b_q + b_q^\dagger)$ is the phonon contribution to the field.

5.2.4 Integrating out phonons, renormalizing the barrier

We focus on the coupling of topological charge states, which are most suited for sensing applications. Thus, we integrate over the phonon modes to determine

the effective interaction between the persistent current states. Following [112–114], we arrive at the following expression for the potential barrier.

$$V = NU_0 e^{2i\theta_0} \langle e^{2i\delta\theta(0)} \rangle_{\delta\theta} + h.c. \tag{5.8}$$
$$= 2NU_{\text{eff}} \cos(2\theta_0)$$

where the brackets denote functional integration over the phonon modes, $U_{\text{eff}} = U_0(\frac{d}{L})^K$ is the renormalized barrier strength, and d is a short distance cutoff. While Luttinger liquid theory has a cutoff above which it loses validity ($E_{LL} \approx \frac{N^2\hbar\omega_0}{4K}$), this renormalization step gives a lower cutoff, $E_{ph} = \frac{N\hbar\omega_0}{4K} \approx \frac{E_{LL}}{N}$. The new cutoff generates a timescale below which the renormalized theory is not valid, which will be important to consider when manipulating the system. Simply put, working below the lowest phonon mode frequency prevents decoherence but lowers the "max velocity" for diabatic processes.

The barrier renormalization depends on both the microscopic details and the Luttinger parameter, K. Here we see the first non-trivial indication of the interactions: in the superfluid limit ($K \to \infty$), a barrier will be weakened significantly by the phononic modes. However, in the strongly repulsive ($K \to 1$) regime, the barrier will remain finite, allowing mixing between current states. The relevant cut-off for this regime is $d \approx \frac{KL}{N}$, so $U_{\text{eff}} = U_0(\frac{K}{N})^K$ [114]. In this limit, the strongest constraint on the barrier is that it must be weak, $2NU_0 < \frac{N^2\hbar\omega_0}{4K}$. This restriction guarantees that the perturbative and adiabatic constraints will be satisfied, since after renormalization $2NU_{eff} = 2N^{1-K}U_0K^K < \frac{N^{2-K}\hbar\omega_0}{4K^{1-K}} < E_{ph}$. Fixing the weakness of the

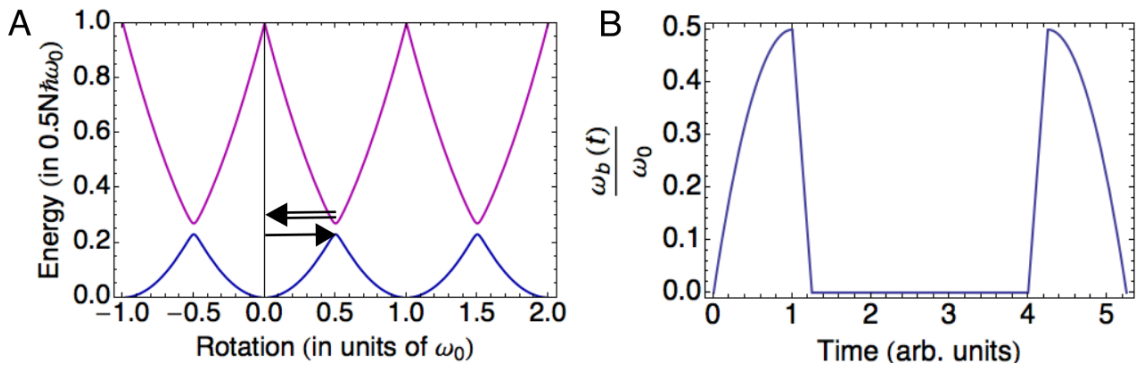

Figure 5.2: A. The energy spectrum for the perturbed current states, blue (magenta) represents the ground (excited) state. The weak barrier creates avoided crossings at rotation $\omega = \frac{2n+1}{2}\omega_0$, $n \in \mathbb{Z}$. The arrows represent the proposed "$\frac{\pi}{2}$-pulse:" the system is adiabatically driven to the avoided crossing (single arrow) and diabatically returned $\omega = 0$ (double arrow). B. A cartoon of the proposed Ramsey sequence. The sequence consists two $\frac{\pi}{2}$-pulses with an observation time τ_{obs} in between.

barrier sets $U_0 = U_{\text{weak}}N$ where $U_{\text{weak}} < \frac{\hbar\omega_0}{8K}$.

This Hamiltonian, similar to the quantum phase-slip junction [103], and is the dual of the standard superconducting charge qubit Hamiltonian [115]:

$$H_{JJ} = E_c(n - n_g)^2 - E_J\cos(\delta) \tag{5.9}$$

where n is the number of Cooper pairs on the island, n_g is set by the gate voltage, δ is the phase difference across the junction, and $[\delta, n] = i$. Under the substitution $n \to J$ and $\delta \to -2\theta_0$, the current states form a charge-qubit-like system with $E_C = \frac{N\hbar\omega_0}{2}$ and $E_J = 2N^{1-K}U_0K^K$ ($E_J \ll E_C$, since the barrier is perturbative).

5.3 A Ramsey sequence for many-body superpositions

Since the barrier couples the current state $|J\rangle$ to states $|J'\rangle = |J \pm 1\rangle$, superpositions can be formed by precisely controlling the rotation rate of the stirring beam. Consider preparing the atoms without any rotation, $|\Psi\rangle = |0\rangle$. Here, only the states $|\pm 1\rangle$ will be coupled by the barrier and only mix weakly into the ground state at $\omega = 0$. We can implement a "$\frac{\pi}{2}$-pulse" in the two steps illustrated in Fig. 5.2a. First, we adiabatically increase rotation to $\omega = \frac{\omega_0}{2}$, where the instantaneous ground state is $\frac{1}{\sqrt{2}}(|0\rangle - |1\rangle)$. Then, the rotation rate is diabatically ramped back to $\omega = 0$ and barrier turned off. This process will be completed in a time $\tau_{\pi/2} = \tau_{\text{adiabatic}} + \tau_{\text{diabatic}}$. These times can be determined from a Landau-Zener analysis of the effective two-level system and will be set by the effective barrier height, $\tau_{\pi/2} \propto \frac{\hbar}{NU_{\text{eff}}}$.

Having established the charge qubit-like behavior and appropriate sequences for preparing topological charge superpositions, we now propose a Ramsey interferometry scheme for rotation sensing, using the persistent current states as the basis. As described above, we create a superposition of current states, $\frac{1}{\sqrt{2}}(|0\rangle - |1\rangle)$, and turn the barrier off. Then, we expose this superposition to a small rotation rate ($\omega \ll \omega_0$) for a time τ_{obs} without the barrier. Over this time, the superposition will evolve into the state $\frac{1}{\sqrt{2}}(|0\rangle - e^{i\phi}|1\rangle)$ where $\phi = N\tau_{\text{obs}}\left(\frac{\omega_0}{2} - \omega\right)$. This phase can be converted into a population difference by performing another "$\frac{\pi}{2}$-pulse." A cartoon of the process is pictured in Fig. 5.2b. The final state can be read out from the persistence of a vortex core in time-of-flight imaging. If the state projects to $|1\rangle$, the vortex will be visible as an absence of density in the center of the ring,

while $|0\rangle$ will expand isotropically, filling the central core [90]. As the relative phase between many-body excitations, the phase scales with the number of atoms while the vortex shot noise is constant. Therefore, the nominal sensitivity to rotation has Heisenberg-like scaling in the absence of noise.

The proposed gyroscope is most viable in the strongly interacting limit which maintains the gap needed to couple persistent current states and keeps $\tau_{\pi/2}$ short. While our analysis has only considered a clean system, it is likely that there will be disorder present in the trap. Disorder leads to localization in 1D for $K < 1.5$ [39]. Therefore, the optimal K is just above this localization limit. While this limit is acceptable for simple experiments, a more detailed analysis of trap imperfections will be necessary for improving future experiments.

5.3.1 Adding noise considerations

We consider realistic sources of noise that could affect the sensitivity. In particular, we will consider shot-to-shot variation in the atom number. Other systematic noise issues, such as laser power and trap configuration fluctuations, could be problematic but can be surmounted with sufficient detuning and laser power.

To compute the effect of shot-to-shot variations in atom number, we assume that number fluctuations are Poissonian, $\sigma_N = \sqrt{N}$. We can consider each individual run of the experiment as having some fixed signal and a random additional noise. We define $F = \frac{\omega_0}{2} - \omega$ and δN_i as the noise in atom number. We consider an average

of many measurements over the noise:

$$\begin{aligned}\langle e^{i\phi}\rangle &= \langle e^{i(NF\tau_{\rm obs}+\delta N_i F\tau_{\rm obs})}\rangle \\ &\approx e^{iNF\tau_{\rm obs}}e^{-F^2\sigma_N^2\tau_{\rm obs}^2}\end{aligned} \tag{5.10}$$

While in the absence of noise, longer evolution times would produce higher sensitivity, the low frequency noise decreases contrast as $e^{-F^2\sigma_N^2\tau_{\rm obs}^2}$ as $\tau_{\rm obs}$ increases. With this noise added in, we can calculate the sensitivity of our approach:

$$\begin{aligned}S &= \left|\partial_\omega \frac{\text{Signal}}{\text{Noise}}\right|^{-1}\Bigg|_{\omega=0}\sqrt{\tau_{\rm obs}} \\ &= \left|\frac{N\omega_0\tau_{\rm obs}\sin(NF_0\tau_{\rm obs}+\phi_0)e^{-F_0^2\sigma_N^2\tau_{\rm obs}^2}}{2F_0}\right|^{-1}\sqrt{\tau_{\rm obs}} \\ &= \frac{e^{\frac{\omega_0^2}{4}\sigma_N^2\tau_{\rm obs}^2}}{N\sqrt{\tau_{\rm obs}}}\end{aligned} \tag{5.11}$$

where in the last line, we have used $F_0 = F(\omega = 0) = \frac{\omega_0}{2}$. We can optimize $\tau_{\rm obs}$ and determine the best sensitivity for the device. Using the optimum observation time, $\tau_{\rm obs}^* = \frac{1}{\omega_0\sigma_N}$, we calculate, $S_{\rm max} = \frac{e^{1/4}\sqrt{\omega_0\sigma_N}}{N}$.

We see that a Poisson-distributed number of atoms per "shot" changes the ideal Heisenberg-like scaling for N fixed to $N^{-3/4}$ scaling. However, this is still an improvement over the shot-noise limit. It could be further enhanced if the time-of-flight images from vortex detection are calibrated to give an sub-Poissonian estimate of atom number, effectively reducing σ_N.

Using a gas temperature of 100 nK and ring radius $R = 19.2$ μm [89–91], we assume a transverse confinement of $l_\perp \approx 200$ nm, which gives $a_s \approx 3600a_0$, where a_0 is the Bohr radius, to set $K \approx 1.6$ for $N = 10^5$. Estimating $\sigma_N = \frac{\sqrt{N}}{10}$, we find that

a sensor with $N = 10^5$ atoms would have $\tau_{\pi/2} = 0.8$ s, $\tau^*_{\text{obs}} \approx 4$ ms, a sensitivity of $2 \times 10^{-4} \frac{\text{rad}}{s\sqrt{Hz}}$ and a bandwidth ≥ 200 Hz. Since the entanglement allows relatively rapid phase accumulation, the sensor has a higher bandwidth than non-interacting sensors. To reasonably compare these techniques, we instead consider a sensitivity per root bandwidth.

5.3.2 Estimating sensitivity

We plot the numerical results for optimum sensitivity as a function of atom number, N, and compare with the noiseless limit and an equal area atom interferometer as described in [28], each evaluated for a fixed time $\tau_{\text{comp}} = \frac{2\pi}{\omega_0} = 0.838$ s in Fig. 5.3. This time is set by the circumnavigation time for atoms moving at the persistent current velocity and is much longer than optimal observation for the Luttinger system, $\tau_{\text{comp}} \approx 6 \times \max(\tau^*_{\text{obs}})$. In the atom interferometer, the atoms will gain a Sagnac phase of $\phi = \frac{2M}{\hbar}\omega A$ where $A = \frac{L^2}{4\pi}$ is the area enclosed by the atoms. This phase can be conveniently rewritten, $\phi = \frac{2\pi MR^2}{\hbar}\omega = \omega\tau_{\text{comp}}$. The sensitivity for the comparison non-interacting system will be:

$$S_{SA} = \frac{1}{|\partial_\omega(\frac{1}{2}\cos(\omega\tau_{\text{comp}} + \phi_0))|}\sqrt{\frac{\tau_{\text{comp}}}{N}} \tag{5.12}$$

$$S_{SA_{max}} = \frac{2}{\sqrt{N\tau_{\text{comp}}}}$$

The sensitivity is improved in the Luttinger ring system, Fig. 5.3a. The non-interacting atomic case shows scaling $\propto N^{-1/2}$ due to the shot-noise limit. Similarly, the noiseless Luttinger system shows Heisenberg-like scaling ($\propto N^{-1}$) while the noisy

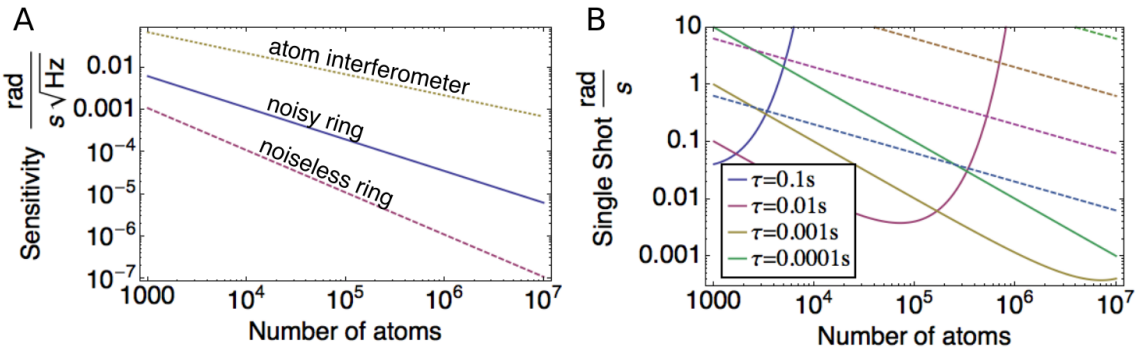

Figure 5.3: A. The sensitivity of our proposed gyroscope (solid) plotted on a log-log scale as a function of atom number. The dashed (dotted) line represents the sensitivity for a noiseless Luttinger (atom interferometer) system with an observation time of $\tau_{\text{comp}} = 0.838$ s. B. Solid (dashed) lines: the single-shot sensitivity for the noisy Luttinger (atom interferometer) system for different observation times, τ, as a function of atom number.

case sits in between. The single shot sensitivity, Fig. 5.3b., demonstrates the trade-offs between longer observation times and atom number.

We note preparing the Luttinger system takes much longer than the observation time. In our example case, $\tau_{\text{prep}} \approx 0.8$s for the $\frac{\pi}{2}$-pulse; so too does $\tau_{\text{measure}} \approx \tau_{\text{prep}}$ which results in a long time between measurements. Faster preparation techniques would substantially improve performance. In addition, atom interferometers can achieve sensitivities much lower than those presented here by using many more atoms and a large enclosed area as shown in Ref. [28].

5.4 Conclusion

While the system shows limited application for high sensitivity rotational sensing, the size of the system makes it a compelling candidate for inertial tests, such as inverse-square law tests, where short length scales are difficult to probe [116–118]. In particular, several high-energy theories predict deviations from Newtonian gravity at the micron scale [116, 119–121]. The ring system described above shows promise in detecting these deviations. However, designing and optimizing such a test will require further research and is beyond the scope of this chapter.

A detailed analysis of the limitations on coherent superpositions in Luttinger liquids will be needed for a complete understanding of this type of gyroscope. Though we controlled the dominant dephasing mechanism by working slowly enough to avoid creating phonons, it is not obvious how stable the superposition will be if particle loss is included. Simulations of superpositions of atoms ($N < 10$) suggest

that the strongly repulsive regime considered here ($K \to 1$) may be robust to particle loss but it is unclear if these results extend to many atoms [108]. Still, the scheme allows the creation of a many-body superposition with sensitivity to small rotation rates and shows favorable scaling, even in the presence of noise. In addition to rotation or inertial sensing, it is possible that creating these superpositions will have other interesting applications, e.g., for use as qubits. [109, 110, 122].

Appendix A: Unraveling the Optomechanical Potential

A.1 Introduction

Optomechanical interactions create a variety of new possibilities for exploring quantum and classical dynamics. These possibilities include drastic improvements in sensing that have enabled the detection of gravitational waves [10,123]. Additionally, using cooling techniques, they also allow for the study of mechanical systems in the quantum domain [124–127]. Experiments in this domain have provided incredibly sensitive measurements of force [9] and allowed for the conversion of quantum information between channels at drastically different frequencies [128]. While the majority of this work has focused on optomechanics in the classical regime, the promise of these new experiments suggests that one needs to deeply examine how optomechanics operates at the border of the quantum regime.

Frequently, the optical fields are assumed to be in a classical steady state while the mechanics can be anywhere in the spectrum from classical to fully quantum. This assumption is well justified when the occupation of the optical cavity (proportional to the driving strength of the laser) is large. Then, we can simply take the photon operators to a coherent state, $a \to \alpha(x) + \delta a$, which depends on other factors in the system. Similar to our previous work, this approximation is also strengthened

by the typical separation of time scales between the optics and the mechanics, i.e., the optics effectively respond instantaneously to the slow motions of the mechanics. This assumption allows one to linearize the dynamics around the steady state, as the fluctuations, δa, are typically small compared to the coherent state. However, the open nature of the system remains and the effect of information loss (through photons exiting the cavity) is likely to have an impact, especially in cases where photon loss is the primary noise mechanism.

In this appendix, we study the quintessential optomechanics interaction, modeled by a cavity with a mirror attached to a spring [8]. First, we walk through the typical semiclassical approximation and derivation of the optomechanical potential for the mechanics. Then, we refine our analysis by including the effect of noise and loss through the quantum jumps method [44, 45]. In this method, the open nature of the system is treated through random processes, called jumps, combined with evolution under a Hamiltonian which includes loss (making it non-Hermitian). We study the evolution of a mechanical coherent state and attempt to reconstruct the effective forces by averaging over the random events.

A.2 Semiclassical analysis

We begin by defining the Hamiltonian of our system. We have a driven optical cavity mode, a, where the cavity frequency depends on the position of a mechanical oscillator, x (similarly, one can understand this interaction in terms of the radiation pressure on the mechanical oscillator). This system can be realized with a moving

cavity mirror, or with the membrane-in-the-middle set up studied in Chapter 3. Moving into a frame with rotates with the driving laser frequency, we arrive at the following Hamiltonian and equations of motion:

$$H_0 = \hbar\left(-\Delta - gx - \frac{i\kappa}{2}\right)a^\dagger a + \hbar\Omega(a + a^\dagger) + \frac{p^2}{2m} + \frac{1}{2}m\omega^2 x^2 \ , \tag{A.1}$$

$$\dot{a} = i(\Delta + gx + \frac{i\kappa}{2})a - i\Omega \ , \tag{A.2}$$

$$\dot{x} = \frac{p}{m} \ , \tag{A.3}$$

$$\dot{p} = -m\omega^2 x + \hbar g a^\dagger a \ . \tag{A.4}$$

In the limit that $|\Delta|, \kappa \gg \omega$, we can assume that the cavity mode responds to the mechanical position instantaneously. In this case, we can find the steady state for a, (which we call α) and substitute it into the equations of motion for the oscillator:

$$\dot{a} = 0 \rightarrow \alpha = \frac{\Omega}{(\Delta + gx) + \frac{i\kappa}{2}} \ . \tag{A.5}$$

Then the radiation pressure force can be found as:

$$\begin{aligned} F_{\text{rad}} &= \hbar g|\alpha|^2 \ , \\ &= \frac{\hbar g|\Omega|^2}{(\Delta + gx)^2 + \frac{\kappa^2}{4}} \ . \end{aligned} \tag{A.6}$$

This force is conservative and can be integrated to find a potential, giving the expected $V(x) = -\frac{\hbar|\Omega|^2}{\kappa/2}\arctan\left(\frac{\Delta+gx}{\kappa/2}\right)$ potential for an optical spring. Now, one may consider the properties of the mechanics (classical or quantum) under this modified potential. We have considered only the optical coherent state amplitude and largely ignored the quantum nature of the optical field. However, as thermal noise decreases, photon loss will have effects on the mechanical system through backaction. To understand these effects, we employ a more sophisticated analysis.

A.3 Quantum Jumps Approach

To treat the quantum and lossy nature of the system, we employ the quantum jump formalism [44, 45]. This formalism allows the simulation of individual quantum trajectories. These trajectories evolve under a non-Hermitian Hamiltonian (to account for cavity decay) and experience noise in which the wavefunction "jumps" to a state with fewer photons. The non-Hermitian Hamiltonian for our system is:

$$H_{\mathrm{QJ}} = H_0 - i\hbar\frac{\kappa}{2}a^\dagger a \ . \tag{A.7}$$

Along with evolution under this Hamiltonian, there are the random "quantum jumps," where the wavefunction is mapped to a system with one fewer photon:

$$|\Psi\rangle \rightarrow \frac{a|\Psi\rangle}{|a|\Psi\rangle|} \ , \tag{A.8}$$

with probability $P = 1 - \langle\Psi(t)|\Psi(t)\rangle$.

Using this method, one maps out the individual "quantum trajectory" which can be used to model a specific instance of an experiment, e.g., tracking the photon number in a cavity by continuous measurement [129]. More commonly, many trajectories are averaged to find expectation values of operators, which matches the master equation result.

A.3.1 Similarity Transformation

We consider what happens in this formalism when we transform the photon operators. As above, we consider an optomechanical cavity driven by a laser field. To

consider excitations away from the coherent state amplitude that we derived above, we make a transformation to shift a to $\alpha + a$. Due to the non-Hermitian nature of the Hamiltonian, this transformation will be only a similarity transformation, not a unitary one. Let $R = e^{-\alpha(a^\dagger - a)}$, where $\alpha \in \mathbb{C}$. $R^{-1} = e^{\alpha(a^\dagger - a)}$, which is not $R^\dagger$ due to the complex nature of α. The creation and annihilation operators transform as:

$$R^{-1} a R = e^{\alpha(a^\dagger - a)} a e^{-\alpha(a^\dagger - a)} = a + \alpha \ , \tag{A.9}$$

$$R^{-1} a^\dagger R = e^{\alpha(a^\dagger - a)} a^\dagger e^{-\alpha(a^\dagger - a)} = a^\dagger + \alpha \ . \tag{A.10}$$

We can then transform the Hamiltonian:

$$\begin{aligned} R^{-1} H R &= \hbar \left(-\Delta - gx - \frac{i\kappa}{2} \right) (a^\dagger + \alpha)(a + \alpha) + \hbar\Omega(a + \alpha + a^\dagger + \alpha) \\ &\quad + R^{-1} \frac{p^2}{2m} R + \frac{1}{2} m\omega^2 x^2 \ , \\ &= -\hbar C \left(a^\dagger a + \alpha^2 \right) + \hbar \left(\Omega - \alpha C \right) (a + a^\dagger) + 2\hbar\Omega\alpha + R^{-1} \frac{p^2}{2m} R + \frac{1}{2} m\omega^2 x^2 \ . \end{aligned} \tag{A.11}$$

where we have defined $C = \Delta + gx + \frac{i\kappa}{2}$, and we have not evaluated the transformation on p because we anticipate that α will depend on x. We began our transformation to eliminate the driving terms on the optical modes. Therefore, we demand $\alpha = \frac{\Omega}{C} = \frac{\Omega}{\Delta + gx + \frac{i\kappa}{2}}$. Substituting in this value for α:

$$H' = -\hbar \left(\Delta + gx + \frac{i\kappa}{2} \right) a^\dagger a + \frac{\hbar\Omega^2}{\Delta + gx + \frac{i\kappa}{2}} + R^{-1} \frac{p^2}{2m} R + \frac{1}{2} m\omega^2 x^2 \ . \tag{A.12}$$

If we inspect the Hermitian parts of the Hamiltonian, we see that they do not include the semiclassical arctangent potential, or any close approximation. We will see that the semiclassical potential must arise through a combination of this potential and

quantum effects that get averaged over. We return to consider the transformation on p:

$$\begin{aligned} R^{-1}pR &= p + i\hbar R^{-1}R' \ , \\ &= p - i\hbar\alpha' \left(a^\dagger - a\right) = p + i\frac{\hbar g\Omega}{\left(\Delta + gx + \frac{i\kappa}{2}\right)^2}\left(a^\dagger - a\right) \ . \end{aligned} \tag{A.13}$$

Now the momentum has a position dependent part which also couples to the photon field. However, as we only consider the transformed photon vacuum, this term can be ignored.

We also compute the probability of a jump, which for small times can be approximated as:

$$\begin{aligned} P_{\text{Jump}} &= 1 - \langle\Psi(t)|\Psi(t)\rangle \ , \\ &= 1 - \langle\Psi(0)| E^{\frac{iH^\dagger t}{\hbar}} E^{-\frac{iHt}{\hbar}} |\Psi(0)\rangle \ , \\ &\approx \frac{t}{\hbar}\langle\Psi(0)|\left(\frac{H^\dagger - H}{i}\right)|\Psi(0)\rangle \ , \end{aligned} \tag{A.14}$$

which is just the expectation value of the anti-Hermitian part of the Hamiltonian. As this will depend on the state we are consider, we delay calculation and specify our ansatz.

A.3.2 Ansatz Wavefunction and Jump Operator Expansion

To more fully understand the effects of these jumps near the classical limit, we consider a system in the vacuum of the transformed photon operator and where the mechanical state is Gaussian wavefunction that is fairly localized in x. With this ansatz, we can study the effect of jumps on the state. We calculate the probability

for the jump and approximate the post-jump state as a transformed Gaussian, which may have a different expectation value of momentum, p_{wp}, position, x_{wp}, and spread, σ. In the subsequent section, we combine these results with evolution under the Hamiltonian to understand the full open system dynamics.

Since our wavefunction is localized in space, if we assume that $g\sigma$ is small compared to other frequencies, we can expand the jump operator around the center of the wavefunction, x_{wp}, that is, $x = x_{wp} + \delta x$. To aid with the mapping onto another Gaussian, we expand the logarithm of the magnitude of the jump operator and re-exponentiate it. Additionally, we expand the phase of the jump operator. These operations allow us to incorporate the post-jump state into a new Gaussian wavefunction with new values for x_{wp}, p_{wp} and σ. Explicitly, the post-jump state is:

$$\begin{aligned}\alpha(x)|\psi\rangle &= \frac{\Omega}{\Delta + gx_{wp} + g\delta x + \frac{i\kappa}{2}} \frac{\exp\left(-\frac{\delta x^2}{2\sigma^2} + \frac{ip_{wp}x_{wp}}{\hbar} + \frac{ip_{wp}\delta x}{\hbar} + i\delta\right)}{\sqrt{\sigma\sqrt{\pi}}} \,, \\ &= \frac{\Omega e^{i\theta}}{\sqrt{(\Delta + gx_{wp} + g\delta x)^2 + \frac{\kappa^2}{4}}} \frac{\exp\left(-\frac{\delta x^2}{2\sigma^2} + \frac{ip_{wp}x_{wp}}{\hbar} + \frac{ip_{wp}\delta x}{\hbar} + i\delta\right)}{\sqrt{\sigma\sqrt{\pi}}} \,. \quad \text{(A.15)}\end{aligned}$$

We define $\Delta' = \Delta + gx_{wp}$ and $w = \Delta'^2 + \frac{\kappa^2}{4}$.We expand the logarithm:

$$\begin{aligned}\log\alpha(x) &= \log\left(\frac{\Omega}{\sqrt{\Delta'^2 + \frac{\kappa^2}{4} + 2\Delta' g\delta x + g^2\delta x^2}}\right) \,, \\ &= \log\left(\frac{\Omega}{\sqrt{(\Delta'^2 + \frac{\kappa^2}{4})(1 + \frac{2\Delta' g\delta x}{w} + \frac{g^2\delta x^2}{w})}}\right) \,, \\ &= \log\left(\frac{\Omega}{\sqrt{(\Delta'^2 + \frac{\kappa^2}{4})}}\right) - \frac{1}{2}\log\left(1 + \frac{2\Delta' g\delta x}{w} + \frac{g^2\delta x^2}{w}\right) \,. \quad \text{(A.16)}\end{aligned}$$

The first term will affect the normalization which we ignore for now. We turn

our attention to the other term which affects expectation value of position, x_{wp}, and the spread, σ:

$$-\frac{1}{2}\log\left(1+\frac{2\Delta' g\delta x}{w}+\frac{g^2\delta x^2}{w}\right)\approx-\frac{1}{2}\left(\frac{2\Delta' g}{w}\delta x+\left(\frac{g^2}{w}-\frac{2\Delta'^2 g^2}{w^2}\right)\delta x^2\right)\ ,$$
$$\approx-\frac{1}{2}\left(\frac{2\Delta' g}{w}\delta x+\left(\frac{g^2(w-2\Delta'^2)}{w^2}\right)\delta x^2\right)\ . \quad \text{(A.17)}$$

We take the expanded jump operator, multiply it by the pre-jump wavefunction and rewrite this new post-jump state as a Gaussian.

We can immediately define:

$$\tau^2=\frac{\sigma^2}{\left(1+\left(\frac{g^2\sigma^2(\frac{\kappa^2}{4}-\Delta'^2)}{w^2}\right)\right)}\ , \quad \text{(A.18)}$$

which will be the new spread of the wavefunction. Looking at τ as a function of Δ', we see some squeezing of the spread near resonance ($|\Delta'|<\frac{\kappa}{2}$), spreading just outside this region and no change far off resonance. With this new spread, we can incorporate the linear term to find the shift of the wavefunction center:

$$2x'_{wp}\delta x=-\frac{2\tau^2\Delta' g}{w}\delta x\ ,$$
$$x'_{wp}=-\frac{g\tau^2\Delta'}{w}=-\left(\frac{\Delta' g\tau}{w}\right)\tau\ . \quad \text{(A.19)}$$

So the wavefunction gets kicked based on the sign Δ'. If the cavity is directly tuned to the mechanical position, there will be no kick of the wavefunction center (though it will still be squeezed). However, away from this point, the wavefunction center moves. We can view this process, occurring at the jump rate, as a kind of velocity. Finally, we need to add and subtract $\frac{x'^2_{wp}}{2\tau^2}$, completing the square. This gives us

wavefunction magnitude:

$$\frac{1}{\sqrt{\sigma\sqrt{\pi}}}\frac{\Omega}{\sqrt{(\Delta'^2+\frac{\kappa^2}{4})}}\exp\left(\frac{x'^2_{wp}}{2\tau^2}\right)\exp\left(-\frac{(\delta x-x'_{wp})^2}{2\tau^2}\right)\ . \tag{A.20}$$

Treating the magnitude alters the position and spread of the wavefunction, but we must also consider the effect that the jumps have on momentum. In coherent states, the momentum is written into the phase. Since the jump operator is complex, it will imprint a phase on the state. The phase of $\alpha(x)$ is:

$$\theta=\arctan\left(\frac{-\frac{\kappa}{2}}{\Delta'+g\delta x}\right)\ . \tag{A.21}$$

In the spirit of the derivation above, we can expand this about $\delta x=0$:

$$\theta\approx-\arctan\left(\frac{\kappa}{2\Delta'}\right)+\frac{g\frac{\kappa}{2}}{\Delta'^2+\frac{\kappa^2}{4}}\delta x+\mathcal{O}(g^2)\ . \tag{A.22}$$

Recalling that the original wavefunction has a phase $\phi\propto\frac{p_{wp}\delta x}{\hbar}$, we can interpret the linear term as a momentum kick:

$$\delta p=\frac{\hbar g\kappa}{2\left(\Delta'^2+\frac{\kappa^2}{4}\right)}\ . \tag{A.23}$$

Again, we can consider this process as an impulse which occurs at the jump rate, resulting in an effective force. We see two major effects after a jump, a stochastic velocity and a correlated stochastic force. This correlated noise could lead to interesting dynamics, but we do not focus on them here.

To complete the equations, we need to calculate the jump rate which will

simply be the probability of a jump divided by time:

$$\begin{aligned} R_{\text{Jump}} = \frac{P_{\text{Jump}}}{t} &\approx \frac{1}{\hbar} \langle \Psi(0)| \left(\frac{H^\dagger - H}{i} \right) |\Psi(0)\rangle \ , \\ &\approx \frac{1}{\hbar} \langle \Psi(0)| \left(\frac{\hbar \kappa \Omega^2}{(\Delta'^2 + \frac{\kappa^2}{4})} \right) |\Psi(0)\rangle \ , \\ &\approx \frac{\kappa \Omega^2}{(\Delta'^2 + \frac{\kappa^2}{4})} \ . \end{aligned} \tag{A.24}$$

Having computed both the approximate post-jump state and the rate at which jumps occur, we can characterize the evolution of our ansatz under quantum jumps. We now turn our attention to the Hamiltonian dynamics to complete our understanding.

A.4 Comparing Quantum Jumps to Semiclassical approach

Having mapped out the effect of quantum jumps, we are now prepared to make a comparison to the semiclassical dynamics that we derived above. We recall that in this limit, the force has the form:

$$\begin{aligned} F &= -m\omega^2 x + \hbar g |\alpha|^2 \ , \\ &= -m\omega^2 x + \frac{\hbar g |\Omega|^2}{(\Delta + gx)^2 + \frac{\kappa^2}{4}} \ . \end{aligned} \tag{A.25}$$

Taking some guidance from Drude model calculations, we can define the momentum as the weighted sum of the momentum of the two possible states after a short time, dt, one where a jump has occurred and one which has simply evolved under the

Hamiltonian. We can then take the limit as $dt \to 0$ and find a differential equation:

$$\begin{aligned} p(t+dt) &= P_{\mathrm{NJ}} p_{\mathrm{NJ}}(t+dt) + P_{\mathrm{J}} p_{\mathrm{J}}(t+dt) \ , \\ &= p(t) + F dt + P_{\mathrm{J}} \delta p_{\mathrm{J}} \ , \qquad \text{(A.26)} \\ \dot{p} &= \frac{p(t+dt) - p(t)}{dt} = F + \frac{P_{\mathrm{J}}}{dt} \delta p_{\mathrm{J}} \ . \qquad \text{(A.27)} \end{aligned}$$

where we assume that the jump probability is small and thus $P_{\mathrm{NJ}} \approx 1$. The conservative terms in F arise from the effective Hamiltonian projected onto the new photon vacuum, which we derive below. The δp_{J} term is the "kick" from the jump operator which we calculated in the previous section. There are also higher order corrections such as the "on-diagonal" Born–Oppenheimer term, i.e., the $aa^\dagger$ term from the shifted p^2, but it will be at higher order in g and we ignore it for the time being.

For the conservative part, we Trotterize the Hamiltonian, where we separate the effects of the standard harmonic evolution and the non-unitary dynamics from the transformation:

$$|\Psi(\tau\rangle \approx e^{\frac{-iV\delta t}{\hbar}} e^{\frac{-iH_0\delta t}{\hbar}} |\Psi(\tau - \delta t)\rangle \ , \qquad \text{(A.28)}$$

where

$$H_0 = \frac{p^2}{2m} + \frac{1}{2} m\omega^2 x^2 \ , \qquad V = \frac{\hbar\Omega^2}{\Delta' + g\delta x + \frac{i\kappa}{2}} \ . \qquad \text{(A.29)}$$

The evolution of a coherent state is simple under H_0 so we choose a state that has instantaneous ($t = \tau$) expectation values $\langle p \rangle = p_{wp}$ and $\langle x \rangle = x_{wp}$. To maintain our ansatz on the coherent state manifold, we expand V in δx, as we did with the

jump operator before:

$$V \approx \frac{\hbar\Omega^2\Delta'}{\Delta'^2+\frac{\kappa^2}{4}} - \frac{i\hbar\Omega^2\kappa}{2\left(\Delta'^2+\frac{\kappa^2}{4}\right)} + \delta x\left(\frac{i\hbar\Omega^2 g\kappa\Delta'}{\left(\Delta'^2+\frac{\kappa^2}{4}\right)^2} + \frac{\hbar\Omega^2 g\left(\frac{\kappa^2}{4}-\Delta'^2\right)}{\left(\Delta'^2+\frac{\kappa^2}{4}\right)^2}\right) . \quad \text{(A.30)}$$

Since $|\Psi(\tau)\rangle \approx e^{-\frac{iV\delta t}{\hbar}}|\Psi\rangle$, we can see that the real terms in V will be a phase imprint and the imaginary terms will give amplitude decay and a drift in x which we will discuss later. Reading off the change in momentum from the imaginary term linear in x, we can write down the conservative force (note the minus sign from $-i$ in the exponent).

$$F = -m\omega^2 x - \frac{\hbar g|\Omega|^2\left(\frac{\kappa^2}{4}-(\Delta+gx)^2\right)}{\left((\Delta+gx)^2+\frac{\kappa^2}{4}\right)^2} . \quad \text{(A.31)}$$

As we noted above, we do not arrive at the semiclassical form of the radiation pressure force and there is a regime where it has the opposite sign from what we would expect.

However, we also have an effective force from the jumps, which we compute by multiplying the momentum kick from a single jump by the jump rate:

$$\begin{aligned}\delta F_{\mathrm{J}} &= \frac{\hbar g\kappa}{(\Delta+gx)^2+\frac{\kappa^2}{4}} R_{\mathrm{jump}} , \\ &= \frac{\hbar g\kappa}{2\left((\Delta+gx)^2+\frac{\kappa^2}{4}\right)} \frac{\kappa\Omega^2}{\left((\Delta+gx)^2+\frac{\kappa^2}{4}\right)} , \\ &= \frac{\hbar g\Omega^2\frac{\kappa^2}{2}}{\left((\Delta+gx)^2+\frac{\kappa^2}{4}\right)^2} . \end{aligned} \quad \text{(A.32)}$$

We see that the average dynamics over jumps produces a κ-dependent force that is twice the size and opposite the sign of the κ-dependent term in the conserva-

tive force. However, we need to consider evolution under both forces, which results in:

$$F \approx -m\omega^2 x + \frac{\hbar g \Omega^2}{(\Delta + gx)^2 + \frac{\kappa^2}{4}} \ , \tag{A.33}$$

which is exactly matches the semiclassical force. Therefore, we see that the semiclassical force arises from the combination of jumps and conservative dynamics in the transformed Hamiltonian.

However, there are additional effects in the Hamiltonian dynamics that we need to consider. We obtain an equation for $\frac{\partial \langle x \rangle}{\partial t}$ by an analogous method. That is, we write:

$$\begin{aligned} x(t+dt) &= P_{\mathrm{NJ}} x_{\mathrm{NJ}}(t+dt) + P_{\mathrm{J}} x_{\mathrm{J}}(t+dt) \ , \\ &= x(t) + v dt + P_{\mathrm{J}} \delta x_{\mathrm{J}} \ , \end{aligned} \tag{A.34}$$

$$\dot{x} = \frac{x(t+dt) - x(t)}{dt} = v + \frac{P_{\mathrm{J}}}{dt} \delta x_{\mathrm{J}} \ . \tag{A.35}$$

Recall from the expansion of V that there is an imaginary term proportional to δx. This term, when multiplied by the $-i$ in the exponential will result in a drift of the wavefunction center. Dividing this drift by dt, we interpret it as a velocity.

$$v_{\mathrm{NJ}} \approx \frac{\Omega^2 g \sigma^2 \kappa \Delta'}{\left(\Delta'^2 + \frac{\kappa^2}{4}\right)^2} \ . \tag{A.36}$$

As we noted in the previous section, there was a similar stochastic drift in the position from jumps. Following our approach from above, we also treat this as a velocity, multiplying the drift by the jump rate. We can now consider both effects

together:

$$\begin{aligned}\dot{x} &= \frac{p}{m} + v_{\mathrm{NJ}} + v_{\mathrm{J}} \ , \\ &= \frac{p}{m} + \frac{\Delta' g\sigma^2\kappa\Omega^2}{\left(\Delta'^2 + \frac{\kappa^2}{4}\right)^2} - \frac{\Delta' g\sigma^2}{\left(\Delta'^2 + \frac{\kappa^2}{4}\right)}\frac{\kappa\Omega^2}{\left(\Delta'^2 + \frac{\kappa^2}{4}\right)} \ , \\ &= \frac{p}{m} \ . \end{aligned} \tag{A.37}$$

The drift in $\langle x \rangle$ from Hamiltonian evolution and the drift caused by the jumps cancel, which matches the semiclassical behavior seen in experiment. However, this calculation suggests that effects from the quantum nature of light are present around these averages and may be accessible in experiment. Further exploration of the variance of mechanical quadratures could help illuminate these effects.

A.5 Conclusion

We have shown how the semiclassical approach to optomechanics can emerge, on average, from the combined effects of Hamiltonian evolution and quantum jumps. In particular, we demonstrate that the lossy nature of the cavity is essential in creating part of the semiclassical potential, as evidenced by the fact that purely Hamiltonian evolution does not reproduce the semiclassical force. We have also quantified some of the deviations from the semiclassical story, namely a trajectory dependent deviation from $\dot{x} = \frac{p}{m}$ and squeezing on the mechanical position depending on the relative size of the detuning to the optical loss rate.

While we have only begun to examine the system, it would be interesting to continue to explore this method, especially in situations where the semiclassical force

exhibits bistability. The strict linearity of quantum mechanics prohibits the existence of multi-stability, so there are likely interesting dynamics which allow multiple solutions to emerge classically. In particular, one could study the optomechanical spring on the blue-detuned side, or a membrane-in-the-middle system where bistability can occur. Given the competition from Hamiltonian evolution and quantum jumps, it is likely that systems with interesting steady states are those where one can have simultaneous eigenstates of the low energy Hamiltonian and the jump operator. However, such studies would necessitate an ansatz that could approximate potential Schrodinger-cat-like states which could emerge.

Appendix B: Observation of optomechanical buckling transitions

nature COMMUNICATIONS

ARTICLE

Received 29 Sep 2016 | Accepted 4 Jan 2017 | Published 1 Mar 2017

DOI: 10.1038/ncomms14481 OPEN

Observation of optomechanical buckling transitions

H. Xu[1], U. Kemiktarak[1,2], J. Fan[2], S. Ragole[1,3], J. Lawall[2] & J.M. Taylor[1,2,3]

Correlated phases of matter provide long-term stability for systems as diverse as solids, magnets and potential exotic quantum materials. Mechanical systems, such as buckling transition spring switches, can have engineered, stable configurations whose dependence on a control variable is reminiscent of non-equilibrium phase transitions. In hybrid opto-mechanical systems, light and matter are strongly coupled, allowing engineering of rapid changes in the force landscape, storing and processing information, and ultimately probing and controlling behaviour at the quantum level. Here we report the observation of first- and second-order buckling transitions between stable mechanical states in an optomechanical system, in which full control of the nature of the transition is obtained by means of the laser power and detuning. The underlying multiwell confining potential we create is highly tunable, with a sub-nanometre distance between potential wells. Our results enable new applications in photonics and information technology, and may enable explorations of quantum phase transitions and macroscopic quantum tunnelling in mechanical systems.

[1] Joint Quantum Institute, University of Maryland, College Park, Maryland 20742, USA. [2] National Institute of Standards and Technology, Gaithersburg, Maryland 20899, USA. [3] Joint Center for Quantum Information and Computer Science, University of Maryland, College Park, Maryland 20742, USA. Correspondence and requests for materials should be addressed to J.L. (email: john.lawall@nist.gov) or to J.M.T. (email: jacob.taylor@nist.gov).

Optomechanical systems provide a unique connection between light and mechanical motion[1–3] due to both their conceptual simplicity—radiation pressure force induces motion in a compliant optical element—and their practical applications in photonics and sensing[4–9]. A canonical example is the modification of the mechanical spring constant via dynamical effects from the radiation pressure associated with the optical modes coupled to the mechanical system. This so-called 'optical spring' effect[10,11] has been employed in the contexts of gravity-wave detection[12], optical trapping of a mirror[13], raising the mechanical quality factor ('optical dilution') of a mechanical oscillator[14] and optical cooling[15]. At the same time, more complex mechanical elements provide new opportunities. For example, nanomechanical devices can be used as memory cells[16–18] or as logic gates. A crucial ingredient for these applications is to develop a robust element that, when driven electronically or optically, can be set to one of two stable static states. Bistability induced by radiation pressure was demonstrated by Dorsel *et al.*[19], using a Fabry–Perot cavity in which the length, and thus the resonant frequency, was modified by the circulating optical power. Shortly thereafter, an analogous experiment was performed in the microwave domain[20]. This work was followed by numerous proposals of applications, including the realization of controllable buckled optomechanical systems[21]. Somewhat surprisingly, the only experiments involving optomechanical bistability reported in the meantime have either involved additional electrostatic feedback[22] or a photothermal mechanism[23–25] rather than radiation pressure. Instead, dynamical effects, necessary for laser cooling and exploration of narrowband behaviour, have been the focus of researchers in nanoscale optomechanics in recent years. At the same time, static properties beyond bistability provide new application spaces for optomechanics in sensing and optical information processing[21,26]. While some experiments with optically driven, pre-buckled devices have yielded successes[18], the mechanical potential was not optically modified in those systems.

Here we report the observation of radiation pressure-induced buckling transitions in an optomechanical system, an effect predicted several decades ago[21]. Our approach relies on a symmetrical optical cavity with a dielectric membrane in the middle[27–29], where the behaviour of the mechanical system can be fabricated and characterized separately from the optics necessary to realize an optical cavity of high finesse. Using this platform, we demonstrate an optomechanical system that realizes controlled first- and second-order buckling transitions. These transitions can be understood as arising when the static optomechanical potential changes smoothly from a single-well to a multiwell potential as the optical driving power is increased. Unlike the situation in the pioneering experiment of Dorsel, in which the bistability was associated with a manifestly asymmetric optomechanical potential[21], our realization results in a spontaneously broken symmetry as the optical drive passes through the transition point. We derive the stability diagram for the buckling transitions, and we show good quantitative agreement between theoretical predictions and experiment.

Results

Experimental set-up. A schematic of our apparatus is shown in Fig. 1a. Two dielectric mirrors, identified as M_L and M_R, form an optical cavity with a length of $\sim$50 mm. At the centre of the cavity is the optomechanical element, a tensioned silicon nitride membrane (see Supplementary Note 4) normal to the cavity mode with long thin tethers connecting the membrane to its frame. An image taken with an optical microscope is shown in Fig. 1b, and a finite element simulation of the fundamental mechanical mode is shown in Fig. 1c. It has a fundamental mechanical frequency of $\omega_m = 2\pi \times 80.3$ kHz, designed to allow for substantial optical spring effects at low laser power. The experiment is performed in the classical regime at room temperature and pressure.

Our approach relies on two different optical modes, denoted a_L and a_R, which have optomechanical couplings of opposite signs. For small displacements of the membrane to the left, mode a_L is shifted up in frequency while a_R is shifted down, and vice versa. A two-dimensional experimental plot of cavity transmission versus membrane position and optical frequency is shown in Fig. 1d; the spectrum is periodic with frequency, so for any membrane positions x except those corresponding to extrema in the spectrum, there is a large set of pairs of modes with opposite optomechanical couplings $g_{L,R}$ (slope of curves in Fig. 1d). The linewidth (FWHM) $\kappa/2\pi$ of the cavity modes is $\sim$1.8 MHz. We move the membrane about 55 nm away from an anti-crossing, where the optomechanical couplings have amplitudes of $g_{L,R} = \pm 2\pi \times 2.1\,\mathrm{kHz\,pm^{-1}}$, and use two such pairs, as illustrated to the right of Fig. 1d. Conceptually, there are four laser fields involved in our experiment, as we now describe.

Two independent probe lasers are locked to a pair of modes with opposite optomechanical couplings by means of the Pound–Drever–Hall (PDH) method, and denoted PDH_1 and PDH_2 in Fig. 1d. The probe fields are actually first-order sidebands generated by electro-optic phase modulators EOM_1 and EOM_2, as shown in Fig. 1a, on independent lasers denoted '$Laser_1$' and '$Laser_2$'. (A detailed description of how the laser fields are generated can be found in the Supplementary Note 3 and Supplementary Fig. 1). Due to the opposite signs of the optomechanical couplings of the modes to which the probe fields are locked, the frequency difference between PDH_1 and PDH_2 is proportional to the membrane displacement, with twice the response of either mode alone. We access this frequency difference by counting the beat signal between the two lasers as detected with photodetector PD_2. At the 2 kHz data acquisition rate employed in this work, the position measurement resolution is better than 1 pm.

We supplement the probe fields with additional fields to create a tailorable, multiwell optomechanical potential. The low coefficient for the absorption of light in silicon nitride at our wavelength ($\lambda = 1{,}550$ nm), combined with the active cooling provided by the ambient air environment, leaves us dominated by radiation pressure for the effective potential (see Supplementary Note 6 and Supplementary Fig. 2). Two strong pump fields, denoted $Pump_1$ and $Pump_2$ in Fig. 1d, are generated by combining light from the lasers, amplifying it, and passing it through phase modulator EOM_3. $Pump_1$ has power P_L and (angular) frequency ν_L and is frequency-offset from probe field PDH_1 by $\sim$2 GHz, the sum of the drive frequencies for EOM_1 and EOM_3, such that it drives mode a_L with (at low pump power) red detuning Δ_L. $Pump_2$ has power P_R and angular frequency ν_R and is similarly offset from probe PDH_2 so as to drive mode a_R with detuning Δ_R. Crucially, the optomechanical coupling of each pump field is of the opposite sign of the probe field to which it is frequency-offset. While a rich variety of phenomena is accessible by taking independent values of P_L, Δ_L, P_R and Δ_R, the experiments described here employ the symmetric situation $P_L = P_R$ and $\Delta_L = \Delta_R$.

Theoretical analysis. In the symmetric configuration, there is only one stable steady state for low to intermediate pump power levels. At higher powers, however, additional steady states appear. For the symmetric case we have constructed, the solutions to the dynamical equations describing these steady states have a

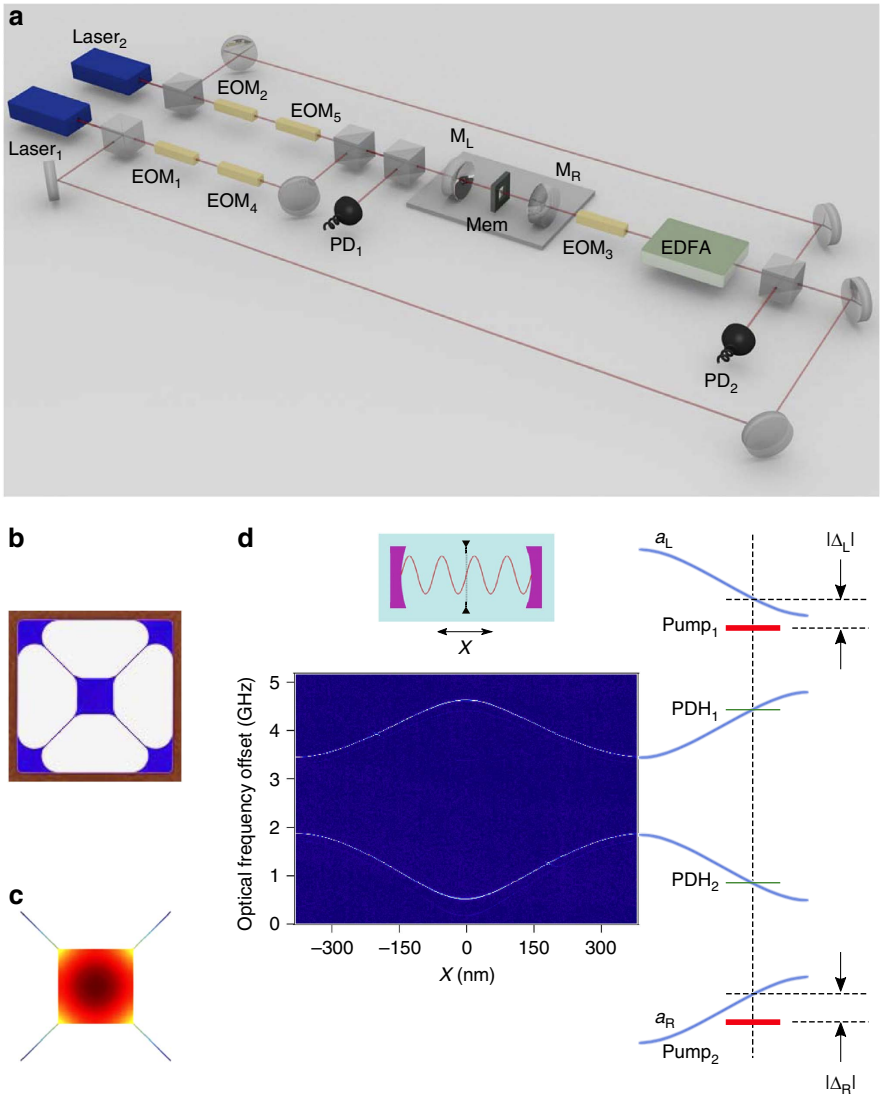

Figure 1 | Experimental set-up. (**a**) Curved mirrors M_L and M_R form a symmetric Fabry–Perot cavity. Tethered membrane Mem that comprises our optomechanical resonator is placed in the centre. The two pump and two probe fields used in the experiment are generated and locked to the cavity by means of independent tunable lasers $Laser_1$ and $Laser_2$, electro-optic phase modulators EOM_1–EOM_5 and an erbium-doped fibre amplifier (EDFA) (details are given in the Supplementary Note 3). Light reflected from the cavity is captured by photodiode PD_1 to lock the lasers to the cavity, and the beat signal between $Laser_1$ and $Laser_2$ is captured on PD_2 to probe the membrane position. (**b**) Microscope image of tethered SiN membrane. The central square is 200 μm on a side. (**c**) Fundamental mechanical mode of membrane determined from finite element analysis; the frequency is 80.3 kHz. (**d**) Optical transmission spectrum for membrane position x near the centre of the cavity. Probe lasers PDH_1 and PDH_2 are locked to adjacent cavity modes whose resonance frequencies have opposite dependences on membrane displacement. Pump laser $Pump_1$ is rigidly offset to probe PDH_1 and detuned to the red of an adjacent cavity mode by Δ_L; similarly, pump laser $Pump_2$ is detuned to the red of an adjacent cavity mode by Δ_R, as shown. When the membrane is displaced to the right, $Pump_1$ is brought closer to resonance and $Pump_2$ is driven further from resonance.

particularly simple form. The optical fields a_L (left-moving) and a_R (right-moving) take the form of coherent states, with amplitudes

$$\alpha_{L(R)} = \frac{\Omega_{L(R)}}{\left(-\Delta_{L(R)} \pm gX\right) - i\kappa/2} \qquad (1)$$

where $\Omega_{L(R)}$ are related to the incident laser powers by $\Omega_{L(R)} = \sqrt{kP_{L(R)}/\hbar\, v_{L(R)}}$, and X is the steady state displacement of the membrane, including the fundamental and higher modes. We note that the fact that the PDH lock tracks the changes in the cavity frequencies leads to a shift $v \to v \pm gX$ for the steady state, effectively enhancing the low-frequency contribution to g by a factor of 2.

As in the experiment, we only focus on the lowest frequency mechanical mode and symmetric driving and detuning, $\Omega_{L(R)} = \Omega$, $\Delta_{L(R)} = \Delta$. This mode feels a radiation pressure force and a spring-based restoring force with spring constant $k = m\omega_m^2$, and the steady state is determined by points where the total force is zero and restorative under small variations in X. Qualitatively, the membrane's motion evolves in a potential combining its internal spring and two competing optical springs. Zeros in the force (minima and maxima of the potential) occur when

$$0 = kX\left(1 - \frac{A}{u^2 + 2u\left(\kappa^2/4 - \Delta^2\right) + \left(\Delta^2 + \kappa^2/4\right)^2}\right) \qquad (2)$$

where $u = (2gX)^2$ is the square of the frequency shift including PDH feedback, and the parameter $A \equiv \frac{-8\hbar g^2 |\Omega|^2 \Delta}{k}$ is proportional to the pump power.

This equation has solutions for $u=0$ and for $u=u_{ss} \equiv \Delta^2-\kappa^2/4 \pm \sqrt{A-\Delta^2\kappa^2}$; physical solutions require $u \geq 0$. Implicitly this requires $A>\Delta^2\kappa^2$, so that u_{ss} is real. For $\Delta<\kappa/2$, there is only one non-zero u solution, and the system continuously goes, as a function of power, from $X=0$ to $X=\pm\frac{\sqrt{u_{ss}}}{2g}$. This is in direct analogy to a second-order buckling transition in a spring, where the broken left/right symmetry is evident even for arbitrarily small values of the displacement. For $\Delta>\kappa/2$, however, there are two solutions for u_{ss}. The smaller corresponds to an unstable branch, while the larger is stable. This leads to a discontinuous change of the membrane displacement at the transition radiation pressure, and provides a first-order buckling transition in the optomechanical system. The overall stability diagram (see Supplementary Note 1 for derivation), including the experimentally probed regimes, is shown in Fig. 2. Both first- and second-order transitions occur, depending upon the detuning, for increasing power. At sufficiently large power levels, the dynamical effects associated with the radiation pressure provide mechanical gain, leading to instability if it overcomes the atmospheric damping. The focus of this work is to study the system at power levels below this threshold.

Experimental results. We now show the experimental buckling of the optically sprung membrane for $\Delta=2\pi\times0.4\,\mathrm{MHz}=0.22\kappa$, where we expect that the dynamics will correspond to a second-order buckling transition. In the absence of a pump laser, the membrane experiences a pure mechanical single-well quadratic potential and fluctuates around the stable position due to both thermal and technical noise. We record the position of the membrane at a sampling rate of 2 kHz for 5 s (see Supplementary Note 5 for position readout); Fig. 3a shows a characteristic subset of the data for 0.4 s, and Fig. 3b shows a histogram of the complete data set, peaked around zero displacement as expected. When the pump fields are turned on, with pump power $P_L=P_R=2.2\,\mathrm{mW}$, the membrane fluctuates around two stable positions, as shown in the time series in Fig. 3c. We attribute the jumping between stable positions primarily to mechanical noise in the nanopositioning stage holding the tethered membrane. As shown in the histogram of the membrane position in Fig. 3d, the membrane buckles to either left or right. As the pump power is raised, the dwell times in the buckled states increase. Figure 3e shows the steady state positions predicted by theory, and implicit in the stability diagram shown in Fig. 2, as a function of pump laser power. Corresponding experimental histograms of the membrane position are shown for the same range of pump powers in Fig. 3f. Both theory and experiment indicate an apparent second-order transition in the membrane displacement X as the pump power is raised.

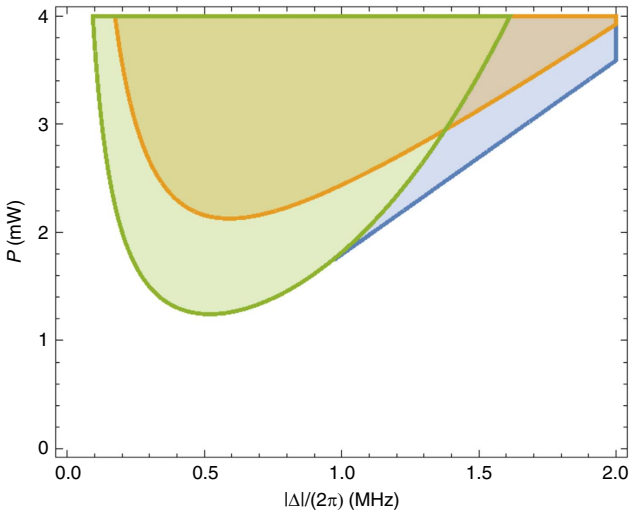

Figure 2 | Theoretical stability diagram. Second-order (green) and first-order (blue) buckling transitions as a function of laser detuning and power $P=P_L=P_R$ are shown. In addition to the stable solutions, the orange overlay indicates the region where radiation pressure provides mechanical gain, raising the quality factor of the mechanical oscillator and potentially causing mechanical instability. Experimental data were taken at detunings $\Delta/2\pi=-0.4$ and -1.2 MHz.

Accompanying the spontaneously broken spatial symmetry as the system passes through the buckling transition is a change in the system dynamics. We observe this by analysing the spectrum of the PDH signal for frequencies higher than the bandwidth ($\sim$3 kHz) of the servos used to lock the lasers to the cavity. Figure 3h shows that as the pump power is raised, the frequency of the optically sprung resonator initially diminishes, and then rises above the frequency of the bare mechanical resonator as the system buckles. This is consistent with the picture that the potential experienced by the membrane evolves from a single well to a double well, the sum of the mechanical and optical potentials.

Curiously, the frequency of the mechanical mode does not go all the way to zero at the buckling transition, as might be expected. This is a consequence of the limited bandwidth of the feedback electronics used to lock the probe lasers to the optical resonances. Specifically, the opposite frequency dependence with position of the pump lasers and their associated probes (Fig. 1d) results in a doubling of the optomechanical coupling for displacements within the bandwidth ($\sim$3 kHz) of the feedback electronics, relative to displacements at substantially higher frequencies. Since the mechanical frequency of the membrane is far above this cutoff, the optical power required to buckle the membrane is well below the power required to drive its frequency to zero in the unbuckled state. Qualitative agreement with the single mechanical mode theory (including the effect of the feedback; see Supplementary Note 2) is obtained and shown in Fig. 3g, but quantitative agreement likely will require inclusion of the higher mechanical modes whose properties remain challenging to fully characterize in the present set-up.

Based on the theoretical model underlying the stability diagram of Fig. 2, we expect the buckling transition to be qualitatively different for detunings $\Delta\geq\kappa/2$. Figure 4 shows our examination of the buckling transition for $\Delta=2\pi\times1.2\,\mathrm{MHz}=0.67\kappa$. Once again, Fig. 4a,b depicts the noise-induced fluctuations of the membrane in the absence of pump lasers. Figure 4c,d shows the time series and histograms of membrane position for $P_L=P_R=3.0\,\mathrm{mW}$; this time, the membrane fluctuates around three stable positions, either remaining unbuckled or buckling to either left or right. When the pump powers are raised to 3.8 mW, only the buckled states remain stable, as shown in Fig. 4e,f.

Theoretical predictions of the steady states as a function of pump power are shown for our experimental conditions in Fig. 4g, and the corresponding experimental histograms of the membrane position are shown in Fig. 4h. In addition to the initial unbuckled state, two more stable positions appear discontinuously as the pump power is increased, indicating that the membrane now experiences an effective triple-well potential. This jump to a finite displacement of the membrane indicates a non-equilibrium first-order buckling transition. As the power is raised still further, the steady state at zero displacement becomes unstable, and the potential becomes a double well. We note that the strong quantitative agreement of our radiation pressure model with these results confirms our neglect of photothermal terms.

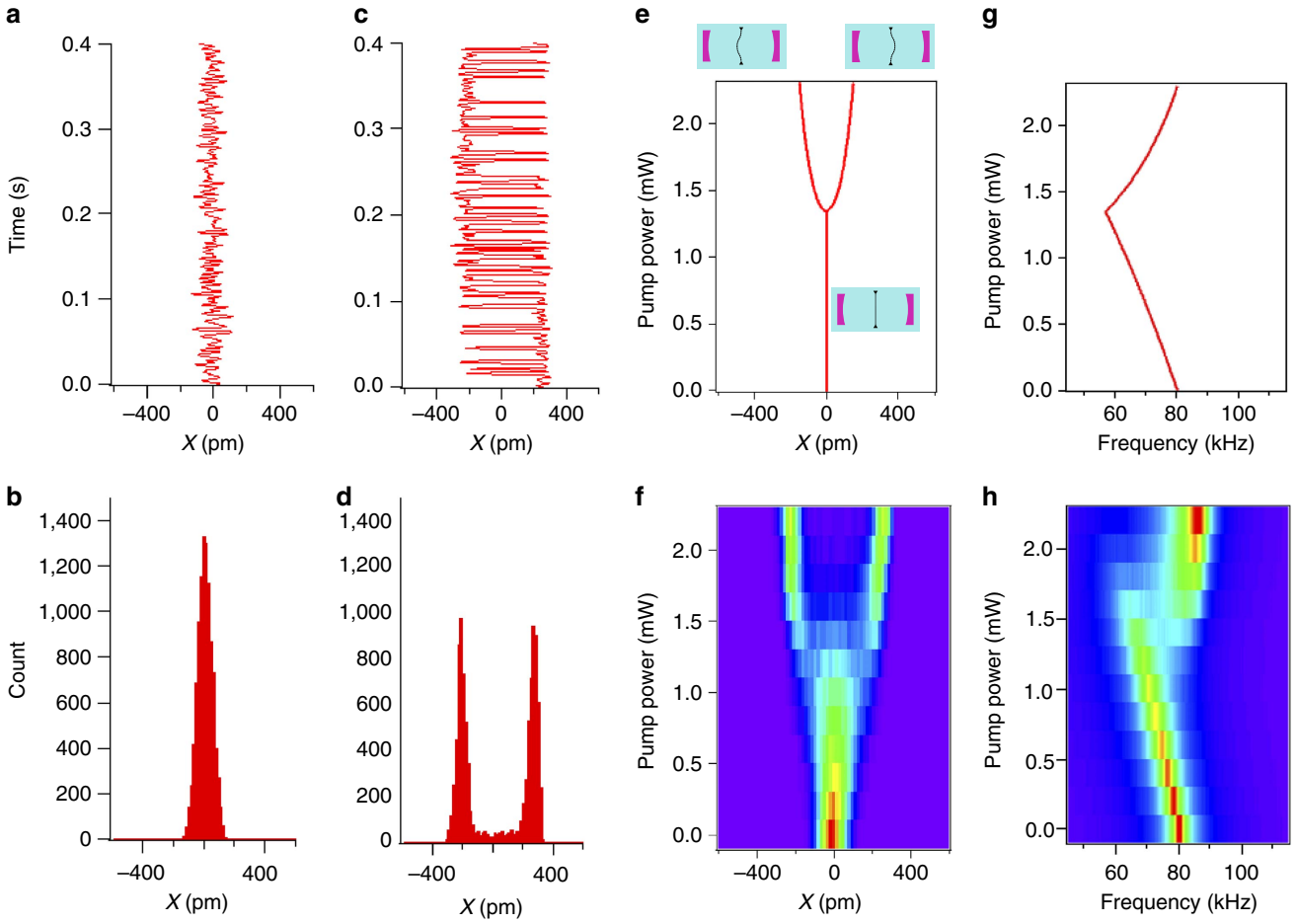

Figure 3 | Second-order buckling transition. (**a**) Real-time data of the membrane position without pump lasers. (**b**) Corresponding histogram. The membrane fluctuates around a single position, resulting from a single-well mechanical potential. (**c**) Real-time data of the membrane position with detuning $\Delta = 0.22\kappa$ and pump power $P_L = P_R = 2.2$ mW. (**d**) Histogram of the membrane position with detuning $\Delta = 0.22\kappa$ and $P_L = P_R = 2.2$ mW. The membrane fluctuates around two stable positions, resulting from a double-well optomechanical potential; the fluctuations are largely induced by mechanical noise in the positioning stage supporting the membrane. (**e**) Calculated stable positions as a function of pump laser power. (**f**) Image of experimental histograms of the membrane position for increasing pump power. The single-well potential develops smoothly into a double-well potential as the power is raised, showing the onset of the second-order buckling transition. (**g**) Calculated mechanical frequency of the membrane for small excursions about the stable positions as a function of pump power. (**h**) Image of mechanical power spectral density inferred from experimental data. The frequency drops as the global potential well initially becomes more shallow, then increases as the membrane buckles into a local potential minimum.

Examination of the mechanical oscillation frequency, Fig. 4j, once again reveals that the frequency of the optically sprung resonator initially diminishes with pump power, but jumps to a value larger than the bare mechanical frequency in the final, double-well regime. For a small range of powers, corresponding to the triple-well regime, the frequency distribution is bimodal. The corresponding theoretical curve, including feedback as discussed previously, is shown in Fig. 4i, where it is clear that different mechanical frequencies are expected in the local potential minima corresponding to the buckled and unbuckled states in the triple-well potential regime. We note that the power levels chosen push into the nominally unstable region of the stability diagram shown in Fig. 2 for the large detuning data. Associated limit cycle behaviour leads to deviations in the experiment from the simple theoretical picture presented earlier, as the system wanders in a potential landscape with position-dependent gain and loss. We believe that this fact, coupled with the feedback and the restriction of our theoretical model to a single mechanical mode, are responsible for the differences in the shapes of the experimental data in Fig. 4h,j from their theoretical counterparts Fig. 4g,i.

Discussion

Our results, which can be generalized to other optomechanical systems, suggest a variety of applications. For laser power near the buckling transition, the response of the membrane to external forces increases dramatically, enabling higher sensitivity for force or acceleration sensing. At higher laser powers, the membrane dwells in its local potential well for significant times, enabling operation as an optomechanical memory, in which the position of the membrane can be switched between the wells by a single laser pulse. Jumps between the potential wells seen in this work arise from technical noise, and may be suppressed by increasing the laser power, using lower-noise positioning stages, and working at low temperature. Our system also provides a platform for studying nonlinear optomechanics and chaotic dynamics, such as dynamical multistability[30]. Furthermore, at low temperatures and with a high mechanical quality factor, a quantum phase transition may be observable in systems of this nature[31]. Specifically, an optomechanical system can be made sufficiently cold—with a nominal dephasing rate slower than its resonance frequency—and sideband resolved to be laser cooled to its ground state before buckling[32]. Then a rapid increase in pump power bringing the

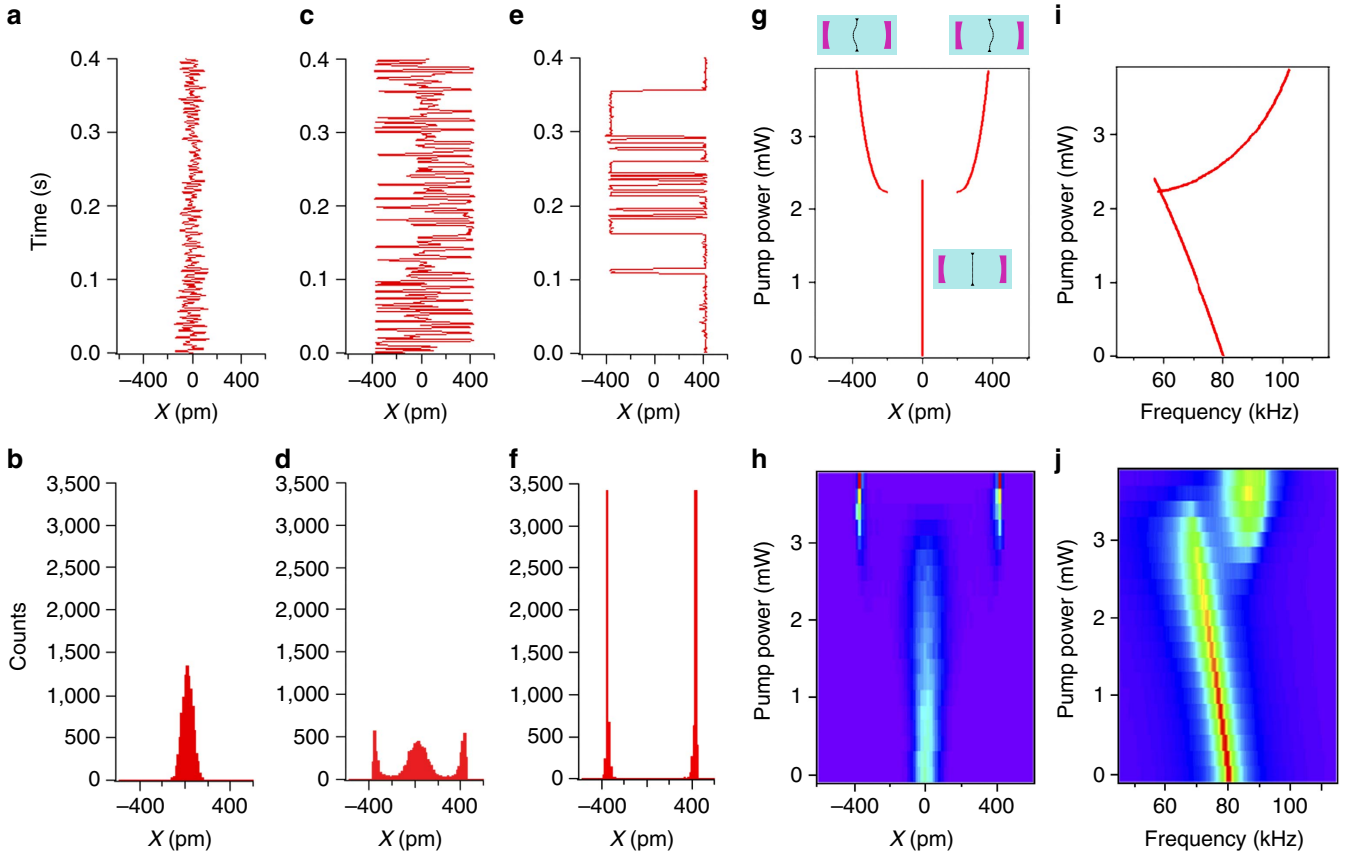

Figure 4 | First-order buckling transition. (**a**) Time series and (**b**) histogram of membrane position, no pump. (**c**) Real-time data and (**d**) histogram of the membrane position with detuning $\Delta = 0.67\kappa$ and pump power $P_L = P_R = 3.0$ mW. The membrane fluctuates around three stable positions, resulting from a triple-well optomechanical potential. (**e**) Real-time data and (**f**) histogram of the membrane position with detuning $\Delta = 0.67\kappa$ and $P_L = P_R = 3.8$ mW. The membrane now fluctuates around just two stable positions, due to a double-well optomechanical potential. (**g**) Calculated stable positions as a function of pump laser power. For a small range of pump powers, there are three stable positions, and as the pump power is raised, the unbuckled state becomes unstable. (**h**) Image of experimental histograms of the membrane position for increasing pump power. (**i**) Calculated mechanical frequency of the membrane for small excursions about the stable positions as a function of pump power. (**j**) Image of mechanical power spectral density inferred from experimental data.

system across the stability boundary could yield a transition driven entirely by quantum fluctuations, a macroscopic version of structural quantum phase transitions such as those in ion crystals[33].

Data availability. Data are stored and saved according to US government policy, and can be made available by request to the authors on an individual basis.

References

1. Milburn, G. & Woolley, M. An introduction to quantum optomechanics. *Acta Phys. Slovaca.* **61,** 483–601 (2011).
2. Meystre, P. A short walk through quantum optomechanics. *Ann. Phys.* **525,** 215–233 (2013).
3. Aspelmeyer, M., Kippenberg, T. J. & Marquardt, F. Cavity optomechanics. *Rev. Mod. Phys.* **86,** 1391–1452 (2014).
4. Metcalfe, M. Applications of cavity optomechanics. *Appl. Phys. Rev.* **1,** 031105 (2014).
5. Abramovici, A. *et al.* LIGO: the laser interferometer gravitational-wave observatory. *Science* **256,** 325–333 (1992).
6. Li, M. *et al.* Harnessing optical forces in integrated photonic circuits. *Nature* **456,** 480–484 (2008).
7. Ludwig, M., Safavi-Naeini, A. H., Painter, O. & Marquardt, F. Enhanced quantum nonlinearities in a two-mode optomechanical system. *Phys. Rev. Lett.* **109,** 063601 (2012).
8. Winger, M. *et al.* A chip-scale integrated cavity-electro-optomechanics platform. *Opt. Express* **19,** 24905 (2011).
9. Krause, A. G., Winger, M., Blasius, T. D., Lin, Q. & Painter, O. A high-resolution microchip optomechanical accelerometer. *Nat. Photonics* **6,** 768–772 (2012).
10. Braginsky, V. B. & Manukin, A. B. *Measurement of Weak Forces in Physics Experiments* (University of Chicago Press, 1977).
11. Sheard, B. S., Gray, M. B., Mow-Lowry, C. M., McClelland, D. E. & Whitcomb, S. E. Observation and characterization of an optical spring. *Phys. Rev. A* **69,** 051801 (2004).
12. Di Virgilio, A. *et al.* Experimental evidence for an optical spring. *Phys. Rev. A* **74,** 013813 (2006).
13. Corbitt, T. *et al.* An all-optical trap for a gram-scale mirror. *Phys. Rev. Lett.* **98,** 150802 (2007).
14. Corbitt, T. *et al.* Optical dilution and feedback cooling of a gram-scale oscillator to 6.9 mK. *Phys. Rev. Lett.* **99,** 160801 (2007).
15. Mow-Lowry, C. M., Mullavey, A. J., Gossler, S., Gray, M. B. & McClelland, D. E. Cooling of a gram-scale cantilever flexure to 70 mK with a servo-modified optical spring. *Phys. Rev. Lett.* **100,** 010801 (2008).
16. Mahboob, I. & Yamaguchi, H. Bit storage and bit flip operations in an electromechanical oscillator. *Nat. Nanotechnol.* **3,** 275–279 (2008).
17. Badzey, R. L., Zolfagharkhani, G., Gaidarzhy, A. & Mohanty, P. A controllable nanomechanical memory element. *Appl. Phys. Lett.* **85,** 3587 (2004).
18. Bagheri, M., Poot, M., Li, M., Pernice, W. P. H. & Tang, H. X. Dynamic manipulation of nanomechanical resonators in the high-amplitude regime and non-volatile mechanical memory operation. *Nat. Nanotechnol.* **6,** 726–732 (2011).
19. Dorsel, A., McCullen, J. D., Meystre, P., Vignes, E. & Walther, H. Optical bistability and mirror confinement induced by radiation pressure. *Phys. Rev. Lett.* **51,** 1550 (1983).
20. Gozzini, A., Longo, I., Barbarino, S., Maccarrone, F. & Mango, F. Light-pressure bistability at microwave frequencies. *JOSA B* **2,** 1841–1845 (1985).
21. Meystre, P., Wright, E. M., McCullen, J. D. & Vignes, E. Theory of radiation-pressure-driven interferometers. *JOSA B* **2,** 1830–1840 (1985).

22. Mueller, F., Heugel, S. & Wang, L. J. Observation of optomechanical multi-stability in a high-Q torsion balance oscillator. *Phys. Rev. A* **77,** 031802 (2008).
23. Metzger, C. *et al.* Self-induced oscillations in an optomechanical system driven by bolometric backaction. *Phys. Rev. Lett.* **101,** 133903 (2008).
24. Hao, F., JiangFang, D., Yong, L. & GengYu, C. Manipulating a micro-cantilever between its optomechanical bistable states in a lever-based Fabry-Perot cavity. *Sci. China Phys. Mech. Astron.* **58,** 1 (2015).
25. Yuvaraj, D., Kadam, M. B., Shtempluck, O. & Buks, E. Optomechanical cavity with a buckled mirror. *J. Microelectromech. Syst.* **22,** 430–437 (2013).
26. Buchmann, L. F., Zhang, L., Chiruvelli, A. & Meystre, P. Macroscopic tunneling of a membrane in an optomechanical double-well potential. *Phys. Rev. Lett.* **108,** 210403 (2012).
27. Thompson, J. D. *et al.* Strong dispersive coupling of a high-finesse cavity to a micromechanical membrane. *Nature* **452,** 72–75 (2008).
28. Jayich, A. M. *et al.* Dispersive optomechanics: a membrane inside a cavity. *New. J. Phys.* **10,** 095008 (2008).
29. Sankey, J. C., Yang, C., Zwickl, B. M., Jayich, A. M. & Harris, J. G. E. Strong and tunable nonlinear optomechanical coupling in a low-loss system. *Nat. Phys.* **6,** 707–712 (2010).
30. Marquardt, F., Harris, J. G. E. & Girvin, S. M. Dynamical multistability induced by radiation pressure in high-finesse micromechanical optical cavities. *Phys. Rev. Lett.* **96,** 103901 (2006).
31. Mumford, J., O'Dell, D. H. J. & Larson, J. Dicke-type phase transition in a multimode optomechanical system: dicke-type phase transition in a multimode. *Ann. Phys.* **527,** 115–130 (2015).
32. Chan, J. *et al.* Laser cooling of a nanomechanical oscillator into its quantum ground state. *Nature* **478,** 89–92 (2011).
33. Shimshoni, E., Morigi, G. & Fishman, S. Quantum zigzag transition in ion chains. *Phys. Rev. Lett.* **106,** 010401 (2011).

Acknowledgements

We acknowledge helpful discussions with J. Harris, A. Schliesser, E. Polzik and J. Foley. Funding was provided by DARPA QuASAR and the NSF-funded Physics Frontier Center at the JQI. Research performed in part at the NIST Center for Nanoscale Science and Technology.

Author contributions

The experiment was conceived by H.X. and J.M.T., and designed by H.X., J.F. and J.L. Data were taken by H.X., U.K. and J.L., and analysed by H.X., S.R., J.M.T. and J.L. All authors helped in the writing of the paper.

Additional information

Supplementary Information accompanies this paper at http://www.nature.com/naturecommunications

Competing financial interests: The authors declare no competing financial interests.

Reprints and permission information is available online at http://npg.nature.com/reprintsandpermissions/

How to cite this article: Xu, H. *et al.* Observation of optomechanical buckling transitions. *Nat. Commun.* **8,** 14481 doi: 10.1038/ncomms14481 (2017).

Publisher's note: Springer Nature remains neutral with regard to jurisdictional claims in published maps and institutional affiliations.

Bibliography

[1] C. J. Davisson. The diffraction of electrons by a crystal of nickel. *Bell Syst. Tech. J.*, 7(1):90–105, 1928.

[2] M. Knoll and E. Ruska. Das Elektronenmikroskop. *Zeitschrift fur Phys.*, 78(5-6):318–339, 1932.

[3] Yuichi Tsuda, Osamu Mori, Ryu Funase, Hirotaka Sawada, Takayuki Yamamoto, Takanao Saiki, Tatsuya Endo, Katsuhide Yonekura, Hirokazu Hoshino, and Jun'Ichiro Kawaguchi. Achievement of IKAROS-Japanese deep space solar sail demonstration mission. *Acta Astronaut.*, 82(2):183–188, 2013.

[4] P. Lebedev. Untersuchungen über die Druckkräfte des Lichtes. *Ann. Phys.*, 311(11):433–458, 1901.

[5] E. F. Nichols and G. F. Hull. The pressure due to radiation. *Astrophys. J.*, 17(5):315–351, 1903.

[6] T. H. Maiman. Stimulated optical radiation in Ruby. *Nature*, 187(4736):493–494, 1960.

[7] A. L. Schawlow and C. H. Townes. Infrared and optical masers. *Phys. Rev.*, 112(6):1940–1949, 1958.

[8] Markus Aspelmeyer, Tobias J. Kippenberg, and Florian Marquardt. Cavity optomechanics. *Rev. Mod. Phys.*, 86(December), 2014.

[9] Sydney Schreppler, Nicolas Spethmann, Nathan Brahms, Thierry Botter, Maryrose Barrios, and Dan M. Stamper-Kurn. Optically measuring force near the standard quantum limit. *Science*, 344(6191):1486–1489, 2014.

[10] B. P. Abbott et al. (Virgo and LIGO Scientific Collaborations). Observation of gravitational waves from a binary black hole merger. *Phys. Rev. Lett.*, 116:061102, Feb 2016.

[11] Mahmood Bagheri, Menno Poot, Mo Li, Wolfram P. H. Pernice, and Hong X. Tang. Dynamic manipulation of nanomechanical resonators in the high-amplitude regime and non-volatile mechanical memory operation. *Nat. Nanotechnol.*, 6(11):726–732, 2011.

[12] Subhadeep Gupta, Kevin L. Moore, Kater W. Murch, and Dan M. Stamper-Kurn. Cavity nonlinear optics at low photon numbers from collective atomic motion. *Phys. Rev. Lett.*, 99(21):2–5, 2007.

[13] Kater W. Murch, Kevin L. Moore, Subhadeep Gupta, and Dan M. Stamper-Kurn. Observation of quantum-measurement backaction with an ultracold atomic gas. *Nat. Phys.*, 4(7):561–564, 2008.

[14] Ferdinand Brennecke, Stephan Ritter, Tobias Donner, and Tilman Esslinger. Cavity optomechanics with a Bose-Einstein condensate. *Science*, 322:235–239, 2008.

[15] E. Gavartin, P. Verlot, and T. J. Kippenberg. A hybrid on-chip optomechanical transducer for ultrasensitive force measurements. *Nat. Nanotechnol.*, 7(8):509–514, 2012.

[16] R. W. Andrews, R. W. Peterson, T. P. Purdy, K. Cicak, R. W. Simmonds, C. A. Regal, and K. W. Lehnert. Bidirectional and efficient conversion between microwave and optical light. *Nat. Phys.*, 10(4):321–326, 2014.

[17] T. J. Kippenberg and K. J. Vahala. Cavity optomechanics: back-action at the mesoscale. *Science*, 321(5893):1172–1176, 2008.

[18] J. D. Teufel, T. Donner, M. A. Castellanos-Beltran, J. W. Harlow, and K. W. Lehnert. Nanomechanical motion measured with an imprecision below that at the standard quantum limit. *Nat. Nanotechnol.*, 4(12):820–823, 2009.

[19] J. P. Gordon, H. J. Zeiger, and C. H. Townes. Molecular microwave oscillator and new hyperfine structure in the microwave spectrum of NH3. *Phys. Rev.*, 95(1):282–284, 1954.

[20] C. L. Degen, F. Reinhard, and P. Cappellaro. Quantum sensing. *Rev. Mod. Phys.*, 89(3):1–39, 2017.

[21] J. Baron, W. C. Campbell, D. DeMille, J. M. Doyle, G. Gabrielse, Y. V. Gurevich, P. W. Hess, N. R. Hutzler, E. Kirilov, I. Kozyryev, B. R. O'Leary, C. D. Panda, M. F. Parsons, E. S. Petrik, B. Spaun, A. C. Vutha, and A. D. West. Order of magnitude smaller limit on the electric dipole moment of the electron. *Science*, 343(6168):269–272, 2014.

[22] William B. Cairncross, Daniel N. Gresh, Matt Grau, Kevin C. Cossel, Tanya S. Roussy, Yiqi Ni, Yan Zhou, Jun Ye, and Eric A. Cornell. Precision measurement of the electron's electric dipole moment using trapped molecular ions. *Phys. Rev. Lett.*, 119:153001, Oct 2017.

[23] Peter W. Graham, Jason M. Hogan, Mark A. Kasevich, and Surjeet Rajendran. New method for gravitational wave detection with atomic sensors. *Phys. Rev. Lett.*, 110:171102, Apr 2013.

[24] S. Kolkowitz, I. Pikovski, N. Langellier, M. D. Lukin, R. L. Walsworth, and J. Ye. Gravitational wave detection with optical lattice atomic clocks. *Phys. Rev. D*, 94(12):1–15, 2016.

[25] Stig Stenholm. The semiclassical theory of laser cooling. *Rev. Mod. Phys.*, 58(3):699–739, 1986.

[26] William D. Phillips. Nobel Lecture: Laser cooling and trapping of neutral atoms. *Rev. Mod. Phys.*, 70(3):721–741, 1998.

[27] L. Pitaevskii and Sandro Stringari. *Bose-Einstein Condensation and Superfluidity (International Series of Monographs on Physics)*. Oxford University Press, 1st edition, 2016.

[28] T. L. Gustavson, P. Bouyer, and M. A. Kasevich. Precision rotation measurements with an atom interferometer gyroscope. *Phys. Rev. Lett.*, 78:2046–2049, Mar 1997.

[29] M. J. Snadden, J. M. McGuirk, P. Bouyer, K. G. Haritos, and M. A. Kasevich. Measurement of the Earth's gravity gradient with an atom interferometer-based gravity gradiometer. *Phys. Rev. Lett.*, 81:971–974, Aug 1998.

[30] J. M. McGuirk, G. T. Foster, J. B. Fixler, M. J. Snadden, and M. A. Kasevich. Sensitive absolute-gravity gradiometry using atom interferometry. *Phys. Rev. A*, 65:033608, Feb 2002.

[31] Vittorio Giovannetti, Seth Lloyd, and Lorenzo Maccone. Quantum-enhanced measurements: beating the standard quantum limit. *Science*, 306(5700):1330–1336, 2004.

[32] Vittorio Giovannetti, Seth Lloyd, and Lorenzo Maccone. Quantum metrology. *Phys. Rev. Lett.*, 96(1):13–16, 2006.

[33] Vittorio Giovannetti, Seth Lloyd, and Lorenzo Maccone. Advances in quantum metrology. *Nat. Photonics*, 5(4):222–229, 2011.

[34] Tomohisa Nagata, Ryo Okamoto, Jeremy L. O'Brien, Keiji Sasaki, and Shigeki Takeuchi. Beating the standard quantum limit with four entangled photons. *Science*, 316(5825):726–729, 2007.

[35] J. Appel, P. J. Windpassinger, D. Oblak, U. B. Hoff, N. Kjaergaard, and E. S. Polzik. Mesoscopic atomic entanglement for precision measurements beyond the standard quantum limit. *Proc. Natl. Acad. Sci.*, 106(27):10960–10965, 2009.

[36] J. A. Jones, S. D. Karlen, J. Fitzsimons, A. Ardavan, S. C. Benjamin, G. A. D. Briggs, and J. J. L. Morton. Magnetic field sensing beyond the standard quantum limit using 10-spin NOON states. *Science*, 324(5931):1166–1168, 2009.

[37] Sin-Itiro Tomonaga. Elementary theory of quantum-mechanical collective motion of particles, ii. *Prog. Theor. Phys.*, 13(5):482–496, 1955.

[38] F. D. M. Haldane. Effective harmonic-fluid approach to low-energy properties of one-dimensional quantum fluids. *Phys. Rev. Lett.*, 47:1840–1843, Dec 1981.

[39] T. Giamarchi. *Quantum Physics in One Dimension*. International Series of Monographs on Physics. Clarendon Press, 2003.

[40] M. A. Cazalilla. Bosonizing one-dimensional cold atomic gases. *J. Phys. B*, 37(7):S1–S47, 2004.

[41] H. Haken. Cooperative phenomena in systems far from thermal equilibrium and in nonphysical systems. *Rev. Mod. Phys.*, 47(1):67–121, 1975.

[42] Haitan Xu, Utku Kemiktarak, Jingyun Fan, Stephen Ragole, John Lawall, and Jacob M. Taylor. Observation of optomechanical buckling phase transitions. *Nat. Commun.*, 8:14481, 2017.

[43] Julian Léonard, Andrea Morales, Philip Zupancic, Tilman Esslinger, and Tobias Donner. Supersolid formation in a quantum gas breaking continuous translational symmetry. *Nature*, 543(7643):87–90, 2016.

[44] H. J. Carmichael. *An Open Systems Approach to Quantum Optics*, volume 18. Springer, Berlin, 1993.

[45] Jean Dalibard, Yvan Castin, and Klaus Mølmer. Wave-function approach to dissipative processes in quantum optics. *Phys. Rev. Lett.*, 68:580–583, Feb 1992.

[46] E. H. Lieb. Exactly soluble models. *Physica*, 73(1):226–236, 1974.

[47] Sudip Chakravarty, Gert-Ludwig Ingold, Steven Kivelson, and Alan Luther. Onset of global phase coherence in Josephson-junction arrays: a dissipative phase transition. *Phys. Rev. Lett.*, 56:2303–2306, May 1986.

[48] B. Derrida. Dynamical phase transition in nonsymmetric spin glasses. *J. Phys. A. Math. Gen.*, 20(11):L721, 1987.

[49] Daniel S. Fisher. Sliding charge-density waves as a dynamic critical phenomenon. *Phys. Rev. B*, 31(3):1396–1427, 1985.

[50] Subir Sachdev. *Quantum Phase Transitions*. Cambridge Univ. Press, 2nd edition, 2011.

[51] Adam T. Black, Hilton W. Chan, and Vladan Vuletić. Observation of collective friction forces due to spatial self-organization of atoms: from Rayleigh to Bragg scattering. *Phys. Rev. Lett.*, 91:203001, Nov 2003.

[52] Kristian Baumann, Christine Guerlin, Ferdinand Brennecke, and Tilman Esslinger. Dicke quantum phase transition with a superfluid gas in an optical cavity. *Nature*, 464(7293):1301–1306, 2010.

[53] G. Labeyrie, E. Tesio, P. M. Gomes, G.-L. Oppo, W. J. Firth, G. R. M. Robb, A. S. Arnold, R. Kaiser, and T. Ackemann. Optomechanical self-structuring in a cold atomic gas. *Nat. Photonics*, 8(4):321–325, 2014.

[54] Helmut Ritsch, Peter Domokos, Ferdinand Brennecke, and Tilman Esslinger. Cold atoms in cavity-generated dynamical optical potentials. *Rev. Mod. Phys.*, 85(2):553–601, 2013.

[55] V. Degiorgio and Marlan O. Scully. Analogy between the laser threshold region and a second-order phase transition. *Phys. Rev. A*, 2(4):1170–1177, 1970.

[56] R. Graham and H. Haken. Laserlight - first example of a second-order phase transition far away from thermal equilibrium. *Zeitschrift fur Phys.*, 237:31–46, 1970.

[57] E. Pytte and H. Thomas. Soft plasma mode and the Gunn instability. *Phys. Rev. Lett.*, 20:1167–1170, May 1968.

[58] Rolf Landauer. Irreversibility and heat generation in the computational process. *IBM J. Res. Dev.*, 5(July):183–191, 1961.

[59] Rolf Landauer. Cooperative effects, soft modes, and fluctuations in data processing. *Ferroelectrics*, 2(1):47–55, 1971.

[60] A. M. Jayich, J. C. Sankey, B. M. Zwickl, C. Yang, J. D. Thompson, S. M. Girvin, A. A. Clerk, F. Marquardt, and J. G E Harris. Dispersive optomechanics: a membrane inside a cavity. *New J. Phys.*, 10, 2008.

[61] J. D. Thompson, B. M. Zwickl, A. M. Jayich, Florian Marquardt, S. M. Girvin, and J. G. E. Harris. Strong dispersive coupling of a high-finesse cavity to a micromechanical membrane. *Nature*, 452(7183):72–5, 2008.

[62] J. C. Sankey, C. Yang, B. M. Zwickl, A. M. Jayich, and J. G. E. Harris. Strong and tunable nonlinear optomechanical coupling in a low-loss system. *Nat. Phys.*, 6(9):707–712, 2010.

[63] H. Xu, D. J. Mason, L. Jiang, and J. G. E. Harris. Topological energy transfer in an optomechanical system with exceptional points. *Nature*, 537:80–83, 2016.

[64] Jasper Chan, T. P. Mayer Alegre, Amir H. Safavi-Naeini, Jeff T. Hill, Alex Krause, Simon Groeblacher, Markus Aspelmeyer, and Oskar Painter. Laser cooling of a nanomechanical oscillator into its quantum ground state. *Nature*, 478:18, 2011.

[65] R. H. Dicke. Coherence in spontaneous radiation processes. *Phys. Rev.*, 93(1):99–110, 1954.

[66] Klaus Hepp and Elliott H. Lieb. On the superradiant phase transition for molecules in a quantized radiation field: the Dicke maser model. *Ann. Phys.*, 76(2):360–404, 1973.

[67] Y. K. Wang and F. T. Hioe. Phase transition in the Dicke model of superradiance. *Phys. Rev. A*, 7(3):831–836, 1973.

[68] Clive Emary and Tobias Brandes. Chaos and the quantum phase transition in the Dicke model. *Phys. Rev. E*, 67(6):066203, 2003.

[69] K. Baumann, R. Mottl, F. Brennecke, and T. Esslinger. Exploring symmetry breaking at the Dicke quantum phase transition. *Phys. Rev. Lett.*, 107:140402, Sep 2011.

[70] P. W. Anderson. Plasmons, gauge invariance, and mass. *Phys. Rev.*, 130:439–442, Apr 1963.

[71] F. Englert and R. Brout. Broken symmetry and the mass of gauge vector mesons. *Phys. Rev. Lett.*, 13:321–323, Aug 1964.

[72] Peter W. Higgs. Broken symmetries and the masses of gauge bosons. *Phys. Rev. Lett.*, 13:508–509, Oct 1964.

[73] G. S. Guralnik, C. R. Hagen, and T. W. B. Kibble. Global conservation laws and massless particles. *Phys. Rev. Lett.*, 13:585–587, Nov 1964.

[74] M. S. Kushwaha, P. Halevi, L. Dobrzynski, and B. Djafari-Rouhani. Acoustic band structure of periodic elastic composites. *Phys. Rev. Lett.*, 71:2022–2025, Sep 1993.

[75] J. V. Sánchez-Pérez, D. Caballero, R. Mártinez-Sala, C. Rubio, J. Sánchez-Dehesa, F. Meseguer, J. Llinares, and F. Gálvez. Sound Attenuation by a Two-Dimensional Array of Rigid Cylinders. *Phys. Rev. Lett.*, 80:5325–5328, Jun 1998.

[76] F. R. Montero de Espinosa, E. Jiménez, and M. Torres. Ultrasonic band gap in a periodic two-dimensional composite. *Phys. Rev. Lett.*, 80:1208–1211, Feb 1998.

[77] Eli Yablonovitch. Inhibited spontaneous emission in solid-state physics and electronics. *Phys. Rev. Lett.*, 58:2059–2062, May 1987.

[78] Marin Soljačić, Steven G Johnson, Shanhui Fan, Mihai Ibanescu, Erich Ippen, and J D Joannopoulos. Photonic-crystal slow-light enhancement of nonlinear phase sensitivity. *J. Opt. Soc. Am. B*, 19(9):2052, 2002.

[79] Martin Maldovan and Edwin L. Thomas. Simultaneous localization of photons and phonons in two-dimensional periodic structures. *Appl. Phys. Lett.*, 88(25):3–6, 2006.

[80] Matt Eichenfield, Jasper Chan, Ryan M. Camacho, Kerry J. Vahala, and Oskar Painter. Optomechanical crystals. *Nature*, 461(7269):78–82, 2009.

[81] Stephen Ragole, Haitan Xu, John Lawall, and Jacob M. Taylor. Thermodynamic limits for optomechanical systems with conservative potentials. *Phys. Rev. B*, 96:184106, Nov 2017.

[82] E. A J Marcatili. Dielectric rectangular waveguide and directional coupler for integrated optics. *Bell Syst. Tech. J.*, 48(7):2071–2102, 1969.

[83] Jasper Chan, Matt Eichenfield, Ryan Camacho, and Oskar Painter. Optical and mechanical design of a "zipper" photonic crystal optomechanical cavity. *Opt. Express*, 17(5):3802–17, 2009.

[84] M. Eichenfield, R. Camacho, J. Chan, K. J. Vahala, and O. Painter. A picogram and nanometer scale photonic crystal opto-mechanical cavity. *Nature*, 459(7246):550–555, 2008.

[85] B. E. A. Saleh and M. C. Teich. *Fundamentals of Photonics*. John Wiley & Sons, Hoboken, 2nd edition, 2007.

[86] Julian Léonard, Andrea Morales, Philip Zupancic, Tobias Donner, and Tilman Esslinger. Monitoring and manipulating Higgs and Goldstone modes in a supersolid quantum gas. *Science*, 358(6369):1415–1418, 2017.

[87] S. Gupta, K. W. Murch, K. L. Moore, T. P. Purdy, and D. M. Stamper-Kurn. Bose-Einstein condensation in a circular waveguide. *Phys. Rev. Lett.*, 95:143201, Sep 2005.

[88] C. Ryu, M. F. Andersen, P. Cladé, Vasant Natarajan, K. Helmerson, and W. D. Phillips. Observation of persistent flow of a Bose-Einstein condensate in a toroidal trap. *Phys. Rev. Lett.*, 99:260401, Dec 2007.

[89] A. Ramanathan, K. C. Wright, S. R. Muniz, M. Zelan, W. T. Hill, C. J. Lobb, K. Helmerson, W. D. Phillips, and G. K. Campbell. Superflow in a toroidal Bose-Einstein condensate: an atom circuit with a tunable weak link. *Phys. Rev. Lett.*, 106:130401, Mar 2011.

[90] K. C. Wright, R. B. Blakestad, C. J. Lobb, W. D. Phillips, and G. K. Campbell. Driving phase slips in a superfluid atom circuit with a rotating weak link. *Phys. Rev. Lett.*, 110:025302, Jan 2013.

[91] Stephen Eckel, Jeffrey G Lee, Fred Jendrzejewski, Noel Murray, Charles W Clark, Christopher J Lobb, William D Phillips, Mark Edwards, and Gretchen K Campbell. Hysteresis in a quantized superfluid 'atomtronic' circuit. *Nature*, 506(7487):200–3, 2014.

[92] Stuart Moulder, Scott Beattie, Robert P. Smith, Naaman Tammuz, and Zoran Hadzibabic. Quantized supercurrent decay in an annular Bose-Einstein condensate. *Phys. Rev. A*, 86:013629, Jul 2012.

[93] C. Ryu, P. W. Blackburn, A. A. Blinova, and M. G. Boshier. Experimental realization of Josephson junctions for an atom SQUID. *Phys. Rev. Lett.*, 111:205301, Nov 2013.

[94] T. P. Orlando, S. Lloyd, L. S. Levitov, K. K. Berggren, M. J. Feldman, M. F. Bocko, J. E. Mooij, C. J. P. Harmans, and C. H. Van Der Wal. Flux-based superconducting qubits for quantum computation. *Phys. C Supercond.*, 372-376, P:194–200, 2002.

[95] Jonathan R. Friedman, V Patel, W Chen, S. K. Tolpygo, and J. E. Lukens. Quantum superposition of distinct macroscopic states. *Nature*, 406:43–46, Jul 2000.

[96] Frederick Wellstood, C. Heiden, and John Clarke. Integrated DC SQUID magnetometer with a high slew rate. *Rev. Sci. Instrum.*, 55(6):952–957, 1984.

[97] B. Yurke, P. G. Kaminsky, R. E. Miller, E. A. Whittaker, A. D. Smith, A. H. Silver, and R. W. Simon. Observation of 4.2-K equilibrium-noise squeezing via a Josephson-parametric amplifier. *Phys. Rev. Lett.*, 60:764–767, Feb 1988.

[98] I. Siddiqi, R. Vijay, F. Pierre, C. M. Wilson, M. Metcalfe, C. Rigetti, L. Frunzio, and M. H. Devoret. RF-driven Josephson bifurcation amplifier for quantum measurement. *Phys. Rev. Lett.*, 93:207002, Nov 2004.

[99] John Clarke and Alex I Braginski. *The SQUID Handbook Fundamentals and Technology of SQUIDs and SQUID Systems*, volume 1. Wiley-VCH, Weinheim, 2006.

[100] S Dimopoulos, P W Graham, J M Hogan, and M A Kasevich. General relativistic effects in atom interferometry. *Phys. Rev. D*, 78(4):42003, 2008.

[101] Raphaël Jannin, Pierre Cladé, and Saïda Guellati-Khélifa. Phase shift due to atom-atom interactions in a light-pulse atom interferometer. *Phys. Rev. A*, 92(1):013616, 2015.

[102] Carlton M. Caves, Kip S. Thorne, R. W P Drever, Vernon D. Sandberg, and Mark Zimmermann. On the measurement of a weak classical force coupled to a quantum-mechanical oscillator. I. Issues of principle. *Rev. Mod. Phys.*, 52(2):341–392, 1980.

[103] J. E. Mooij and Yu. V. Nazarov. Superconducting nanowires as quantum phase-slip junctions. *Nat. Phys.*, 2(3):169–172, 2006.

[104] Toshiya Kinoshita, Trevor Wenger, and David S Weiss. Observation of a one-dimensional Tonks-Girardeau gas. *Science*, 305(5687):1125–1128, 2004.

[105] F. Meinert, M. Panfil, M. J. Mark, K. Lauber, J.-S. Caux, and H.-C. Nägerl. Probing the excitations of a Lieb-Liniger gas from weak to strong coupling. *Phys. Rev. Lett.*, 115:085301, Aug 2015.

[106] R. Citro, A. Minguzzi, and F. W J Hekking. Quantum stirring as a probe of superfluidlike behavior in interacting one-dimensional Bose gases. *Phys. Rev. B*, 79(17):1–4, 2009.

[107] N. Didier, A. Minguzzi, and F. W. J. Hekking. Quantum fluctuations of a Bose-Josephson junction in a quasi-one-dimensional ring trap. *Phys. Rev. A*, 79:063633, Jun 2009.

[108] David W. Hallwood, Thomas Ernst, and Joachim Brand. Robust mesoscopic superposition of strongly correlated ultracold atoms. *Phys. Rev. A*, 82:063623, Dec 2010.

[109] Dmitry Solenov and Dmitry Mozyrsky. Metastable states and macroscopic quantum tunneling in a cold-atom Josephson ring. *Phys. Rev. Lett.*, 104:150405, Apr 2010.

[110] Dmitry Solenov and Dmitry Mozyrsky. Macroscopic two-state systems in trapped atomic condensates. *Phys. Rev. A*, 82:061601, Dec 2010.

[111] Y. Cai and K. C. Wright. Private communication. *Priv. Commun.*, 2015.

[112] C. L. Kane and Matthew P. A. Fisher. Transport in a one-channel Luttinger liquid. *Phys. Rev. Lett.*, 68:1220–1223, Feb 1992.

[113] C. L. Kane and Matthew P. A. Fisher. Transmission through barriers and resonant tunneling in an interacting one-dimensional electron gas. *Phys. Rev. B*, 46:15233–15262, Dec 1992.

[114] Marco Cominotti, Davide Rossini, Matteo Rizzi, Frank Hekking, and Anna Minguzzi. Optimal persistent currents for interacting bosons on a ring with a gauge field. *Phys. Rev. Lett.*, 113:025301, Jul 2014.

[115] Alexander Shnirman, Gerd Schön, and Ziv Hermon. Quantum manipulations of small Josephson junctions. *Phys. Rev. Lett.*, 79:2371–2374, Sep 1997.

[116] E. G. Adelberger, B. R. Heckel, and A. E. Nelson. Tests of the gravitational inverse-square law. *Annu. Rev. Nucl. Part. Sci*, 53:77–121, 2003.

[117] Jens H. Gundlach. Laboratory tests of gravity. *New J. Phys.*, 7(1):205, 2005.

[118] D. J. Kapner, T. S. Cook, E. G. Adelberger, J. H. Gundlach, B. R. Heckel, C. D. Hoyle, and H. E. Swanson. Tests of the gravitational inverse-square law below the dark-energy length scale. *Phys. Rev. Lett.*, 98:021101, Jan 2007.

[119] David B Kaplan and Mark B Wise. Couplings of a light dilaton and violations of the equivalence principle. *J. High Energy Phys.*, 2000(08):037–037, 2000.

[120] Raman Sundrum. Fat gravitons, the cosmological constant and submillimeter tests. *Phys. Rev. D*, 69(4), 2004.

[121] Nima Arkani-Hamed, Savas Dimopoulos, and Gia Dvali. Phenomenology, astrophysics, and cosmology of theories with submillimeter dimensions and TeV scale quantum gravity. *Phys. Rev. D*, 59(8):086004, 1999.

[122] Davit Aghamalyan, Marco Cominotti, Matteo Rizzi, Davide Rossini, Frank Hekking, Anna Minguzzi, Leong-Chuan Kwek, and Luigi Amico. Coherent superposition of current flows in an atomtronic quantum interference device. *New J. Phys.*, 17(4):045023, 2015.

[123] Mark F. Bocko and Roberto Onofrio. On the measurement of a weak classical force coupled to a harmonic oscillator: experimental progress. *Rev. Mod. Phys.*, 68:755–799, Jul 1996.

[124] F. Diedrich, J. C. Bergquist, Wayne M. Itano, and D. J. Wineland. Laser cooling to the zero-point energy of motion. *Phys. Rev. Lett.*, 62:403–406, Jan 1989.

[125] I. Wilson-Rae, P. Zoller, and A. Imamoğlu. Laser cooling of a nanomechanical resonator mode to its quantum ground state. *Phys. Rev. Lett.*, 92:075507, Feb 2004.

[126] Florian Marquardt, Joe P. Chen, A. A. Clerk, and S. M. Girvin. Quantum theory of cavity-assisted sideband cooling of mechanical motion. *Phys. Rev. Lett.*, 99:093902, Aug 2007.

[127] A. D. O'Connell, M. Hofheinz, M. Ansmann, Radoslaw C. Bialczak, M. Lenander, Erik Lucero, M. Neeley, D. Sank, H. Wang, M. Weides, J. Wenner, John M. Martinis, and A. N. Cleland. Quantum ground state and single-phonon control of a mechanical resonator. *Nature*, 464(7289):697–703, 2010.

[128] A. P. Reed, K. H. Mayer, J. D. Teufel, L. D. Burkhart, W. Pfaff, M. Reagor, L. Sletten, X. Ma, R. J. Schoelkopf, E. Knill, and K. W. Lehnert. Faithful conversion of propagating quantum information to mechanical motion. *Nat. Phys.*, 13:1162–1167, 2017.

[129] Christine Guerlin, Julien Bernu, Samuel Deléglise, Clément Sayrin, Sébastien Gleyzes, Stefan Kuhr, Michel Brune, Jean-Michel Raimond, and Serge Haroche. Progressive field-state collapse and quantum non-demolition photon counting. *Nature*, 448(7156):889–893, 2007.